Universidade de Aveiro Departamento de Engenharia Mecânica
2011

Diana Rebecca
Esteves Cardoso
Gavazzo Rodrigues

Biomechanical Analysis of Surgical Treatments of the Cervical Spine

Análise Biomecânica de Tratamentos Cirúrgicos da Coluna Cervical

Universidade de Aveiro Departamento de Engenharia Mecânica
2011

Diana Rebecca
Esteves Cardoso
Gavazzo Rodrigues

Biomechanical Analysis of Surgical Treatments of the Cervical Spine

Análise Biomecânica de Tratamentos Cirúrgicos da Coluna Cervical

Thesis submitted to Universidade de Aveiro (University of Aveiro) in order to satisfy the necessary requirements for the Master's Degree in Mechanical Engineering, performed under the scientific orientation of António Manuel Godinho Completo, Assistant Professor of the Mechanical Engineering Department of the University of Aveiro and co-oriented by Abel Fernando Queirós e Nascimento, Invited Assistant Professor of the Mechanical Engineering Department of the University of Aveiro and Director of "Instituto de Cirurgia Reconstrutiva de Coimbra".

Dissertação apresentada a Universidade de Aveiro para cumprimento dos requisitos necessarios a obtenção do grau de Mestre em Engenharia Mecânica, realizada sob a orientação científica de Professor Doutor António Manuel Godinho Completo, Professor Auxiliar do Departamento de Engenharia Mecânica da Universidade de Aveiro e co-orientada pelo Professor Doutor Abel Fernando Queirós e Nascimento, Professor Auxiliar Convidado do Departamento de Engenharia Mecânica da Universidade de Aveiro e Director do Instituto de Cirurgia Reconstrutiva de Coimbra.

o júri / the jury

presidente / president

Professor Doutor Francisco José Malheiro Queirós de Melo
Professor Associado do Departamento de Engenharia Mecânica da Universidade de Aveiro

vogais / examiners' committee

Professor José António de Oliveira Simões
Director da Escola Superior de Artes e Design - Matosinhos
Professor Associado com Agregação da Universidade de Aveiro

Professor Doutor António Manuel Godinho Completo
Professor Auxiliar do Departamento de Engenharia Mecânica da Universidade de Aveiro

Professor Doutor Abel Fernando Queirós e Nascimento
Professor Auxiliar Convidado do Departamento de Engenharia Mecânica da Universidade de Aveiro
Director do Instituto de Cirurgia Reconstrutiva de Coimbra

To Mummy, Daddy and Pedro.
I love you always.

agradecimentos / acknowledgements

Firstly I'd like to thank my teacher Professor Antonio Completo, for his patience, availability, dedication and perseverance, without whom this project would not have been possible.

I would also like to thank Professor Abel Nascimento, for his help and enthusiasm regarding this thesis. A big thank you to Doctor Elizabeth Nogueira for her availability and input regarding my thesis and her answers to any questions I may have had regarding the human spine.

Thank you to Aveiro University, for existing.

From this point onwards let it be clear that order of appearance is NOT relevant!

A special thank you to Joana Pereira and Ricardo Duarte for their input to this thesis, and to the rest of the Biomechanical Laboratory. Working alongside all of you was a lot of fun!

Thank you, Sophie; you are one of the kindest people I ever met, for always being there for me. Thank you, Ricardo, for your bounce, excitement and for reminding me that life is not to be taken too seriously! Thank you to the Neta family who were so kind to me for the most part of my university years. Thank you to the Brunas who adopted the four of us, and have consistently been such good friends and for also showing me the value of working hard. Thank you to the Graças for their friendship. Thank you Maria José, my second mother, for always being present in my life.

Thank you: Guida, for always putting me and everyone else before you; Avô Raul, for all the times I needed to go to Lisbon; Tété, for the homemade meals and your motherly ways; Mariana, for providing so many lunches; Pedro, Xico, Miguel, João Pedro and Freddy for being lovable idiots; Nana, for your inner glamour, I'm proud to have your name; Uncle Miguel, you're just wonderful; To Kristine and the German branch of the family and Diane too, for all the emails, pictures and advice; To the rest of my family (Avó Teresa and Avô Quim included, who were always cheering from above) and to all my friends (Palheiro Golf included).

Thank you to Edgar Wright for your unorthodox views and all the editing.

Thank you, to the best maths teacher in Portugal (if not the world) Padre Salesiano António Vieira, and to all the great teachers I had who made a difference because they cared.

To Becky, Mango, Reebok, Jack, Zarco and all the others who provided so many hours of fun.

To P.B. for his presence and comfort ever since before I was here.

Last but not least Daddy and Mummy, nothing I write could ever do you justice...even then: for all the magic and fleecy lambs, and teaching me that there is nothing I can't do, no matter how utterly ridiculous, unfeasible and impossible it may seem to the entire world, thank you.

Keywords

Biomechanics, Arthroplasty, Arthrodesis, Finite Element Method, Cervical Spine Implants, CT Images.

Abstract

The main objective of this thesis was to study the biomechanical implications related to different surgical procedures for decompressing the intervertebral discs in the cervical spine.

The different surgical techniques were evaluated so as to assess how load transfer to the adjacent vertebrae would be affected, thereby ascertaining the potential risks of failure of these vertebrae when compared to the vertebrae in the native (healthy) state. For this purpose an initial analysis of the cervical spine was performed, specifically on the C4-C6 segment, from an anatomical, biomechanical and pathological point of view. An analysis of surgical reconstructive processes was also carried out, with particular focus on the two procedures known as arthrodesis and arthroplasty.

Finite element models were then developed from CT images obtained from a healthy male patient, with the purpose of comparing the surgical cases of arthrodesis and arthroplasty to the native case. For these tests the selected implants were the Fidji PEEK cage (Zimmer, Inc) for the arthrodesis case and the ProDisc-C (Synthes, Inc.) for the arthroplasty case. The different models generated from medical CT imaging were reconstructed with the help of 3D modelling and finite element software and submitted to loading conditions that simulated the weight of the human head in the anatomical (upright) position.

The results obtained for each model enabled the evaluation, and therefore the comparison, of the alterations in load transfer from one model too another. These alterations were determined through the measurement of the variations in the principal strain values in the cortical bone of vertebrae C5 and C6, adjacent to the implant, and in vertebra C4, which was positioned directly above vertebra C5. Compressive strain values were also analysed in the trabecular bone for all three vertebrae.

The principal strain values in the anterior vertebral body of vertebrae C5 and C6, obtained from the numerical models developed, were compared with the respective results obtained from the experimental models subsequently used in this study.

In addition to the numerical models developed, experimental models of the C5-C6 segment in rigid polyurethane foam were created. The different surgical techniques (arthroplasty and arthrodesis) were performed in-vitro. The purpose behind the development of these models was to ascertain the extent to which the results obtained for the numerical models could be experimentally replicated. Alterations in load transfer in these models was registered by means of rosette strain gauges placed in the anterior region of the vertebrae, allowing the evaluation of the principal strain values on the model's surface. These experimental models were submitted to the same loading conditions as the numerical models.

A high correlation between the principal strain values was obtained when comparing the numerical models with the experimental models, thus revealing the ability of the numerical models to recreate the mechanical behaviour of the experimental models.

The comparison made between the native numerical model (in which mechanical bone properties had not been simplified) and the model where mechanical properties were discretized, into cortical and trabecular bone properties, revealed differences that should not be overlooked. When comparing implanted models with the native model an increase in principal strain values of cortical and trabecular bone, particularly in the lateral areas of the vertebral body were revealed, relatively to the native model. On average these increases were lower in the cortical bone for the arthroplasty case than in the arthrodesis case, but higher in the trabecular bone.

Thus, it is concluded that both surgical techniques contribute to the increase of mechanical strain on the vertebrae adjacent to the implants, and thus possibly increase the risk of failure of the bone structure due to fatigue.

Palavras-chave

Biomecânica, Artroplastia, Artrodese, Metodo dos Elementos Finitos, Implantes Coluna Cervical, Images TAC.

Resumo

Procurou-se especificamente avaliar como cada uma das diferentes técnicas cirúrgicas altera a transferência de carga as vértebras adjacentes, aferindo assim potenciais riscos de falência destas quando comparadas com a situação das vértebras no estado nativo (saudável). Para o efeito, numa primeira fase procurou-se realizar uma naálise detalhada a coluna cervical, especificamente ao segmento C4-C6, na sua vertente anatómica, biomecânica e patológica, assim como dos processos cirúrgicos de reconstrução com especial enfoque na artrodese e artroplastia cervical.

Numa fase posterior procedeu-se ao desenvolvimento de modelos numéricos de elementos finitos a partir de imagens de TAC de um paciente saudável, com o propósito de comparar as técnicas de artroplastia e artrodese com a situação nativa. Para estas análises foram seleccionados os implantes Fidji PEEK cage (Zimmer, Inc) para a técnica da artrodese, e ProDisc-C (Synthes, Inc) para a técnica da artroplastia. Estes diferentes modelos, gerados a partir das imagens médicas de TAC, foram reconstruídos com o auxílio de softwares de modelação 3D e de elemento finitos, e submetidos a condiç oes de cargas idênticas, correspondente ao peso da cabeça humana na postura anatómica.

Os resultados obtidos com estes modelos permitiram avaliar de forma comparativa as alterações de transferência de carga através das deformações principais no osso cortical das vértebras C5-C6 imediatamente adjacente aos implantes, assim como na vértebra C4 do segmento anexo. Em complemento destas deformações foram também analisadas as deformações de compressão no osso esponjoso das mesmas vértebras.

As deformações principais no cortex anterior das vértebras C5-C6 dos modelos experimentais desenvolvidos foram comparadas com os resultados obtidos nos modelos numéricos correspondentes criados neste estudo.

Em complemento aos modelos numéricos anteriores, desenvolveram-se modelos experimentais do segmento C5-C6, em espuma rígida de poliuretano, onde as diferentes técnicas cirúrgicas (artrodese e artroplastia) foram implementadas através de cirurgias "in-vitro". O desenvolvimento destes modelos pretendeu aferir até que ponto os resultados obtidos nos modelos numéicos se reproduziam experimentalmente. As alterações de transferência de carga nestes modelos foram realizadas com recurso a rosetas de extensómetros colocadas na região anterior das vértebras, permitindo a avaliação das deformações principais na sua superfície. Estes modelos foram submetidos ao mesmo caso de carga dos modelos numéricos.

Um elevado valor de correlação entre as deformações principais foi obtido na comparação dos modelos numéricos com os modelos experimentais, revelando uma boa capacidade dos modelos numéricos replicarem o comportamento mecânico dos modelos experimentais.

Os resultados obtidos na comparação do modelo numérico nativo com o modelo em que as propriedades mecânicas foram discretizadas, em osso cortical e esponjoso, revelaram diferenças não desprezáveis. Os resultados obtidos entre os diferentes modelos implantados e o modelo nativo revelaram aumentos das deformações no osso cortical e esponjoso, em particular nas zonas laterais aos implantes, relativamente ao modelo nativo. Em média estes aumentos foram inferiores na técnica da artroplastia relativamente a artrodese no osso cortical e foram superiores no osso esponjoso.

Assim, conclui-se que as ambas as técnicas cirúrgicas contribuem para o agravar da solicitação mecânica sobre as vértebras adjacentes aos implantes, e desta forma possivelmente potenciar o risco de falência por efeito do processo de fadiga.

Contents

List of Figures

List of Tables

Introduction

The human spine is an extremely complex and sound structure. It is the main support system for the entire body, protects the spinal cord from possible damage whilst also enabling a very wide range of motion for the body. The spine is divided into four main parts: the cervical spine (neck area), the thoracic spine, the lumbar spine and the sacrum. This study is focused on the cervical spine, associated problems, corresponding surgical treatments and how these treatments alter the biomechanics of the human neck.

One of the main problems associated to the cervical spine is degenerative disc disease. During the last 50 years, the most popular treatment for this pathology has been decompression via surgical procedure performed by anterior intersomatic arthrodesis (vertebral fusion). Results show a short and long term decrease in neurological complications and pain symptoms. Arthrodesis is the surgical procedure consisting of the artificial induction of joint ossification between two bones (in this case adjoining vertebrae), in order to align, strengthen and stabilize the affected area.

In the majority of arthrodesis cases, the fixing device is filled with bony tissue in order to increase bone fusion success rates. Although arthrodesis limits the patients' spinal mobility, the majority of patients who have undergone this procedure are still able to perform all their daily tasks normally. However, functional limitations, loss of mobility (as far as the affected spinal segments are concerned), additional strain now allocated to the vertebrae directly above and below the now fixed vertebrae, plus aggravation of any disc degeneration caused by this extra strain are still cause for concern. These factors justify the search for new and safer solutions in order to preserve mobility and integral spinal structure.

At the present time, cervical arthroplasty represents a promising technique which solves most of the above mentioned problems. It enables spinal decompression, preserves the cervical segment's movement, maintains the initial cervical segment's length, minimizes degenerative alterations to adjacent discs as well as enabling a quick recovery. Disc prosthesis have been used mainly in cases that cannot be treated by fixing vertebrae permanently. This operation may affect one, or, a maximum of two inter-vertebral discs, and posterior spinal articulations must be in good condition. During this procedure the disc is replaced by a high density polyethylene and metal prosthesis. This prosthesis enables the disc (source of pain) to be removed without causing any blockage as far as spinal movement is concerned, thus maintaining a natural spinal balance. As cervical arthroplasty is a fairly recent technique, long term results are still undetermined so this practice has not yet been consolidated.

The main objective of this project is, (from a biomechanical point of view, to compare the two afore-mentioned surgical procedures: cervical arthrodesis and arthroplasty). In addition, to identify potential risks associated with the surrounding structures after surgery in comparison to the intact and healthy cervical spine. This study will be based on thorough research of existing bibliography concerning these two surgical procedures. In addition, clinical situations will be simulated, through modelling instruments and a numerical technique (finite element method - FEM), in order to evaluate a number of biomechanical parameters that would otherwise be very difficult or even impossible to determine.

Another objective of this study is to numerically and experimentally quantify the structural alterations caused to the bone before and after each one of these two surgical procedures. The two implants studied were the Fidji PEEK Cage for Arthrodesis, and ProDisc-C for Arthroplasty. The C4-C6 spinal segment was focused on in this study since C5-C6 intervertebral area is the most common section to suffer degeneration. So implants were positioned in the C5-C6 intervertebral space. Vertebra C4 was also recreated as a means to ascertain what the implant's effect is on a vertebra that is not in direct contact with the implant. This thesis is organizes into five chapters.

The first chapter is dedicated to Cervical Spine anatomy and biomechanics. It identifies main cervical spinal elements, tissues, range of motion, main actuating forces and stability. Some previous studies on the cervical spine were also mentioned here. This chapter's purpose is not to extensively analyse the anatomy of the spine, but a brief anatomical description seemed appropriate in order to set the initial framework for this project.

In chapter two most clinical problems associated to the cervical spine are mentioned, along with causes, some symptoms and surgical and non surgical treatments. This chapter is also dedicated to cervical arthrodesis and arthroplasty. A revision was made regarding the different types of implants and biomaterials used throughout the years, along with surgical procedure, problems that may arise and success rates for some of the main implants.

In chapter three the steps to creating each one of the numerical models is explained.

Implanted and native numeric models were created from CT images. The final versions of these models, of the studied spinal segment (C4-C6), were created through the use of different software packages. Computational results and a discussion on these are also presented here, with the objective of investigating structural behaviour of the cervical spine for each one of the three main cases (native spine, spine with cage, spine with prosthetic disc).

Chapter four regards the experimental approach. Model construction is explained along with used methodology and materials, results and their respective discussion. In this chapter numeric results, mainly stress/strain levels in the cortical bone near implant fixation area, are also compared with the experimental results.

In the last chapter general conclusions of this study are presented, along with suggestions for possible future projects.

Chapter 1

The Cervical Spine

1.1 Human Spine

In this chapter a brief explanation of the cervical spine's function will be made along with its anatomy and main components, since this topic is the starting point of this study.

The human spine is the structural pillar of the human body. In a simplified way this pillar is firm but flexible at the same time. Its flexibility and stability is guaranteed by the fact that is it composed of various smaller pieces, called vertebrae. These vertebrae are joined together by articulations, muscles, ligaments and tendons. Even though the spine is technically composed purely of bones, from a more practical point of view it also entails all the spine's content and annexes such as muscles, nerves, veins, etc.

The spine is built up of 24 movable vertebrae and 5 fixed vertebrae. The 24 movable vertebrae are the 7 cervical vertebrae, 12 thoracic vertebrae and 5 lumbar vertebrae, the 5 fixed vertebrae make up the lower part of the spine and form the sacrum (figure 1.1).

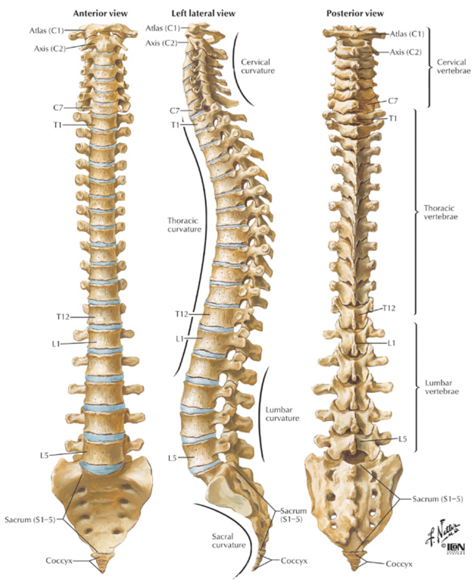

Figure 1.1: Human Spine: Anterior View, Sagital View, Posterior View.
[www.netterimages.com]

1.2 Cervical Spine Anatomy

Since this study is based on the cervical spine, this is the portion of the spine that will be focussed on.

The cervical spine (figure 1.2) is the topmost part of the spine, and this is where the head is supported. The seven vertebrae are known as C1, C2, C3, etc, all the way down to C7. The cervical spine is divided into two main parts the upper cervical spine (C1 or Atlas and C2 or Axis) and the lower cervical spine (C3 to C7). The C1 and C2 vertebrae's geometry is very different to that of all other vertebrae and also from each other's. These two vertebrae are responsible for most of rotation and flexion of the head.

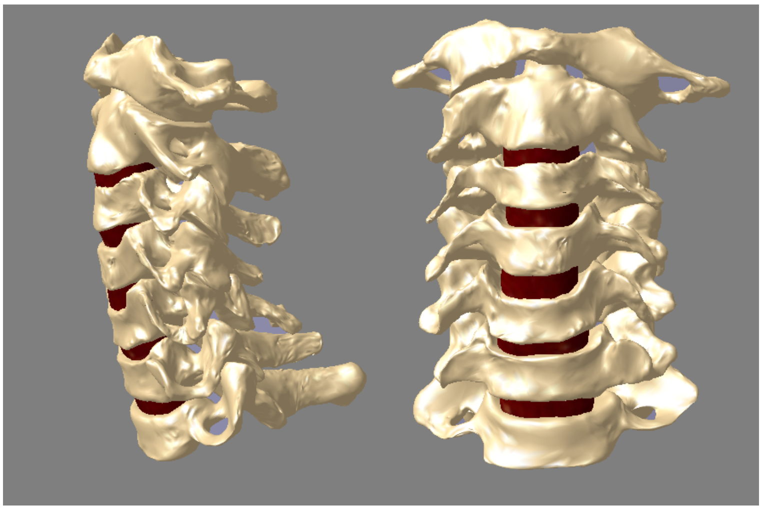

Figure 1.2: Cervical Spine.

1.2.1 Vertebrae

With the exception of the C1 and C2 vertebrae all other vertebrae follow the same basic structure, a body, the lamina, the vertebral arch and the posterior spinous process. When all the vertebrae are positioned one on top of the other they form an interior tunnel (created by the vertebral foramen) through which the spinal cord passes through.

Figure 1.3 represents the top view of vertebra C7 and a Side view of a typical cervical vertebra.

Vertebrae are attached to each other through the two superior and inferior articular surfaces that form synovial joints. In other words the superior articular surface of, for example vertebra C5 is in contact with the inferior articular surface of vertebra C4. This interface is responsible for spinal movement (rotation and translation).

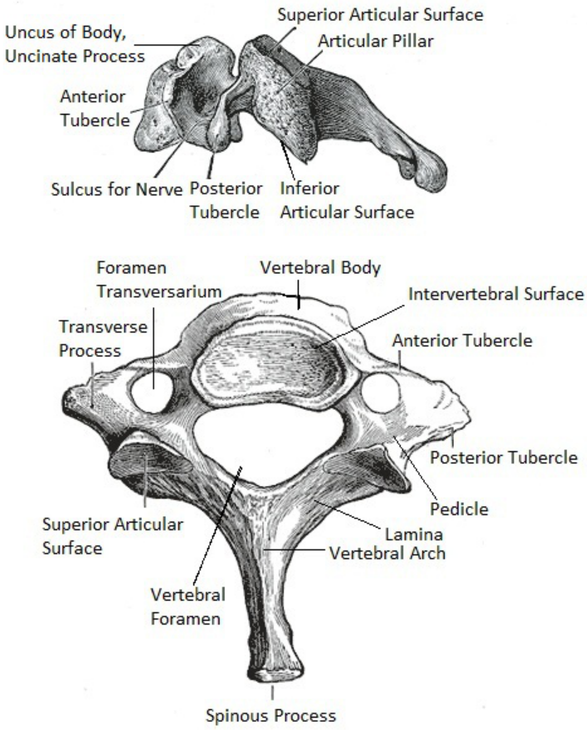

Figure 1.3: Vertebral anatomy.
[Gray, H., *Anatomy of the Human Body*, 1918]

1.2.2 Spinal Cord

The medulla spinalis or spinal cord forms the elongated, nearly cylindrical, part of the central nervous system which occupies the upper two-thirds of the vertebral canal. Its average length in a male is about 45 cm, and 42 to 43 in a female, whilst its weight amounts to about 30gr. It starts at the level of the upper border of the atlas and ends at the lower border of the first or upper border of the second, lumbar vertebra. Above, it is continuous with the brain; below, it ends in a conical extremity, from the apex of which a fragile filament descends as far as the first segment of the coccyx. The position of the medulla spinalis varies with the movements of the vertebral column since its lower extremity is drawn slightly upward when the column is flexed [24].

1.2.3 Intervertebral Discs

Vertebrae are also attached to each other through intervertebral discs (with the exception of the C1/C2 interface). The discs are positioned in the intervertebral surface on the vertebral body. The Uncinate Process helps to keep the disc positioned on the vertebrae. This articular entity is responsible for the flexion and extension movement of the spine and is known as an amphiarthrosis joint since this joint is categorized as a slightly movable joint. It is made up of two vertebral horizontal planes and the intervertebral disc.

The intervertebral disc's structure is a very particular one, it's divided essentially into two parts: the central part, the Nucleus Pulposus and the outer part, the Annulus Fibrosus. In figure

1.4 three images of the intervertebral disc are visible. From left to right the whole intervertebral disc, the nucleus pulposus with surrounding sections of the annulus fibrosus and a section of the intervertebral disc.

Figure 1.4: Intervertebral disc.

The nucleus pulposus is formed of a gelatine like substance that derives from the spinal cord in the embryo. This gelatine is transparent and composed of 88% of water, thus being highly hydrophilic, and chemically formed by a substance fundamentally composed of Mucopolysaccharides. Mucopolysaccharides are long chains of sugar molecules that are found throughout the body, often in mucus and in fluid around the joints. They are more commonly called glycosaminoglycans. Also identified in this substance was sodium chondroitin sulfate-protein complexes, a form of hyaluronic acid and kerato sulfate. From a histological[1] point of view the nucleus contains collagen fibbers and chondrocyte like cells. There are no blood vessels or nerves in the nucleus [35].

The outer part of the intervertebral disc is the annulus fibrosis. It is composed by a succession of concentric fibber layers. The direction of the fibbers from one layer to another are crossed. The direction of the fibbers on the outermost layer are almost vertical and gradually tilt so that in the innermost layer they are practically horizontal. In a healthy disc this intertwinement of fibbers makes it impossible for any substance to permeate into the disc and nucleus. The nucleus is constantly under slight pressure in such a way that if the disc were to be cut horizontally the nucleus would protrude over the annulus fibrosus [35].

1.2.4 Ligaments

Spinal ligaments surround the cervical spine in order to stabilize and control its movement. The cervical spine's ligaments are divided into six main groups according to their whereabouts:

- Anterior longitudinal ligaments - set on the anterior facet of the vertebral bodies;
- Posterior longitudinal ligaments - set on the posterior facet of the vertebral bodies;
- Ligamentum Flavum - join the lamina of one vertebra to the lamina of the adjoining vertebra;
- Capsular ligaments - join the inferior articular surfaces of a vertebra with the superior articular surfaces of a vertebra directly bellow it;
- Interspinous ligaments - join the spinal process of one vertebra to another;
- Supraspinal ligaments - are set on the posterior surfaces of the vertebrae's spinal process.

[1] Histology: The study of the microscopic anatomy of cells and tissues of plants and animals

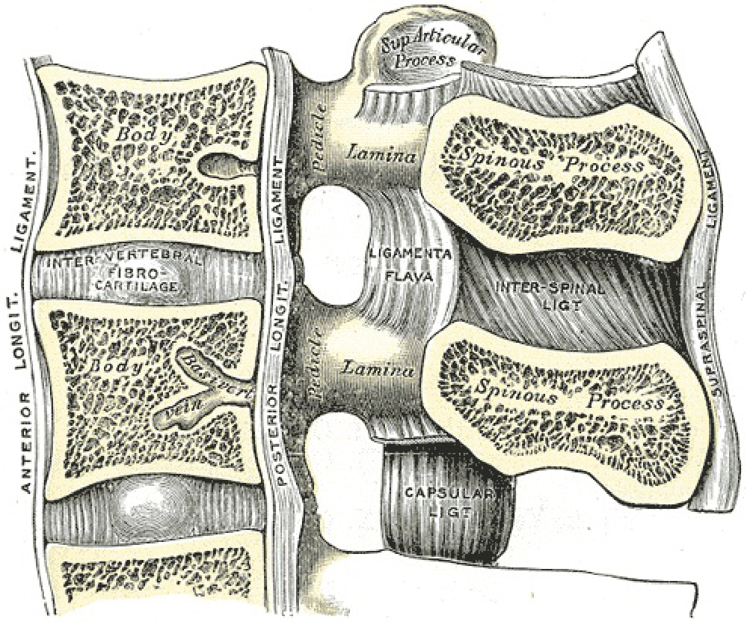

Figure 1.5: Vertebral ligaments.
[Gray, H., *Anatomy of the Human Body*, 1918]

For a better understanding of the positioning of the various groups of ligaments, these have been made visible in figure 1.5. The figure shows a sagital cut of a portion of the cervical spine with the six groups of ligaments.

1.2.5 Muscles

Tendons, just like ligaments, are made of a fibrous tissue, however, instead of joining bone to bone they connect muscle to bone.

There are hundreds of muscles in the body, and the muscular system of the spine is a complex one, in as much as there are various "main" muscles in the neck with important roles. The muscular system of the spines' main purpose is to support and stabilize the spine. The neck muscles help to support the neck but also, due to their complexity, enable a wide range of motion (flex, rotate and extend).

The neck muscles are divided into two main sections, these are the deep muscles and the superficial muscles.

The deep muscles are directly connected to the lower cervical spine. Most of these muscles follow an oblique course starting from the C3 vertebral area and heading downwards in a back and inwards direction. Bearing in mind that the neck is, for all effects and purposes, symmetrical, the deep muscles determine the extension, flexion (frontal and sagital) and rotation of the side of their contraction. Contrarily to this, the superficial muscles determine the extension and flexion of the side of their contraction but the rotations is determined by the contraction of superficial muscles on the opposite side of this particular movement.

The superficial muscles are attached to the skull and upper cervical spine (C1 and C2), and even though they also follow an oblique direction they go in a downwards, forward and outwards direction. This way the neck muscles create a crisscross net over the cervical spine [35].

In figures 1.6, 1.7 and 1.8 most neck muscles are visible.

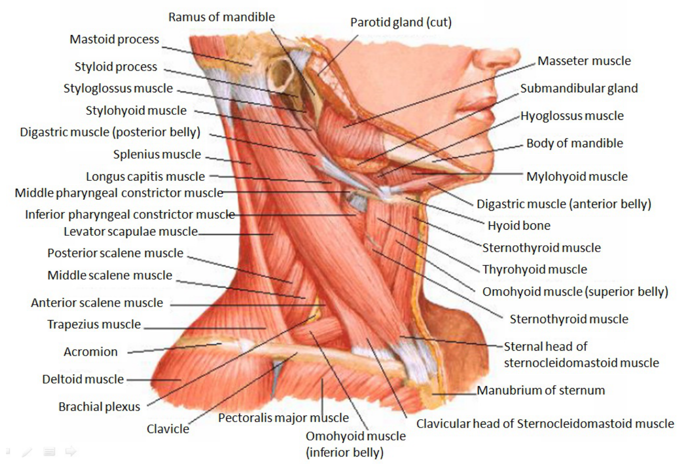

Figure 1.6: Neck Muscles-Lateral view.
[Netter, F. H., *Atlas de Anatomia Humana*, 2000]

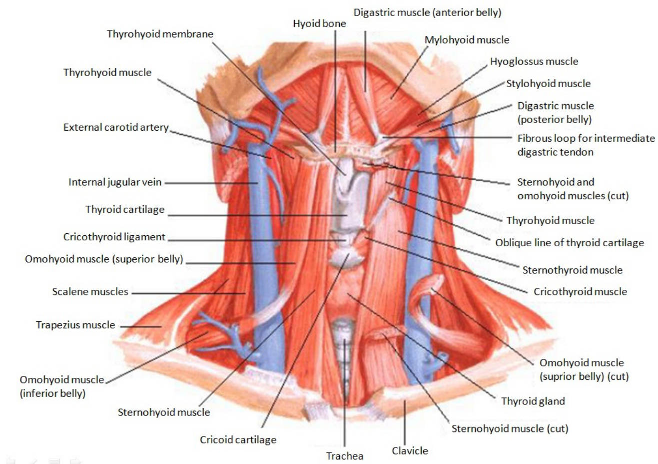

Figure 1.7: Neck Muscles-Infrahyoid and Suprahyoid Muscles.
[Netter, F. H., *Atlas de Anatomia Humana*, 2000]

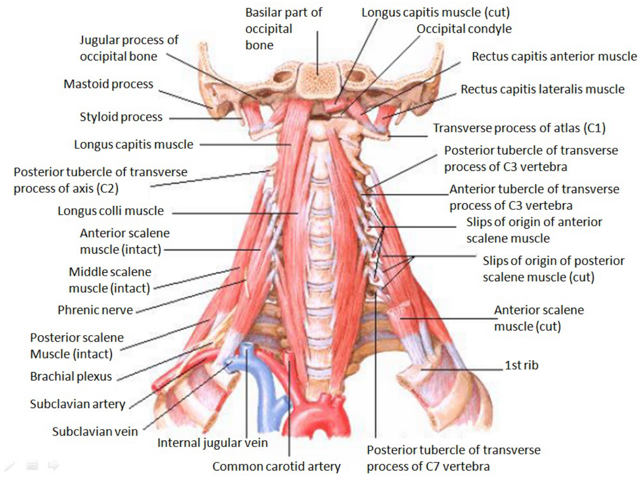

Figure 1.8: Neck Muscles-Scalene and Prevertebral.
[Netter, F. H., *Atlas de Anatomia Humana*, 2000]

1.2.6 Arteries and Veins

The neck is extremely rich in veins and arteries since the brain requires so much oxygen. The main differences between veins and arteries are that veins are usually thinner and are responsible for the transportation of blood low in oxygen to the heart, whilst arteries are more muscular and take blood rich in oxygen from the heart to all other organs.

The main cervical blood flow is guaranteed by the external and internal carotid arteries, the internal and external jugular veins. In figures 1.7 and 1.8 it's possible to identify the external carotid artery, the internal jugular vein and also the subclavian vein and artery. These last two blood vessels are situated at the base of the neck.

1.3 Biomechanics of the Cervical Spine

The objective of studying the biomechanics of the cervical spine is so that actuating forces and caused movement may be better understood, in order to allow manipulation of these forces as a means to solve or prevent any malformation. In order to better understand movement and force directions three main plains are commonly used as a reference point: the frontal or coronal plane, the sagittal or median plane and the horizontal or transverse plane (figure 1.9).

Figure 1.10 represents a simplified diagram of actuating forces of a human head on the cervical spine.

The head is in equilibrium with the neck when the body is in the upright static position (anatomic position). In other words the positioning of the head in this anatomic position would be in the upright position when an imaginary card pressed between one's teeth (masticatory plane) would create a horizontal plane (see figure 1.10 **P.M.** plane).

Point **O** represents the point where the occipital bone fits into the atlas (C1).

The point **G** represents the centre of gravity of the head and on this point the force corresponding to the head weight is represented by an arrow pointing down. Force **F** represents the resulting neck muscle force that counterbalances the weight of the head.

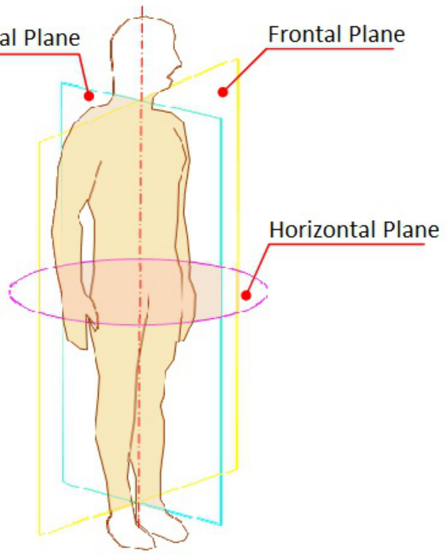

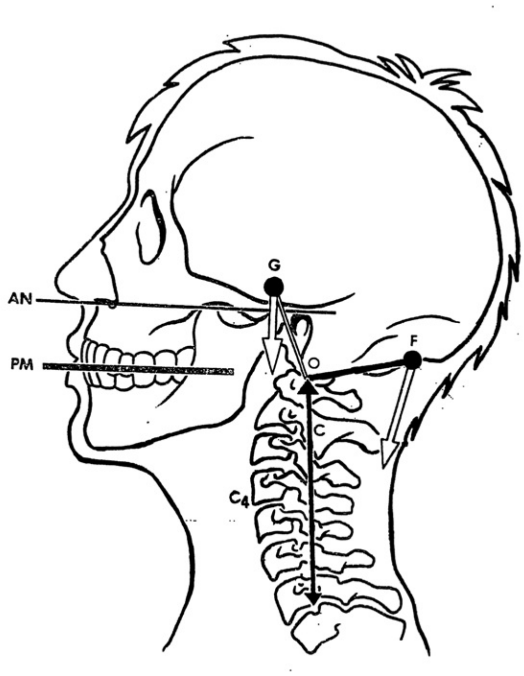

Figure 1.9: Reference planes for thehuman body [Completo, A. M. G., *Estudo Numérico e Experimental da Biomecânica da Prótese do Joelho*, 2006]

Figure 1.10: Actuating forces on a human cervical spine. [Kapandji, I. A., *Fisiologia Articular: Esquemas Comentados de Mecânica Humana - Vol. 3.*, 1987]

The cervical spine is not vertical, it's shaped like a "C", this natural curvature of the cervical spine is known as natural cervical lordosis. Usually males have larger median cervical lordosis than females (20 and 14 degrees respectively) [33].

By comparing profile x-rays during maximum flexion-extension (see figure 1.11: **A**) it's possible to ascertain that:

The total range of flexion-extension of the inferior cervical spine is from 100 to 110°;

The total range of flexion-extension of the whole of the cervical spine is around 130° (with the masticatory plane as our plane of reference).

Thus determining that the range of flexion-extension of the upper cervical spine (C1 and C2) is about 20 to 30°.

Through x-rays of the neck on a frontal plane whilst tilting the head, the value of approximately 45° was determined as being the maximum value of lateral bending the head can support (figure 1.11 **B**). The upper cervical spine has a lateral bending value of about 8° this angle is obtained solely by the Atlanto-occipital joint (joint between the Atlas and the Occipital bone) since the Axis (C2) doesn't tilt.

Rotation on the horizontal plane was determined as being between 80 to 90° to each side. Being 12° of these 80 or 90° due to the Atlas' rotation and another 12 due to the Axis' rotation (figure 1.11 **C**).

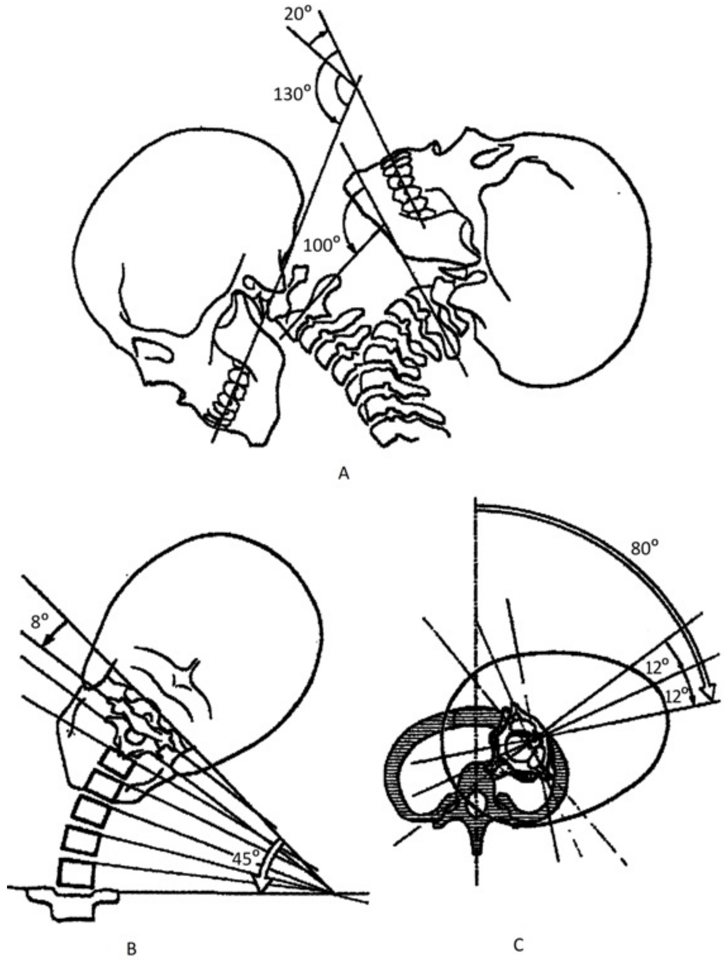

Figure 1.11: Cervical spine range of motion.
[Kapandji, I. A., *Fisiologia Articular: Esquemas Comentados de Mecânica Humana - Vol. 3.*, 1987]

Intervertebral disc movement

The nucleus' shape is similar to that of a sphere, bearing this in mind it may be compared to a swivel head articulation. This articulation features three different movements:

- Tilting
    In the sagital plane (flexion or extension)
    In the frontal plane (lateral flexing)
- Rotation of one vertebra in relation to the second one.
- Sliding/Translation

In total this joint allows for 6 degrees of freedom: frontal and lateral flexion-extension, sagital sliding, transversal sliding, left and right rotation, however all these movements have a small amplitude, it is thanks to the fact that there are many of these articulations in the spine that enable the body to perform movements with greater amplitude.

These different movements and how they affect the forces in the intervertebral disc will now be discussed. Firstly compression and extension movement shall be considered (1.12 **A**, **B** and **C**). Before any kind of pressure is put upon the disc (**A**) this disc has interior forces of its own since the annulus' fibbers put pressure upon the nucleus, this is can be defined as being a state of pre-restriction of the disc.

When an extension force is put upon the disc (**B**), the vertebral endplates retract from the disc, disc width decreases, disc height increases as does the tension in the fibbers of the annulus. The nucleus which is usually cylindrical will now present a more spherical shape. The elongation of the disc decreases pressure on the nucleus; this is the basis for treatments of herniated discs, however depending on the state of the disc this may not work).

When axially compressing the spine (**C**), the disc is squeezed between the vertebral endplates, the nucleus flattens, it's internal pressure increases and transmits itself laterally towards the innermost fibbers of the annulus. This way a vertical force is transformed into a lateral force and tension in the annulus fibbers increases.

When observing the intervertebral discs as a parts of the whole cervical spine during the movements of extension (**D**) what happens is that the upper vertebra deviates slightly backwards making the intervertebral disc's height at the back smaller, consequently pushing the nucleus forwards. When this happens the annulus fibbers' tension grows and pulls the top vertebra forwards to its initial position. The same principle applies to lateral bending (**E**) and flexion movement (**F**). During the flexion movement the top vertebra moves forward; the nucleus is pushed backwards and supports its self on the annulus, and the tension in the annulus' fibbers increases pulling the vertebra back towards its initial position.

Bearing in mind that the annulus fibbers' are oblique (the outer layers are almost vertical and the inner layers are almost horizontal), and that they change direction from one layer to another. When rotation movement is applied on the vertebrae, what happens is the following:

- The fibbers of the layers of the annulus whose direction is the same as the rotation direction are extended.

- The fibbers of the layers of the annulus whose direction is opposite to the direction of rotation are flexed.

- The maximum tension is felt in the inner layers of the annulus since this is where the fibbers are almost horizontal. The nucleus is now submitted to the highest compression forces in the disc and this pressure increases proportionally with rotation angle.

As a general rule, taking all these movements into consideration (lateral flexion, sagital flexion and extension, compression and rotation, it's safe to conclude that during movement there is always a heightening of the pressure applied on the nucleus, as well as of the tension in the annulus' fibbers. Thanks to the ability of the disc to adapt to all these different movements and to the varied direction of the annulus fibbers the disc tends to compensate for whatever forces motion may create upon it, in such a way that the spines' tendency is for the spine to return to its natural, stable and balanced position.

For this study in particular the value of 50 N was considered for simulations on the cervical spine. The choice of 50 N was based on a simulation of static-loading conditions which could be achieved for a man standing [25].

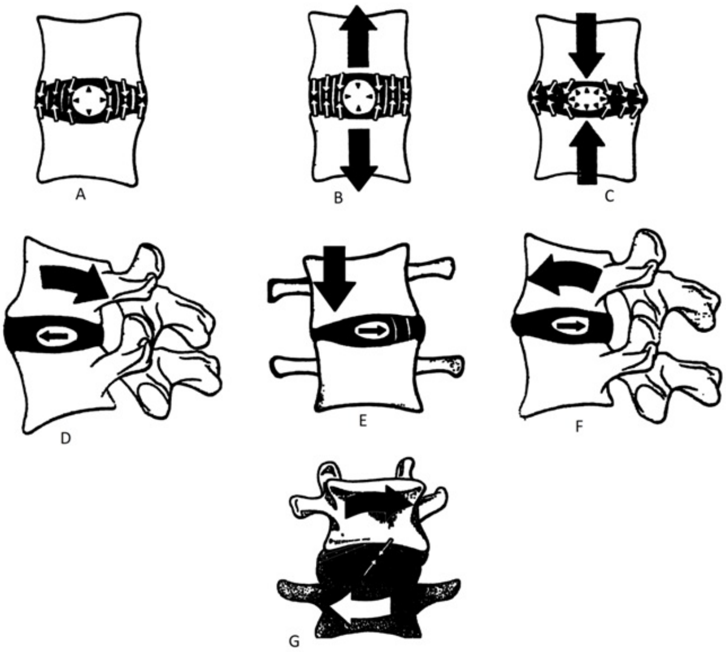

Figure 1.12: Intervertebral disc, actuating forces.
[Kapandji, I. A., *Fisiologia Articular: Esquemas Comentados de Mecânica Humana - Vol. 3.*, 1987]

1.3.1 Previous Cervical Spine Studies

Different studies have been performed on the cervical spine. Studies are very varied, differing in loading conditions (compression, flexion, rotation, applied forces and moments), spinal segment (whole cervical spine, implants, upper cervical spine, lower cervical spine, or a shorter segment of the lower cervical spine), boundary conditions (ligaments [46], muscles [15] [7] [47], vertebral fixation), the nature of the segment (numerical or experimental), whether the study is in-vivo or in-vitro, what is evaluated (vertebral or disc strain, muscle force, displacement [40] [44], mechanical properties [39]), etc..

In this study, the segment was subjected to an axial compressive force when in the anatomical position. However, the cervical spine has been studied in-vivo during other activities such as during cycling [41], neck flexing when lying down on oneâs back [48] or just simple voluntary isometric contractions [14] and [15].

Maicon Pasini et. al. studied the cervical spine in 9 subjects during cycling (in three different postures) with the objective of estimating internal forces. For this, the image of the sagittal posture of the spine was recorded through filming and the muscle activity of the cervical extensors was registered. Reflexive markers were placed on anatomical points on the head and the cervical spine. One subject was submitted to radiological exam of the head and cervical spine in the sagittal plane with lead markers placed on the same anatomical points of reference. Muscular force was calculated using the inverse dynamics technique. The results demonstrate that muscular strength and the root mean square (RMS) value increase significantly ($p<0.05$) when the cervical spine is more extended and the head is pushed forward [41].

Barton et. al. studied the reliability of a new method for measuring muscular strength, efficiency, and relaxation times of the neck flexor musculature by evaluating healthy adult patient and patients who had unilateral neck pain and headache. In order to do this 20 subjects (10 pain free and healthy: 3 male and 7 female, and 10 pain subjects: 3 male and 7 female) lay supine, and isometrically flexed their necks against a force transducer attached to the back of a webbing and velcro helmet. Electromyograms (EMGs) were recorded from surface electrodes on the stemo-cleidomastoid (SCM) muscles. Two consecutive sessions of five contractions of varying levels of effort from minimal through moderate and maximal effort were analyzed. Results showed that in the control group (10 healthy subjects), the interclass correlation coefficients (ICCs) for the first two maximum neck flexion contractions were: for peak force ICC=0.81; peak force/body weight ICC=0 .75; average force ICC= 0.75; and for force relaxation time ICC=0.73; stemocleidomastoid muscles electromyogram relaxation times: right ICC=0.60 and left ICC=0.67. Comparing sessions 1 and 2 the interclass correlations for stemocleidomastoid muscles efficiencies were right ICC=0.58 and left ICC=0.97.

The peak force registered in the control group was reduced by 50% in the neck pain subjects. Similarly, peak force/body weight in the neck pain subjects was 46% of control group, and average force in the neck pain subjects was 43% of control group. In two neck pain subjects, SCM EMG and force relaxation times were abnormally long in both the affected and the unaffected SCM muscles, exceeding the control values by greater than 3 standard deviations. The difference between the right SCM efficiency of the control subjects and the affected SCM efficiency of the neck pain subjects approached the $p<0.05$ criterion for significance ($p=0.055$). The technique was found to be highly reliable for the measurement of neck flexor peak force, peak force/body weight, average force, and force relaxation time, and moderately reliable for the quantisation of SCM EMG relaxation times and SCM efficiency. All force values were significantly lower in the neck pain population compared with the control group. In the neck pain population, force and SCM EMG relaxation times, as well as efficiencies, suggested abnormalities. Neck pain subjects showed no significant differences in SCM EMG relaxation time or SCM efficiency between affected and unaffected SCM muscles. [48]

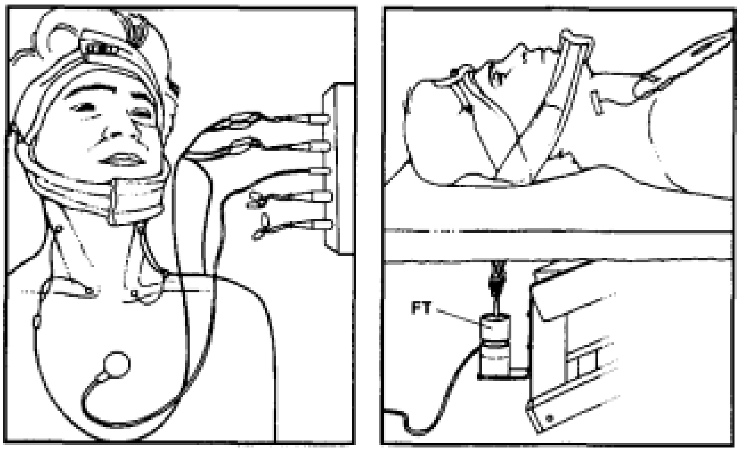

Figure 1.13: Setup for Barton et. al.'s study.
[P. M. Barton, *Neck Flexor Muscle Strength, Efficiency and Relaxation Times in Normal Subjects and Neck Pain and Headache*, 1996]

Hyeonki Choi performed at least two studies regarding neck contractions ("Analysis of Human Neck Loads During Isometric Voluntary Ramp Efforts" [14] and "Quantitative assessment of co-contraction in cervical musculature" [15]). In 2000 he analysed human neck loads during Isometric voluntary ramp efforts in the C4 and C5 vertebrae level. Neck muscle forces and spinal loads at the C4-C5 level that result from isometric voluntary ramp efforts gradually developing to maximums in flexion, extension, left lateral bending and right lateral bending were estimated . Electromyographic (EMG) activities, a three-dimensional anatomic data of the neck and a hybrid model, EMG-assisted optimization (EMGAO) model, were used. The model computed the cervical loads at 25%, 50%, 75%, and 100% of peak moments. The highest model-predicted C4-C5 joint compressive forces occurred during flexion: 361 ($\pm$ 164) N, 811 ($\pm$ 288) N, 1207 ($\pm$ 491) N and 1674 ($\pm$ 319) N in 25%, 50%, 75% and 100% of peak moment respectively. Variations in load distribution among the agonistic muscles and co-contractions of antagonistic muscles were estimated during ramp efforts. Results suggest that higher C4-C5 joint loads, than previously reported, are possible during isometric voluntary muscle contractions. These higher physiological loads at C4-C5 level must be considered possible during orthopaedic reconstruction at this level [14].

In 2006 Sung Kyu Ha et. al. performed a biomechanical analysis of a finite element model of the C3-C6 segment with an elastomer-type prosthetic disc. For this a three-dimensional finite element (FE) model for the multi-level lower cervical spinal segment C3âC6 was developed using computed tomography (CT) data, and applied to study of the effects of the fusion and the artificial disc prosthesis on the biomechanical behaviour of the lower cervical spine. The NURBS computer aided design (CAD) data used in this study for modelling the vertebrae facilitate adding surface patch layouts for seamless attachment of the soft tissues, such as intervertebral discs onto the vertebrae. A FE model was completed by generating mesh out of this geometry. Its accuracy was validated by comparing with previously published experimental and numerical results for the flexion-extension, axial rotation, and lateral bending moments. An implantation of an elastomer-type disc prosthesis or fused graft between C4-C5 vertebrae was considered in the FE model by modifying the intact disc. It is shown that the fusion reduced the mobility at its level by about 50-70% for the considered loading cases [28].

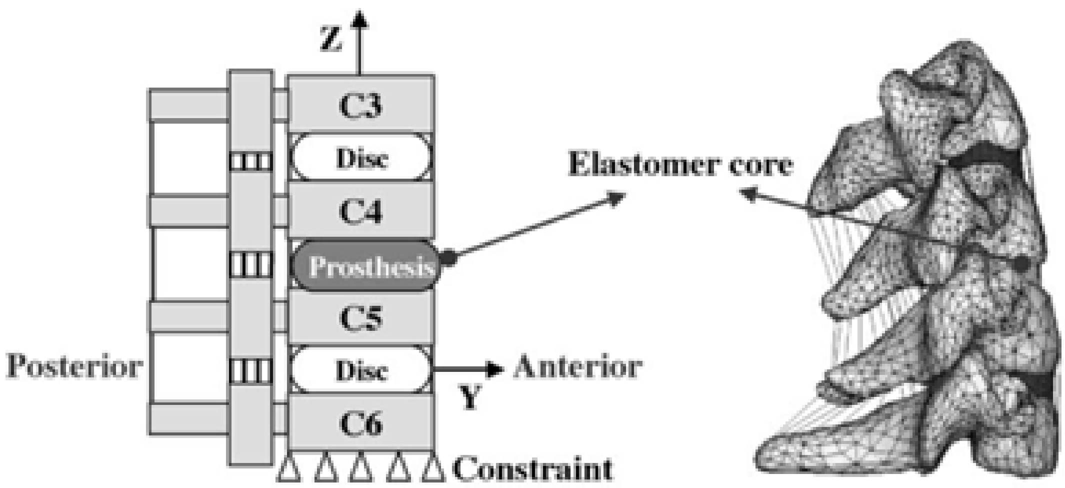

Figure 1.14: Fe model of the C3-C6 segment used in Sung Kyu Ha ‘s study.
[S. K. Ha, *Finite element modeling of multi-level cervical spinal segments (C3âC6) and biomechanical analysis of an elastomer-type prosthetic disc.*, 2006]

Another numerical study of a cervical spine segment was performed by Matthew B. Panzer et. al.. This study was focused on the C4-C5 segment with an accurate representation of each tissue within the segment. This model incorporated more than double the number of elements of existing models until then, required for accurate prediction of response. The most advanced material data available were then incorporated using appropriate non-linear constitutive models to provide accurate predictions of response at physiological levels of loading. This tissue-scale segment model was validated against a wide variety of experimental data including different modes of loading (axial rotation, flexion, extension, lateral bending, and translation), and different load levels (0 to 125 N, 0.3 Nm and 1 Nm). Vertebral Range of motion, ligament deflection and pressure in synovial facet joints was evaluated. In general, the predicted response of the model was within the single standard deviation response corridors for both low and high load levels. Importantly, this model demonstrates that appropriate refinement of the finite element mesh, representation at the tissue level, and sufficiently detailed material properties and constitutive models provide excellent response predictions without calibration of the model to experimental data. [38]

Teo et. al. conducted a numerical study to evaluate the roles of ligaments, facets, and disc nucleus in the transmission of load from superior to inferior vertebral level of human lower cervical spine (C4-C6) using the finite element (FE) approach. Accordingly, a 3-dimensional FE model of the C4-C6 cervical spine, (consisting of 11,187 nodes and 7,730 elements), modelling the bony vertebrae, articulating facets, intervertebral discs, and associated ligaments, was developed and its predicted results were validated against published data under axial compression load configurations. Displacement for the basic model (with all components) was evaluated and was maximum (1 mm) for 800 N. The FE model was further modified accordingly to investigate the role of disc, facets and ligaments in preserving cervical spine motion segment stability under same load configuration. The passive intact FE model predicted the non-linear force displacement response of the human cervical spine, with increasing stiffness at higher loads. For the model without disc nucleus displacement reached 1 mm when applying only a 100 N load [21].

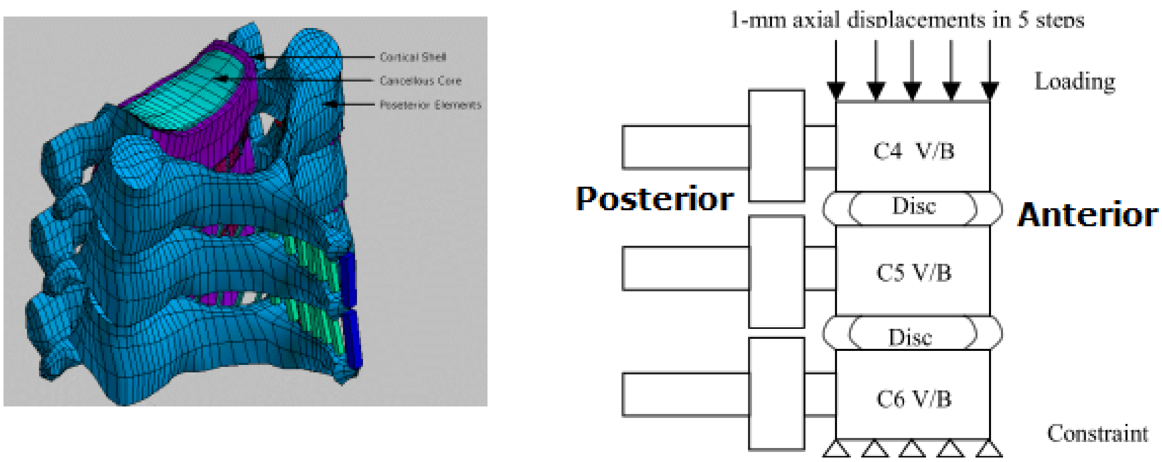

Figure 1.15: Left: C4-C6 FE Model, Right: Loading Configuration.
[E. C. Teo, H. W. Ng, *Evaluation of the role of ligaments, facets and disc nucleus in lower cervical spine under compression and sagittal moments using finite element method*, 2001]

Yoganandan et. al. used 15 human cadaver cervical spines to determine the biomechanics of the human cervical spinal structures under distractive forces. A 'part-to-whole' approach was used in the study. Four experimental models from the 15 unembalmed human cadavers were used to demonstrate the feasibility of the methodology. Structures included isolated cervical spinal cords, intervertebral disc units, skull to T3 preparations, and intact unembalmed human cadavers. Axial tensile forces were applied, and the failure load and distraction were recorded. Stiffness and energy absorbing characteristics were computed. Maximum forces for the spinal cord specimens were the lowest (278 N +/- 90). The forces increased for the intervertebral disc (569 N +/- 54), skull to T3 (1555 N +/- 459), and intact human cadaver (3373N +/- 464) preparations, indicating the load-carrying capacities when additional components are included to the experimental model. The experimental methodologies outlined in the present study provide a basis for further investigation into the mechanism of injury and the clinical applicability of biomechanical parameters [44].

Chapter 2

Clinical Problems Associated to the Cervical Spine

2.1 Introduction

This thesis is based on two cervical spinal surgeries (Arthrodesis and Arthroplasty). As a first approach to cervical spine treatments, different pathologies that affect this portion of the spine were considered in order to better understand when surgery is, or not, considered as a possible treatment for cervical spine illnesses.

Back pain is a common complaint for people of all ages. An estimated 80-90% of people will experience back pain sometime in their lifetimes [45].

Some cases of back injury can be completely healed quite easily (i.e. minor sprains); however just about any injury if not treated properly can lead to more serious problems at a later date. An injury can change the spine's motions and this may be enough to cause "extra" damage to the spine. In addition, throughout a person's life joints tend to degenerate and this is usually associated to pain and/or difficulty in performing certain everyday tasks.

In this chapter some of the most common pathologies of the cervical spine will be listed, and of these the illnesses that lead to surgery will be explained along with corresponding causes and symptoms.

2.2 Pathologies: Causes, Symptoms and some forms of Treatment

As a means to simplify the presentation of cervical spine pathologies, these were divided into 5 different categories:

- **1 - Injuries/Accidents**
- **2 - Degenerative Diseases**
- **3 - Infections/Illnesses/Inflammations**
- **4 - Defects/Deformation**
- **5 - Nerve Dysfunctions**

1 - Injuries/Accidents

- Vertebral Subluxation [36]
  - Spondylolisthesis
  - Retrolisthesis
- Cervical Compression Fracture [49]
- Whiplash [4]
- Torticollis [36]
  - Congenital Torticollis

2 - Degenerative Diseases

- Cervical Spondylosis - Degenerative Spinal Osteoarthritis [36]
  - Cervical Myelopathy
  - Stenosis
- Cervical Disc Disorders [36]
  - Herniated Nucleus Pulposus
  - Degenerative Disc Disease
  - Internal Disc Disruption
- Facet Joints Syndrome [36]
- Cervical Osteoporosis [36]

3 - Infections/Illnesses/Inflammations

- Spondylitis [36]
- Rheumatoid Arthritis [36]
- Spinal Osteomyelitis [13]
- Discitis (disc infections) [13]
- Epidural Abscess (spinal canal infection)
- Cervical Spine Cancer [36]

4 - Defects/Deformation

- Spondylolysis
- Hyperlordosis
- Hyperkyphosis

5 - Nerve Dysfunction

- Cervical Radiculopathy [13]

2.2.1 Cervical Spondylosis - Degenerative Spinal Osteoarthritis

Pathophysiology: Cervical spondylosis is a degenerative disorder of the cervical spine characterized by disk degeneration with disk space narrowing, bone overgrowth producing spurs and ridges and hypertrophy of the facet joints and ligaments which may calcify [52].

Surgical Treatment: Restores intervertebral disc space, by removal of the degenerated disc and insertion of a prosthetic disc in the case of Arthroplasty or a Cage in the case of arthrodesis.

2.2.2 Cervical Stenosis and Myelopathy

Pathophysiology: Cervical stenosis is the name for the actual narrowing of the canal, while cervical myelopathy indicates injury to the spinal cord and its function [56].

Cervical myelopathy is the most serious condition of cervical spondylosis and is the most commonly acquired cause of spinal cord dysfunction among those aged over 55 years; it entails compression of the spinal cord by cartilaginous nodules of degenerated disc material [16].

Figure 2.1: Narrowing of the spinal canal in the cervical spine

.

[Sekhon L. H. S., *The Role for Cervical Arthroplasty for Symptomatic Cervical Stenosis: The Case Against.*,2007]

Surgical Treatment: Removal of the intervertebral disc causing compression to the spinal cord. In this case (intervertebral disc causing spinal cord compression) arthroplasty or arthrodesis may be performed in order to decompress the spinal cord.

2.2.3 Cervical Disc Disorders

- Herniated Nucleus Pulposus
- Degenerative Disc Disease
- Internal Disc Disruption

Pathophysiology: Cervical disc disorders encountered in physiatrist practice include herniated nucleus pulposus (HNP), degenerative disc disease (DDD), and internal disc disruption (IDD). HNP implies extension of disc material beyond the posterior margin of the vertebral body. Most of the herniation is made up of the annulus fibrosus. DDD involves degenerative annular tears, loss of disc height, and nuclear degradation. IDD describes annular fissuring of the disc without external disc deformation [53],[60].

Herniated nucleus pulposus (HNP) can be subdivided into three stages.

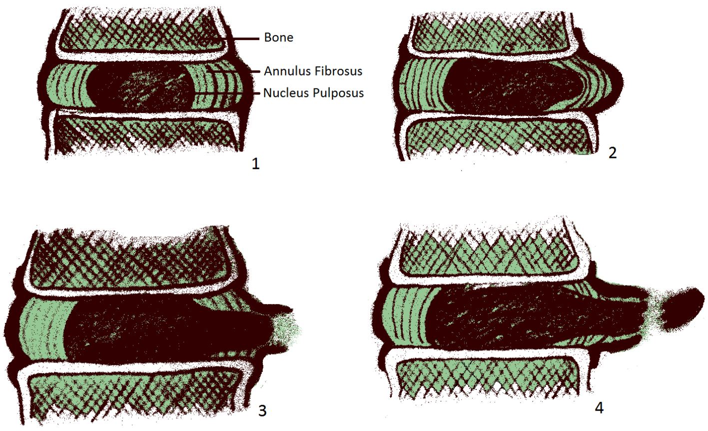

Figure 2.2: Stages of a herniated intervertebral disc.

Figure 2.2 depicts four images that characterize the stages of a herniated intervertebral disc. Classification of a herniated disc: 1- Normal healthy intervertebral disc, 2- Disc protrusion (when the nucleus penetrates the annular fibers without any tissue tearing), 3- Disc extrusion (when the nucleus bursts the annular fibers and goes beyond these), 4- Disc sequestration (when the nucleus starts to fragment, separating itself from the disc altogether)

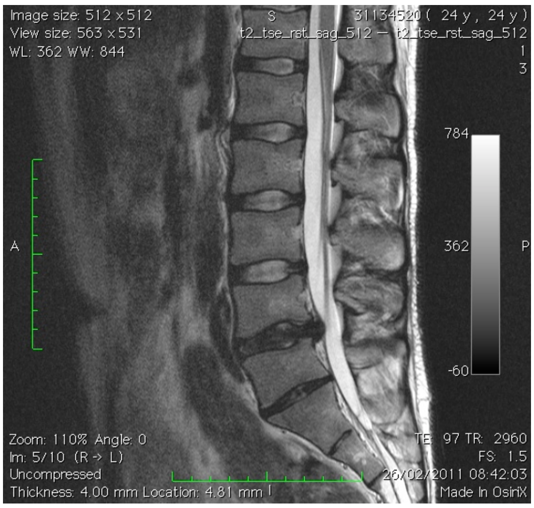

Figure 2.3: Disc protrusion in the lumbar spine - 24 year old male.

Surgical Treatment: When confronted with a disc degeneration illness, surgery is usually the most effective treatment. Disc disorders can easily lead to more problems when they are not treated straight away (i.e. Cervical stenosis). Arthroplasty and/or arthrodesis are usually performed in these cases.

2.2.4 Rheumatoid Arthritis

Pathophysiology: An inflammatory condition that affects synovial joints (most frequent joints in the human body), characterized by a destruction of ligaments, tendons, cartilage, and bone. The cervical spine is composed of multiple small synovial articulations that make it particularly susceptible to RA involvement. The occipitoatlantal (occiput-C1) and atlantoaxial (C1-C2) joints are at high risk because of the extensive presence of synovial tissue in these regions [5].

Surgical Treatment: Spinal fusion is the hallmark of surgical management of the rheumatoid neck. For patients with significant atlantoaxial subluxation, C1-C2 fusion is the procedure of choice [5].

2.2.5 Discitis

Pathophysiology: Infection of the intervertebral disc. Surgical Treatment: Disc removal, arthroplasty or arthrodesis may be performed.

Figure 2.4: Discitis.
[Pradilla, G., Ardila, G. P., Hsu, W., Rigamonti, D.,*Epidural abscesses of the CNS.*, 2009]

Note: It is important to refer that other cervical illnesses may lead to further illnesses, i.e. Disc Herniation may lead to Myelopathy, in which case arthroplasty and arthrodesis are considered as a way of treating the herniated disc and Myelopathy.

There is a wide variety of existing illnesses and accidents that could have various variations of each other so patients must be individually assessed. One may not initially consider surgical treatment such as arthrodesis and arthroplasty but these may well be a solution to allot of different problems associated to the cervical spine.

2.3 Surgical Treatments

Before surgical treatments are discussed it's important to note the existence of non-surgical ones.

There are two main types of treatments for cervical spine disorders: **conservative** and **surgical**. Depending on the illness/disorder it's the orthopaedic doctor's job to ascertain which of these will be most suited.

Conservative treatment is considered a non-invasive procedure, in other words, it doesn't require anaesthesia, being admitted into hospital, etc.; however it is usually a slow and gradual process to recovery. Various resources are used such as: immobilization, specific exercises, pain killers, anti-inflammatories, physiotherapy and chiropractic care.

For those cases where conservative treatment proves unsuccessful, then, most likely, surgery may be the option.

It's important to mention that surgery should only be performed as a **last resort**.

Even though clinical experience and scientific calculations help decrease surgical risks, these should always be taken into account.

It is important to be aware of the fact that the risks involved during a surgery depend a lot on the patient, and therefore most of the risks involved are not due to a possible mistake made by the surgeon. Even though all precautions are taken to avoid complications, there are others that cannot be pre-empted such as infection, haemorrhage, and side effects to the anaesthetic. Other complications directly associated to cervical arthroplasty and arthrodesis are damage to the larynx nerve that may cause a hoarse voice (permanent or not), damage to the nervous roots or spinal cord, that may result in various problems associated to body movement, and also damage to various blood vessels.

Even though synthetic implants are produced in biocompatible[1] materials, the implant may still suffer some extent of rejection by the patient, since the biocompatibility of a material with its environment depends of the interaction between the implant (made of such a material) and its surrounding tissues, as well as other factors, that may vary from one person to another, and also from one region of the body to another.

The biocompatibility of a material for an implant is considered optimal when, firstly, is sustains surrounding tissue growth; and, secondly, when it establishes an interface with its biological surroundings, which is capable of supporting any forces to which that particular area (where the implant is inserted) is exposed.

Even when a material is biocompatible it suffers wear and tear. Although body tissues also suffer wear and tear they have the ability to regenerate, and though such regeneration may be fast or slow, it's never the same wear and tear that an implant is subject to. So implants have to be checked upon, and may need to be substituted (partially or totally depending on their state).

For all these reasons biocompatible materials suffer a constant evolution, therefore different areas of the body have different implants available that last longer.

Usually implants are made of metal or polymeric materials.

Polymeric materials used are usually high density polymers. They are very rigid thermoplastics and usually make up the support structure of the implant.

[1]Biocompatible = compatibility between a material and the environment it is surrounded by.

Metal materials are usually aluminium, stainless steel and titanium.

Aluminium is usually considered as a lighter alternative to steel. It's not as resistant, but usually its resistance is enough to satisfy the implant's force-bearing criteria.

Steel is a very resistant metal, but a heavy one at that. In order to make the most of its resistance, steel may be used to create the structure of the implant instead of the whole of the implant; this way steel is usually coupled with a second material in order to create a lightweight and resistant implant. Titanium is both resistant and light; however it is also an expensive material so usually it isn't used for a whole implant.

Other metallic materials are also used such as titanium alloys, cobalt and chromium.

Healing and Recovery

The healing process is the natural way in which the body repairs damaged tissues. Healing is a natural phenomenon; however if the patient is in good health to begin with, has a healthy diet, gets enough activity and rest, healing will, of course, be easier. Recovery, on the other hand, does require some effort on the patient's side. Recovery does not depend on healing the wounds alone, it also requires some amount of effort and persistence in order to regain physical strength. Some patients may have complete healing of all wounds, but never regain full movement of the operated area (even when surgery is successful).

2.3.1 Arthrodesis

2.3.1.1 Introduction

This section is dedicated to the surgical procedure known as Arthrodesis. Once again, besides a brief explanation regarding the procedure's steps, prosthetic implants will also be mention here along with materials used for their fabrication plus success rates for each of these. Arthrodesis or fusion implies an artificial fixing of one or more articulations.

2.3.1.2 Surgical Procedure

Cervical arthrodesis is a surgical procedure focused on the upper region of the spine. The main purposes of this procedure is relieving pain caused by compression of either nerve roots or the spinal cord, and/or caused by a deteriorated or malfunctioning intervertebral discs.

Cervical arthroplasty involves the fixation of two or more vertebrae. Throughout the years various methods and different types of instruments have been used to establish this fixation: Metal plates, screws, bone grafts and synthetic grafts. The main techniques and implants used for cervical arthrodesis were:

- use of Bone grafts: Autograft if the graft was made of the patient's own bone, extracted from another part of the body, or allograft if the graft was made of a donors bone;

- use of Metal plaque: In this procedure sometimes the disc wasn't removed and a metal plaque was attached to two or more vertebra in order to restrain their movement so as to allow any inflation to heal;

- use of Synthetic graft: Procedure used now a days, in which the disc is substituted for a graft made out of a biocompatible material.

The most commonly used implant at present is the synthetic graft. This graft is usually known as a Cage. Even though this graft is a snynthetic implant, it possesses a hollow centre in order for some of the extracted tissue from the operation to be inserted in the cage and then inserted in the spine.

According to Steven M. Kurtz [57] the use of PEEK cages has expanded as an alternative to autograft alone as well as to plate and screw stabilization

The main reasons the other techniques and implants fell out of use were:

- For the Autograft: when this graft was used surgery took longer, (implying greater blood loss) and another incision had to be made on the body in order to retrieve bone tissue to form the graft.

- For the allograft: since this graft is made of bone from a donner, the patient's risc in the body rejecting the graft increases, leading to other complications.

- For the metal plaque: since this plaque was attached to the vertebra through metal screws this could damage the vertebrae and, once more lead to further problems.

Cervical arthrodesis is associated with a movement restriction regarding the vertebrae involved, and this implies a **biomechanical alteration** of the cervical spine. ADD or Adjoining Disc Disease is a problem that sometimes arises after a patient has been submitted to cervical arthrodesis and is associated to an excess movement of the vertebrae directly above and under the fixed vertebrae in order to compensate the lack of movement of the fixed cervical elements.

During cervical arthrodesis the patient is under a general anaesthetic and the disc is substituted by the cervical cage, thus assuring correct intervertebral high, and decompression of any nerve or even the spinal cord that may be occurring.

The surgeon accesses the cervical area through a small incision on the anterior neck region to then remove the damaged disc and insert the cage. Since the implant is made in of biocompatible material (metal and/or polymeric material) the implants aren't usually rejected by the body.

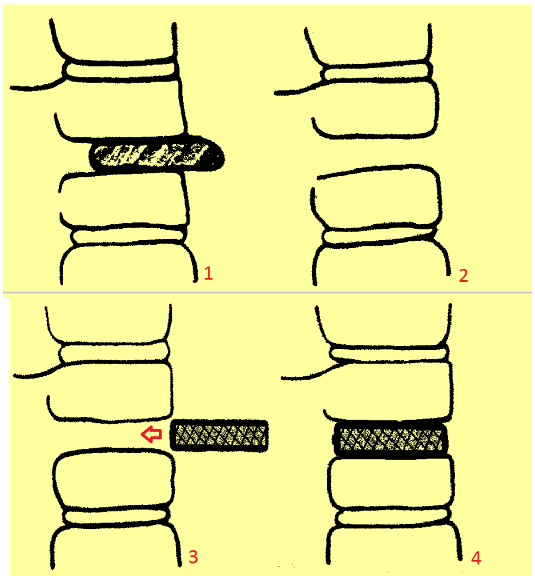

Figure 2.5: Arthrodesis surgical steps.

In figure 2.11 the various steps for cervical arthrodesis have been ilustrated:

- Incision - Surgery is performed with the patient lying on their, a small incision of approximately 3 to 4 cm on the anterior region of the neck is made.
- Exposing and cervical disc removing - After the incision is made, a retractor is used to pull aside neck muscles and other neck components, so as to enable a clear view of the disc that needs to be removed. This disc is then removed (figure 2.11, 1) until the nervous roots and spinal cord are cleared from whatever damage the disc was causing (figure 2.11, 2).
- Widening - Once the disc has been removed the intervertebral space is usually widened slightly in order to regain intervertebral height and also so the surgeon may insert the cervical cage easily.
- Inserting the cage - After the disc has been removed measurements are taken in order to insert a cage with the correct size. The cage is then placed between the vertebrae, where the disc was previously (figure 2.11, 3).
- Wound closure - Vertebrae are then freed and a natural compression of the cage occurs (figure 2.11, 4) and the retractor is removed. The incision is usually then sown up internally (like in plastic surgery) and in most cases the thread used to close up the incision is one that the body absorbs, so as not to require stitch removal.

This procedure is monitored by x-rays, in order to be sure about the exact placement of the prosthetic disc.

2.3.1.3 Surgical Complications

Cervical arthrodesis is now a relatively straightforward surgical procedure. Since the implant's geometry is a simple one it's quite easy to insert. The fact also that the implant is composed of a single piece and doesn't require screws or any further fixing device also simplifies the procedure.

2.3.1.4 Synthetic Grafts - Cervical Cages

Since cervical cages are, at this point, the norm, and since this study is based also on a cervical cage, in this section some cervical cages used in arthrodesis shall be presented.

According to Blumenthal et. al. [55] the first interbody fusion was performed in 1933, an autogenous tibial peg was used to anteriorly treat the lumbar spine of an adolescent with spondylolisthesis.

More or less seven years later the first posterior lumbar interbody fusion was performed (1940s). These early posterior procedures involved packing bone fragments into the disc space after discectomy.

Bagby first described the use of a basket cage (Bagby's Basket) to hold bone graft used for cervical spinal fusion in horses. This concept evolved into threaded fusion cages for use in humans. Other types of cages have also been developed for spinal fusion, such as ringlike cages, rectangular cages, plates connected with struts, tapered cylinders and threaded hollow bone dowels [55].

The first anterior internal cervical fixation device was developed by Bohler in the 1960s, and this was the foundation of the numerous plates available from there onwards [51].

Although anterior cervical instrumentation was initially used in cervical trauma, because of obvious benefits of this instrumentation, indications for its use have expanded over time to degenerative cases, including patients with multilevel decompressions. Due to this expansion a progressive increase in the number of surgeries with anterior cervical arthrodesis and plating has been evident.

Along with increased use of plating systems, implant designs evolved over the last three decades. In the 1970s the 'H' and 'HH' plates' designs appeared and were used throughout Europe in anterior cervical spine surgery. Other designs such as the caspar plate for the cervical spine were created in the 1980s. Some of these plates came in diferent sizes in as much as they could be used for more that one level of fusion.

Early devices required penetration of the posterior cortex of vertebral body (bicortical purchase) and the fear of dural penetration and subsequent neurologic catastrophe delayed acceptance of the use of these devices worldwide, particularly in the United States. The most popular, second generation systems (e.g., CSLP from Synthes, Orion from Sofamor-Danek, Codman plate) featured screws fixed to the implant and permitted screw convergence on placement. The latest, third generation systems are the dynamic semi-constrained plates to prevent stress shielding and to allow subsidence [58].

It's important to stress the fact that these plates were usually combined with the intervertebral graft.

Cervical interbody cages have been developed in hopes of improving on an already highly successful operation. The goals of the interbody device include immediate stability, restoration of the normal sagittal alignment of the cervical spine, elimination of bone grafting, and high fusion rates without supplemental fixation.

Three general structures for interbody devices have been developed. Horizontal cylinders (figure 2.6), vertical rings (figure 2.7), and open boxes based on the tricortical graft are commonly used interbody devices. Although many comparative animal, clinical, and biomechanical studies are available on interbody fusion cages the literature remains sparse in their application to the cervical spine. The most extensively studied clinically have been the threaded cylindrical interbody cervical cages [59].

Figure 2.6: BAK/C cage image.
[Yu, W. D., Tripuraneni, K. R.,*Cervical Interbody Cage Fusions.*, 2004]

A study of this metal cage (BAK/C) in the cervical spine was performed and surgical outcomes with the use of this cage (group 1) were compared to patients submitted to arthrodesis with the use of bone grafts (autograft or allograft), (group 2).

Complications in group 2 were 20.4% compared with 11.8% in group 1. This difference was mainly due to graft collapse or failure and incisional problems.

At 12 months, BAK/C cage group had a significantly higher rate of fusion (97.9%) compared with the bone graft group (89.7%).

Hacker reported on 54 patients comparing iliac bone graft and BAK/C cages in one and two-level anterior cervical fusions. For single levels, the fusion rate was 100% in the BAK/C group and 93% in the autograft group [59].

Whitecloud reported on 20 patients using a vertical ring titanium surgical mesh interbody device packed with harvested bony tissue. Successful fusion rates were observed (92%) with 85% having good or excellent clinical results [59].

Figure 2.7: Example of two vertical ring cages of different sizes.
[Yu, W. D., Tripuraneni, K. R.,*Cervical Interbody Cage Fusions.*, 2004]

Historically, spinal fusion instrumentation was fabricated from metallic biomaterials, including stainless steel and titanium alloy, because of their strength and fatigue resistance.

However, one key drawback of these metallic implants is incompatibility with diagnostic imaging, including MRI and CT scans, which are crucial for visualizing changes to the spinal cord and vital soft tissue structures of the spine. Laboratory studies during the 1990s confirmed that PEEK (polyetheretherketone) implants had the requisite combination of strength, wear, creep and fatigue resistance to replace metallic biomaterials for spine implants [57].

In 1999 the first cervical cage made out of a material other than metal was created. This material was PEEK [57].

Cervical PEEK cages are relatively new and not many different modes have yet available, however the Solis PEEK cage (figures 2.9 and 2.10) has been used in a number of cases and some studies are available. Information on other PEEK cages such as the Vista-S and the Fidji (figure 2.8) cages is scarce and no studies were found regarding these cages. These three cages share more or less the same geometry, they are ring like objects (so that bony tissue may be inserted in its centre for better ossification - see figure 2.9) and have several fissures on its top and bottom surface that prevents the cage from sliding about on the vertebrae. These cages are made available by companies such as Zimmer Spine Corporate and Abbott Spine.

Figure 2.8: Fidji Cervical Cage.
[The Art & Science of Spine Surgery, *Fidji Cervical Interbody Fusion System - Abbott Spine*,2006]

According to a study done by Dr. N. Oblu [10] 29 patients with radiculopalthy underwent cervical arthrodesis with the Solis PEEK cage and after a one year all of them had improved and returned to their respective jobs successfully.

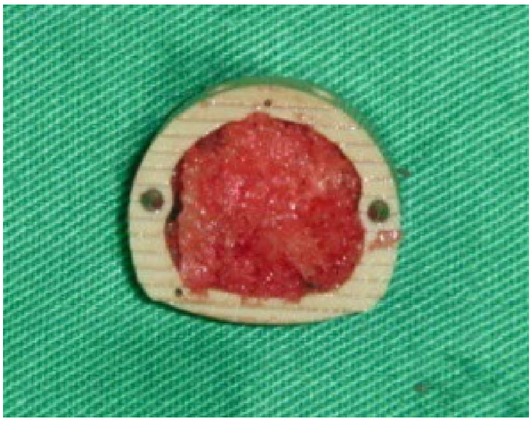

Figure 2.9: Solis Cage filled with cancelous bone.
[Popescue, C. E., Muller, J., Costachescu, B.,*1 Year Experience with Solis PEEK cages in cervical disectomy and fusion.*, 2010]

Figure 2.10: Solis PEEK cage.
[Popescue, C. E., Muller, J., Costachescu, B.,*1 Year Experience with solis PEEK cages in cervical disectomy and fusion.*, 2010]

The fusion rate seems to be superior to the autologus bone graft application. In this study no cage migration or breakage was observed and only one case of subsidence occurred. No plate fixation was used and it was suggested that the cage's bottom pins are enough to keep the cage in the disc space. Oblu stated that in these last years there has been a growing trend in the implantation of the cage device for cervical interbody fusion [10].

Currently it seems to be accepted that there is no universally accepted anterior cervical disectomy and fusion method nor that the ideal implant has been found.

Hopefully in the near future study outcomes will be published on the Fidgi and other similar cages in order to give way to other cervical cage models in order to obtain even better results in cervical arthrodesis.

2.3.2 Arthroplasty

2.3.2.1 Introduction

This section is dedicated to the surgical procedure known as Arthroplasty. Once again, besides a brief explanation regarding the procedure's steps, prosthetic implants will also be mention here along with materials used for their fabrication plus success rates for each of these.

2.3.2.2 Surgical Procedure

Cervical arthrodesis is a surgical procedure focused on the upper region of the spine. The main purposes of this procedure is relieving pain caused by compression of either nerve roots or the spinal cord, and/or caused by a deteriorated or malfunctioning intervertebral discs.

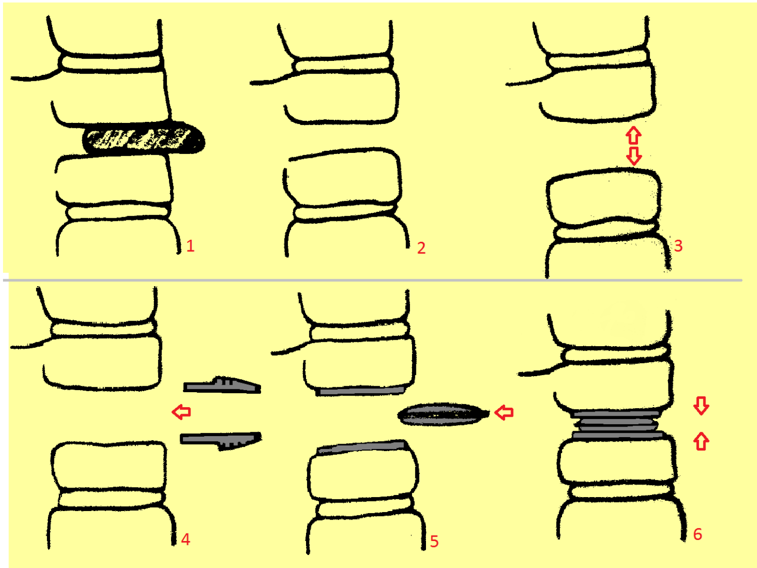

Figure 2.11: Arthroplasty surgical steps.

In figure 2.11 the various steps for cervical arthroplasty have been illustrated:

- Incision - Surgery is performed with the patient lying on their back, a small incision with approximately 3 to 4 cm on the anterior region of the neck is made.

- Exposing and cervical disc removing - After the incision is made, a retractor is used to pull aside neck muscles and other neck components, so as to enable a clear view of the disc that needs to be removed. This disc is then removed (figure 2.11, 1) until the nervous roots and spinal cord are cleared from whatever damage the disc was causing (figure 2.11, 2).

- Widening - Once the disc has been removed the intervertebral space is usually widened slightly in order to regain intervertebral height and also so the surgeon may insert the cervical prosthetic disc easily (figure 2.11, 3).

- Inserting the prosthetic disc - After the intervertebral disc has been removed measurements are taken in order to insert a prosthetic disc with the correct size. The prosthetic disc is then placed between the vertebrae, where the intervertebral disc was previously (figure 2.11, 4 and 5).

- Wound closure - Vertebrae are then freed and a natural compression of the prosthetic disc occurs (figure 2.11, 6) and the retractor is removed. The incision is usually then sown up internally (like in plastic surgery) and in most cases the thread used to close up the incision is one that the body absorbs, so as not to require stitch removal.

This procedure is also monitored by x-rays, in order to be sure about the exact placement of the prosthetic disc.

2.3.2.3 Surgical Complications

Cervical arthroplasty is more challenging to perform than arthrodesis. Usually the prosthetic disc is made up of more than one piece, thus complicating the insertion process. Prosthetic discs usually have fin like structures on it's upper and lower surfaces so as to insure short term fixation, this means that the surgeon very often must remove more vertebral bone than that removed for the insertion of a cervical cage. This bone removal may also be a challenge to a surgeon who may not be used to performing arthroplasties.

2.3.3 Prosthetic discs

This section addresses main cervical implants used in arthroplasty. Implants for this surgery will be mentioned chronologically.

The first arthroplasty was performed by Dr. Ulf Fernsotröm in Sweden in 1957 [26]. This arthroplasty consisted in the insertion of a stainless steel sphere in place of the intervertebral disc. The spheres were produced with different diameters in order to maintain intervertebral height from one patient to another.

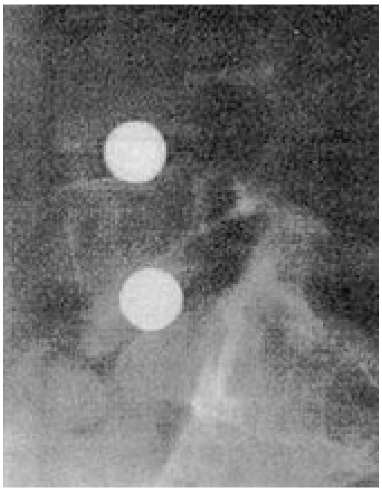

Figure 2.12: Fernstrom's implanted steel ball.
[Bono, C. M., Garfin, S. R.,*History and evolution of disc replacement.*, 2004]

This implant failed mainly due to the fact that the sphere was only touching each of the two vertebrae at only one point. From a medical point of view this isn't very important; however, from a mechanical point of view it is crucial. The area where the vertebra contacted with the intervertebral disc had been reduced to a single point. Movement transmission and range was altered significantly causing problems to the patients who had undergone this procedure. In time the bone could succumb and the steel balls subside. Intervertebral height restoration was lost in about 88% of cases at 4 to 7 year follow-ups. The sheer forces produced at the metal-bone interface were most likely a contributing factor [11]. Even though Fernstrom's sphere wasn't a very successful solution it made way for a sequence of alternatives that lead to the current prosthetic discs witch are a lot more reliable nowadays.

Prosthetic disc evolution has been a slow albeit progressive process due to the fact that this device is restricted in its size; must perform the same function as the disc; must be produced in a biocompatible material; and surgery that ensures the prosthetic discs' insertion must be feasible since it's to be placed so closely to the spinal cord.

For over 20 years no prosthetic disc design seemed to fulfil the necessary requirements. In the 1980s two new devices were developed: the SB Charité and the ProDisc. The novelty of these designs was the introduction of synthetic-on-synthetic articulating surfaces. It was designed by Shellnack and Büuttner-Janz. This device consisted of a sliding core of ultra-high-molecular-weight polyethylene (UHMWPE) between two endplates produced in a cobalt-chromium-molybdenum (CoCrMo) alloy; in order to induce osseointegration the endplates were coated with a titanium layer [11].

Figure 2.13: Assembled and component views of the current SB Charité III disc replacement device.
[Bono, C. M., Garfin, S. R.,*History and evolution of disc replacement.*, 2004]

The SB Charité still suffered some changes that lead to the third and current version of the disc (SB Charité III) in 1987 [11]. There are hardly any studies done on this prosthesis for the cervical spine since this version of this prosthesis only appeared much later. However, quite a lot of studies have been done regarding the Charité lumbar spine prosthesis. As far as the lumbar spine is concerned a study showed that the complication rate, as a result of disc migration or dislocation and device failure, was 6.5%. Forty-six patients with the SB Charité III disc were studied a mean of 3.2 years after implantation: 63% reported satisfactory results. The success rate was 69% in patients who underwent isolated disc replacement and 77% in patients who had undergone previous back surgery. Two patients had the prosthesis removed. Seven patients underwent posterolateral fusion without removal of the device [42].

In the late 1980s after the SB Charité III, the ProDisc prosthetic disc emerged. The ProDisc was developed by Marnay and it was composed of two metal end plates [11]. Both end plates possess a finlike protrusion that enables fixation during surgery. This disc made way for the ProDisc-C specifically for the cervical spine in 2002. The ProDisc-C has a polyethylene core fixed (unlike the SB Charité III) to the inferior endplate.

The ProDisc-C cervical disc is a metal-on-polyethylene articulating device (see figure 2.14). This modular implant consists of two cobalt-chromium-molybdenum endplates and an ultra-high molecular weight polyethylene (UHMWPE) inlay. The endplates of the prosthesis are initially secured to the vertebral bodies with central keels, and they have a plasma-sprayed titanium coating for long-term fixation stability. The UHMWPE inlay is pre-assembled into the inferior endplate [43].

Figure 2.14: ProDisc-C disc.
[McKhann, G. M., *Clinical Neurosurgery: A Publication of the Congress of Neurological Surgeons.*, 2006]

A study with 209 patients was performed by Rick B. Delamarter et. al. [18] with insertion of the ProDisc-C and overall results for a two year period were positive, and at least as successful, if not more so, than cervical fusion. Results over a long period of time have not yet been obtained with most recent cervical prosthetic discs, precisely because they are recent devices.

In a study done by Daniel Murrey et. al. 103 patients were studied and subjected to cervical arthroplasty with the ProDisc-C. Outcomes were good after 2 years with a success rate of 98%. The most common treated level was C5-C6 [18].

In 1991 the Cummins prosthetic disc emerged in Bristol (UK). This implant was composed of only two pieces (ball-and-socket design) and was produced in 316L stainless steel. Both pieces are fixed to the anterior side of the vertebrae with the use of screws. The upper piece has a convex inferior side, whilst the inferior piece supports the upper piece with a concave upper side (figure 2.15).

This disc suffered various alterations, one in 1998, another in 1999 and, finally, one in 2000. This latter disc is known as the Prestige Disc. The Cummins disc proved itself unreliable when it was discovered that the prosthetics' disc height was greater than the intervertebral disc's. The fact that this disc was fixed to the vertebra through screws made surgery a complicated and fiddly process [26].

The Cummins/Bristol disc was implanted in 26 patients and clinical outcomes were good in a 2.4 year follow up. However, and unfortunately, the stainless steel devices may have suffered from a production error since there were five cases of hardware failure, one of which required surgical revision [42].

As the Cummins disc was being developed, the Cervidisc was designed in 1999 and implanted by Aymen Ramadan. The materials used in Cervidisc are a combination of titanium endplates bearing zirconia ceramic gliding surfaces. Eleven cases of subsidence out of 50 implants were registered and alterations were made. After these alterations there was improvement. Short term fixation of the Cervidisc is guaranteed by segments of triangular rims that can be observed in figure 2.16

Figure 2.15: Lateral and anterior views of the Cummins/Bristol disc.
[Gerber, M. S., Galler, R. M., Papadopoulos, S. M.,*Spinal Disk Arthroplasty.*, 2003]

whilst long term fixation is guaranteed by a coating of hydroxypatite to encourage bone growth. As with the Prestige the Cervidiscs' range of motion is limited by metal rims around the ceramic joint components. Various sizes are available for this disc model [26].

Figure 2.16: Cervidisc.
[Link, H. D., McAfee, P. C., Pimenta, L.,*Choosing a cervical disc replacement.*, 2004]

The Bryan cervical disc was created just before the year 2000. It's a device manufactured in polyurethane and titanium. The titanium makes up the upper and lower surfaces, whilst the polyurethane makes up the centre of the implant. Polyurethane was selected over polyethylene since theoretically it has a greater capacity for shock absorption. It was the first non metal on metal disc to be produced. It is available in five different sizes, but only in one height. In January of the year 2000 it was first implanted in Europe. It is the most restricted prosthetic disc implant in terms of motion range. A study on 63 patients was performed by Jan Goffin et. al [31], that showed good results after four years. Over 50% of patients showed excellent results and only one case was unsuccessful, proving that the Bryan disc might be a good solution for some cases. A longer patient follow-up would be necessary to confirm these facts.

Figure 2.17: Bryan cervical disc.
[McKhann, G. M., *Clinical Neurosurgery: A Publication of the Congress of Neurological Surgeons.*, 2006]

In the year 2002 the Porous Coated Motion (PCM) disc was first implanted. Even though the PCM disc is composed of cobalt-chromium alloy and polyethylene it is inserted as a single piece. It is available in three different sizes and two different heights. The polyethylene centre is responsible for maintaining intervertebral movement. Its initial fixation is done with anterior flanges and posterior screws [26].

Pimenta and coworkers [37] presented 2-year follow-up data for an ongoing PCM arthroplasty trial. Fifty-three women and thirty-four men, with a mean age of 57 years,were evaluated (post-operatively) every 3 months for a period of 24 months.

Figure 2.18: Porous Coated Motion (PCM) disc.
[McKhann, G. M., *Clinical Neurosurgery: A Publication of the Congress of Neurological Surgeons.*, 2006]

The mean clinical values were favourable after 2 years. In this study the NDI scale was considered in order to evaluate patient outcome.

The NDI consists of 10 items, each with a score up to 5, for a total score of 50. The lower the score, the less self-rated disability. Dr. Vernon established the following guide to interpretation of a patient's score [27]:

- 0 - 4 = No disability
- 5 - 14 = Mild disability
- 15 - 24 = Moderate disability
- 25 - 34 = Severe disability
- 35 or over = Complete disability

The mean preoperative NDI value was 45, becoming 28.4 at one week follow-up, 21.85 at one month, and the final score at the follow-up at two years was 24.1 [37].

In 2002 the Prestige disc was developed from the Cummins/Bristol disc and is now produced in 6 different sizes.

Like the ProDisc and SB Charité, the Bryan Total Cervical Disc also had an articulating core. However, it was made of polyurethane rather than PE (polyethylene) since, polyurethane is considered to have greater shock absorbing capability. This might be considered a small forward step on the evolutionary scale of total disc replacements [11]. Its long-term fixation is guaranteed by triangular fins (see figure 2.19), thus solving the Cummins discs' problems. This disc's range of motion is limited within the coupling borders, so as to prevent excessive motion.

Wigfield and coworkers [9] concluded that motion was successfully preserved after 2 years, as all patients radiographically demonstrated motion within an appropriate physiologic range and that prosthetic disc stability was confirmed since none of them had dislocated.

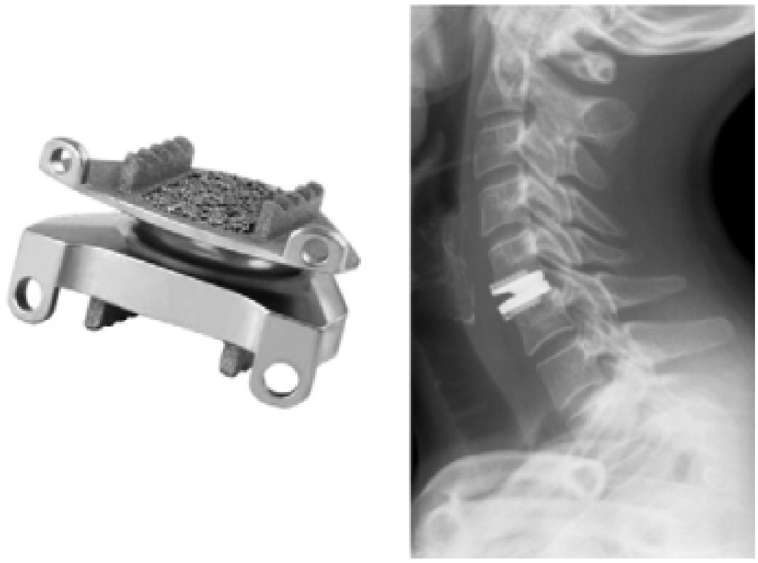

Figure 2.19: Isolated and implanted PRESTIGE LP Cervical Disc.
[Smucker, J. D., Sasso, R. C.,*Cervical Disc Replacement: The State of the Data. Seminars in Spine Surgery*, 2006]

Thanks to all the past designs and studies in 2004 a new generation of prosthetic discs began with the Mobi-C disc. This prosthetic disc is made of a UHMWPE (ultra high molecular weight polyethylene) layer between two metal base plates. The movement is limited by two lateral stops both on the top plate and on the bottom plate visible in figure 2.20.

Short-term fixation is guaranteed once again by the fins on the upper and lower disc plates.

A study was performed on 65 patients, 21 were submitted to anterior cervical disectomy and fusion whilst the remaining 44 were implanted with the Mobi-C disc. Patients were observed 3, 6, 12 and 18 months after surgery. Even though surgery time was less for cervical fusion, resulting data favoured the Mobi-C prosthesis with regards to severity of dysphagia, return to work status and patient satisfaction. The long-term success of the Mobi-C disc arthroplasty procedure will depend on further investigation [50].

In 2005 more models for cervical implants appeared, mainly the Secure-C and the Kineflex cervical disc.

The SECURE-C consists of two cobalt-chrome alloy endplates that are secured to the top and bottom surfaces of vertebrae and have an ultra-high-molecular-weight polyethylene core that fits

Figure 2.20: Mobi-C prosthetic cervical disc.
[Villavicencio, A. T., Burneikiene, S., Pashman, R., Johnson, J. P.,*Spinal Artificial Disc Replacement: Cervical Arthroplasty: Part II: Indications, Surgical Technique, and Complications.*, 2007]

between the two plates. The design of the Secure-C disc aims to simplify the insertion technique of artificial discs in the cervical region [30].

Figure 2.21: Secure-C disc.
[Goldstein, J. A., Sharan, A. D.,*Cervical Artificial Disc Replacement Technologies*, 2006]

A study performed by Joseph Marzluff, Jason Highsmith and Kelly Baker [32] on 5 patients showed that a year after they had been treated with the Secure-C disc not only were they all pain free but also that symptoms had subsided. A longer follow-up of these patients would be required (over 3 years) for there to be any conclusions about long-term feasibility of this prosthetic disc.

The Kineflex cervical disc is a metal on metal disc with a semiconstrainted core.

The Kineflex-C is a 3-piece modular design consisting of two cobalt chrome molybdenum (CCM) endplates and a CCM core that allows certain movements such as translation during flexion-extension, lateral bending, and axial rotation. Movement of the disc is allowed within limits, since these are restricted by a retention ring. The theory behind the metal-on-metal design is that it should last longer than other materials [30].

This disc along with others such as the Discover-C, CerviCore, Cerpass or the M6 cervical discs are still being studied and some have even been implanted. However, results regarding these prosthetic discs are still to be obtained, and conclusions to be drawn.

Chapter 3

Finite Element Models of Segments C4-C6 and C5-C6

3.1 Introduction

In this chapter the whole construction process of the various finite element models will be explained. In addition to a brief explanation of Computer Tomography (CT) and the Finite Element Method (FEM), this chapter will also cover 3D bone models and the material properties that were used.

Due to the fact that the geometry of the studied segments is a complex one, numeric models were created so that they could then be submitted to a numeric computational technique so as to obtain stress-strain levels. The purpose of determining maximum and minimum stress-strain levels, was that this would clarify when the structural integrity of the studied structures (C4-C6 segments) were in jeopardy.

3.2 Materials and Methods

As previously mentioned, the point of this project was to study the mechanical alterations caused by two cervical spine surgeries, cervical arthroplasty and arthrodesis. For this purpose three different main situations were compared: Native Model, implanted ProDisc-C Model and implanted Fidji Cage Model.

Later on in this study experimental models were also created and studied, the experimental studied segment was the C5-C6 segment. For the validation of the numerical models (segment C4-C6) other numerical models, referred to as the Numerical Foam Models (since the material associated to the vertebrae was polyurethane rigid foam), of the C5-C6 segment were created so as to compare with experimental results. However, throughout most of this chapter the main focus is on the C4-C6 segment.

A representation of the C4-C6 segment models may be seen in figure 3.1.

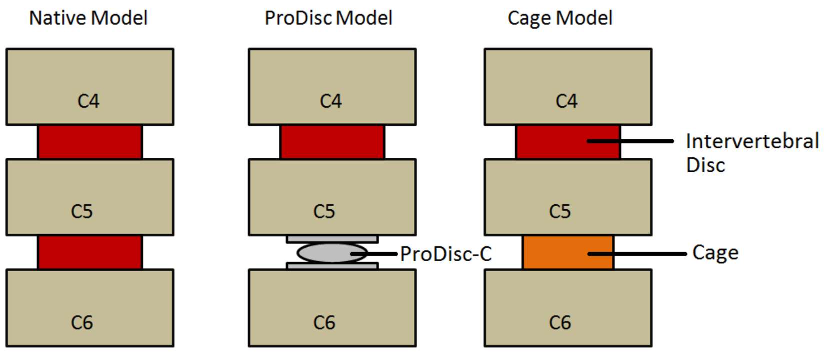

Figure 3.1: Studied C4-C6 segment models: simplified illustration.

Four main models were created for the study of the C4-C6 segment, and three of the C5-C6 segment, and for simulation purposes, more than one scenario was fashioned for some of these cases. These different models were:

1^{st}st - Native C4-C6 segment model created for simulation using MSC Marc Mentat program. This model will be referred to as the **Specific Patient Native Model**;

2^{nd} - Native C4-C6 segment model created for simulation using CAD software - CATIA - Dassault Systémes. This model will be referred to as the **Discretized Patient Native Model**.

3^{rd} - C4-C6 segment model with a cervical prosthetic disc between vertebrae C5 and C6. The prosthetic disc used in this study was the ProDisc-C. This model will be, from here on after, referred to as the **Discretized Patient ProDisc-C Model**.

4^{th} - C4-C6 segment model with a cervical cage between vertebrae C5 and C6. The cage used in this study was the cervical Fidji PEEK cage. This model will be referred to as the **Discretized Patient Cage Model**.

5^{th} - C5-C6 segment model with an intervertebral disc but instead of bone material properties those of Polyurethane Rigid Foam (PUR) were used. This model will be referred to as the **Numerical Foam Native Model**.

6^{th} - C5-C6 segment model with a cervical cage (Fidji PEEK cage) between vertebrae C5 and C6, with Polyurethane Rigid Foam (PUR) material properties for the vertebrae. This model will be referred to as the **Numerical Foam Cage Model**.

7^{th} - C5-C6 segment model with the ProDisc-C between vertebrae C5 and C6, with Polyurethane Rigid Foam (PUR) material properties for the vertebrae. This last model will be referred to as the **Numerical Foam ProDisc-C Model**.

All these models were created from CT images and converted into models with the use of Simpleware ScanIP software.

In figure 3.2 a simplified diagram is shown of the different models that were studied.

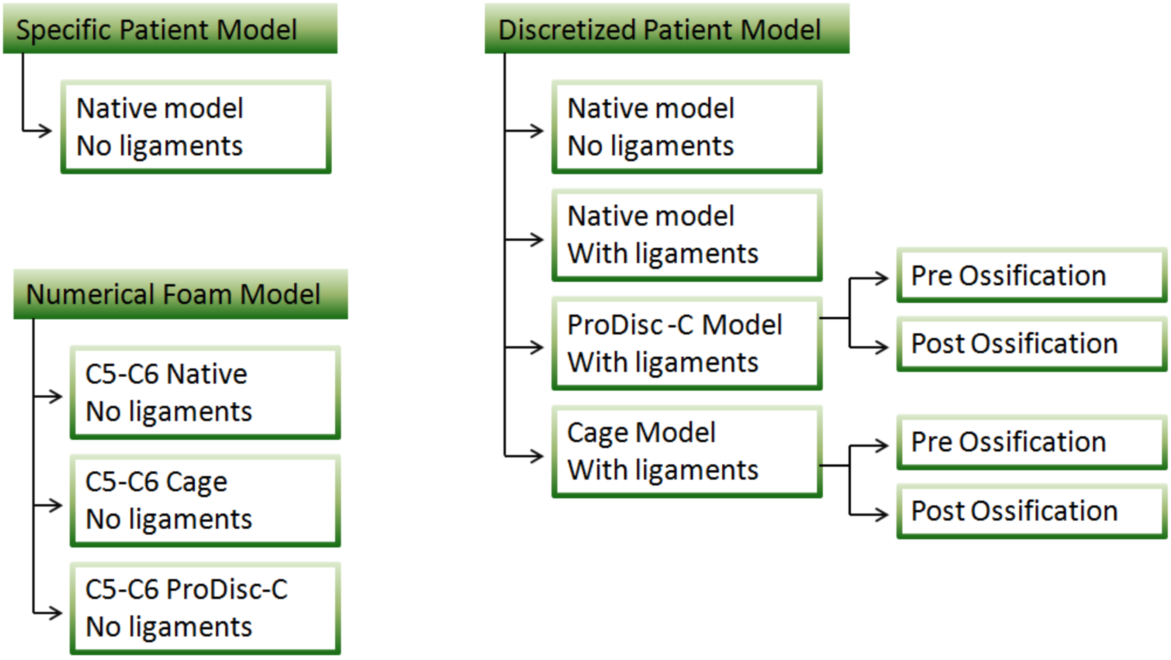

Figure 3.2: Diagram of all numerical studied models.

3.2.1 Computer Axial Tomography

For this study the models were created from CT images. These images were obtained from a computed tomography center in Aveiro, Portugal: CENTAC, (Centro de Tomografia Computorizada de Aveiro LDA.). The images provided were the result of a CAT (Computer Axial Tomography) scan performed on a male patient's spine.

Computer Axial Tomography is widely used nowadays for a comprehensive variety of things. It is used mainly for obtaining information concerning the geometry of internal structures of a greater body. This makes Computer Axial Tomography a non-invasive technology since it is used instead of having to destroy the outer layer surrounding the components one may wish to study. For this reason Computer Axial Tomography is mostly used for the study of living/breathing creatures. A CT image (figure 3.3) is the result of a Computer Axial Tomography 2D scan.

The end result of the CAT-Scan is but a succession of radiographies of different portions of the cervical spine. These scans are then converted by a computer into the so-called tomographic slices (a slice/image for every scan). With the use of appropriate software all these images are then stacked onto each other to create a 3D model of the scanned internal structures of the cervical spine area. Every scan had a spacing of 0.5 mm in relation to the next one. Bigger spacing is usually used, however the smaller the spacing the greater the detail of the final model.

3.2.2 Finite Element Method

Currently numerical methods are practically a necessity when it comes to solving engineering related problems.

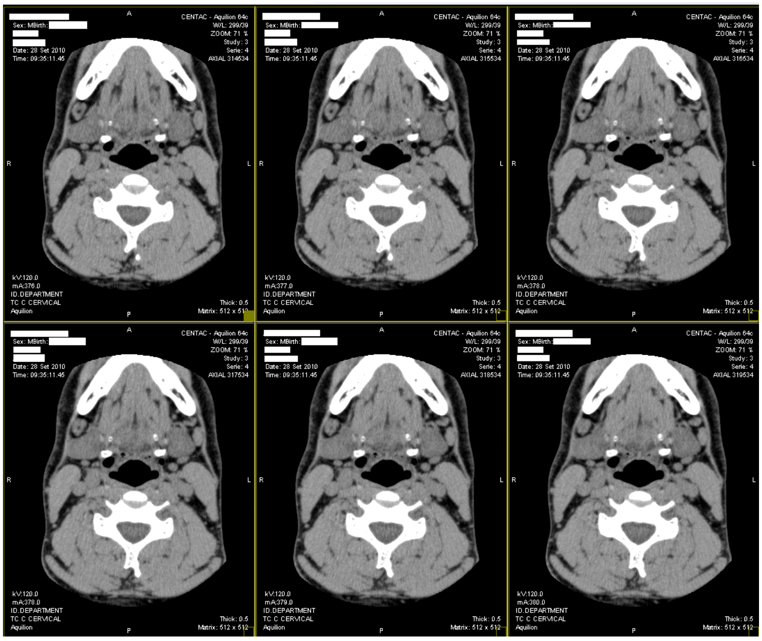

Figure 3.3: Example of CT images.

The Finite Element Method (FEM) is a numerical computational technique developed originally as a means to obtain stress-strain levels in complex problems that usually entail more than one structure. For this reason, it has been widely used in numerous engineering studies, and biomechanics is no exception.

There are many studies that use the FEM essentially due to the clinical need to determine the stress and strain levels on bony tissues alone or bone and implant systems that are subjected to different forces.

One of the main advantages of the FEM is its ability to predict the behaviour of a given system.

However, in order to predict this behaviour it is necessary to be able to replicate the entire system, otherwise results either won't be valid or they will, at the very least, have quite a large margin of error.

When applying the FEM, the studied system is divided into a number of smaller areas or volumes, called finite elements. This step, in which the system is broken down into elements, is known as discretization.

The union of all these finite elements creates the finite element mesh. This mesh should be created in order to maximize the alignment of all elements to the object which was discretized, so that the mesh will look as much as the initial object as possible.

In a linear elastic analysis, the first quantity to be determined by the FEM is usually the displacement of a finite number of points in the system. These points are vertices of the elements, and are called nodes. Once the nodal displacement is determined, the corresponding deformation for each node is calculated and from this deformation the final stress/strain state of each node is calculated.

Nowadays, specific programs exist for the automatic generation of these meshes. Usually these programs are the same ones that generate FEM solutions for the given problem.

These programs can usually create meshes with different sized elements; in other words, for a given structure one may define the element size for the whole mesh. The smaller the element size, the closer the mesh is to the initial geometry of the object.

Nevertheless, the use of meshes that may coincide with the smallest detail on the meshed object is not sufficient for obtaining results with no error whatsoever. The main disadvantage of a very small element size is that this goes hand in hand with greater computational time and the need for a computer with allot of memory in order for the program to be able to compute and store results. It's important to be aware of the fact that even with the ability to generate results with the smallest of element sizes these may not be "perfect" results, since there is some error associated to each element and therefore the more the elements the bigger this error becomes. Thus, depending on the problem at hand the appropriate element size should be carefully determined, since this is crucial for obtaining valid results.

The main reason for the development of finite element models in this study was to be able to investigate various biomechanical aspects, such as stress/strain and deformation levels, between the various components entailed in cervical arthrodesis and arthroplasty which would be difficult, if not impossible, to determine otherwise (i.e. in-vitro studies).

3.2.2.1 Inicial Modeling Considerations

Before the explanation on the creation of the models starts it's important to understand the concept of Grey Scale. In this case a grey scale is a list of all the different grey tones (Hounsfield Units - HU) captured in the CT image (one grey value for each different toned pixel). The CT image is really nothing more than a capture of the different densities inside the body. Since, for example, bone density is higher than muscle density, these two tissues show up on the image in different grey tones.

As mentioned, CT images (DICOM format) were imported into the ScanIP program. Right after the images were imported, the available ScanIP "bone" option was selected in order for the program to automatically associate the images' grey scale to different bone densities.

After setting the "bone" condition in ScanIP, a threshold filter was applied on all the imported images. Since bone tissue shows up on the images as being the white areas, and since threshold values go from 0 (black) to 255 (white), a threshold interval with high values was chosen in order to create a mask that would encompass all bone tissue. It's important to refer the fact that image's grey tones go from 0 to 255, but that the default ScanIP HU scale for bone tissue goes from -700 to 1300, so the image's grey tone that corresponds to 0(black) will be associated to the HU value of -700, and the image's grey tone that corresponds to 255(white) will be associated to the HU value of 1300. Another consideration is that not all the HU values (ranging from -700 to 1300) will be present on the created mask. It's very unlikely that there will be any values with HU values below 40 present in the bone mask (since trabecular bone is associated to darker grey colored pixels that don't go below the value of 40 HU [22]).

Once this mask was created (HU interval of [107;1300]) it was possible to preview a 3D view off this mask (figure 3.4). Since the threshold interval usually captures more than just the bone one intends to create a model from, parts of the mask were added or removed with the use of the commands Paint and Unpaint respectively, slice by slice, to create a model of each necessary bone; this can be observed in figure 3.5.

During this process the program user must be very aware of the geometry of the bone being modelled, since one is dealing directly with horizontal sections (2D images) of the bone, in order for the end result to be a 3D model. ScanIP did have the ability to show a plane that corresponded to the slice on the 3D preview model, thus making it slightly easier to know which parts of what vertebrae were on that slice. Figure 3.7 shows the CT image on the right, and on the left a

Figure 3.4: Fist filter application: Threshold.

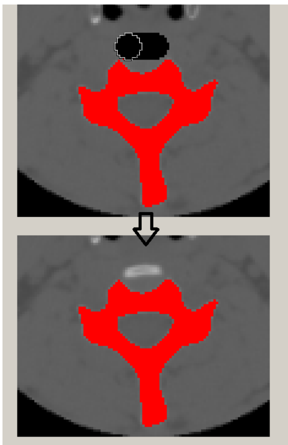

Figure 3.5: "Unpaiting" what doesn't belong to the required vertebra.

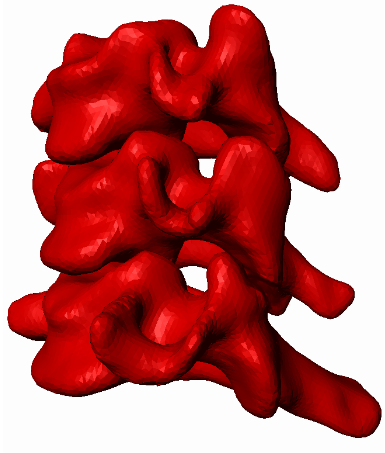

Figure 3.6: Cleaned final mask containing the three vertebrae.

preview of the 3D model with a plane indicating the whereabouts of the slice; in this case the plane corresponds to the slice that intersects vertebrae C5 and C6.

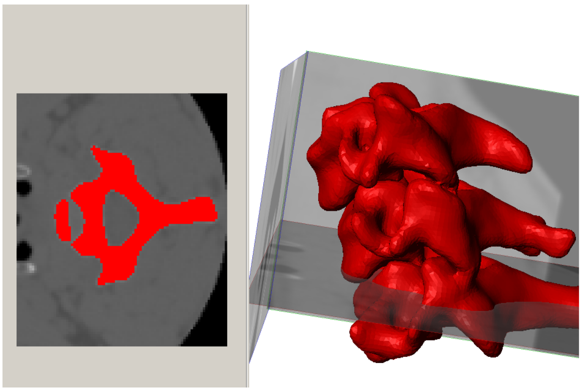

Figure 3.7: On the left slice image, on the right 3D model.

Initially this study was to be based on different numerical models (native model, prosthetic model and cage model) all simulated using MSC Mark Mentat software. However, due to computational difficulties, and after thoroughly and exhaustively exploring every single permutation thought possible so as to try and solve the computational problems, it was decided that the only model that was to be simulated using Marc Mentat software was the native model and all other models would be simulated using CATIA software.

The main problem was due to very fine element size (due to CT images with high resolution) and the use of a grey scale to define the material properties of the bone.

As mentioned, the use of grey scale values makes it possible to associate different mechanical properties (Young's modulus and Poisson ratio) to each grey tone (density) in the created mask. This is a huge advantage since bone isn't homogeneous, so the trouble of manually associating a variation of mechanical properties to the various grey levels or the need to simplify bone as a homogeneous material is thus eliminated. However, it should be noted that from the programs available only Marc had the ability to recognize imported material properties (HU) from the Simplware generated model.

Initially it was impossible to import the created model from ScanFE to Marc since ScanFE would shut down when trying to export the model. This was due to the relation between element and model size. So if the model was very big whilst being composed of very small elements then this would cause the program to crash. This problem was solved by creating a mask for each of the vertebrae in ScanIP (see figure 3.8) and from there an individual finite element model for each mask was created in ScanFE. Exporting each vertebrae from ScanFE was now possible, since the global model size had been reduced to a third (global model included the three vertebrae).

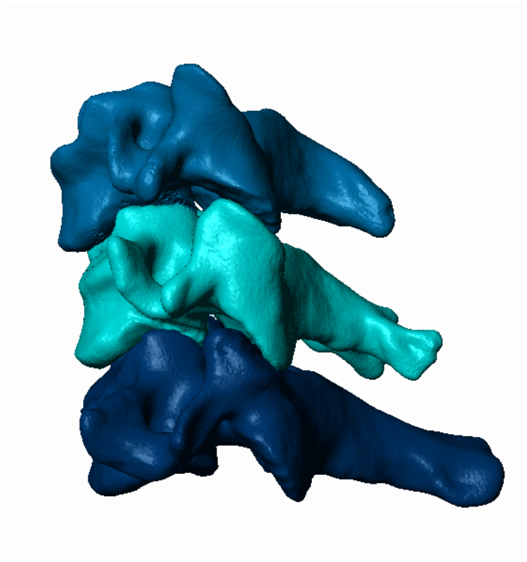

Figure 3.8: Representation of the three masks, one for each vertebrae.

However, Marc was unable to compute these three vertebrae and two created discs since now it was clear that the native model created in Marc was too "heavy".

It was then ascertained that the mesh created by default in ScanFE depended solely on the resolution of each one of the CT images. By decreasing image resolution element size was increased, at the cost of some detail in the image, and the Marc file decreased. So, once the balance between image resolution, image size and element size was reached, the full model (3 vertebrae and 2 discs) was successfully computed in Marc, thus from here on this native Marc model will be referred to as the Specific Patient Native Model. The one mask per vertebrae was still taken into account in this balance so as to be able to get as much detail of the vertebrae as possible.

Up to this point the only model created was the native model. Once work started on the implanted models it was quickly understood that these models would not work in the same way the native Marc model had worked.

In the case of the vertebrae and discs, element size wasn't very small; however, when creating a mesh for the cervical cage or the prosthetic disc element size was by default very small, and this small element size was then applied to the rest of the model (three vertebra and disc with minute element size). The alternative would be to force a bigger size element to be used for the whole implant, but when this was done too much information was lost regarding the implant's geometry.

This fine-sized mesh was due to the fact that the available Simpleware software did not have the ability to adapt the element size to the geometry that was to be meshed. So for example if the smallest length of a part of the piece one wished to mesh was 2 mm then **all** elements would have 2mm in size.

Since Catia program has the ability to create an adaptive mesh this seemed like the obvious solution, however Catia doesn't recognize imported material properties, and so Catia would imply a simplification regarding material properties, in other words, the vertebrae would be discretized into cortical bone and trabecular bone.

In order to solve this problem, it was decided that only the native model would be simulated using Marc, since this way material properties would be maintained and mesh size would still be acceptable for Marc since there was no implant in this model that required a very small element size. As for all the other models, they would be simulated using Catia.

A native discretized model for simulation using Catia would also created (Discretized Patient Native Model). This Discretized Patient Native Model was created so as to be able to compare the Specific Patient Native Model with the Discretized Patient Native Model and thus be able to know how realistic the results from the other Discretized Patient Models would really be.

3.2.2.2 Specific Patient Native Model

This model began, like all the others, with the use of the ScanIP program; the three vertebrae were created using threshold filters, and paint/unpaint commands. Once these masks were satisfactory the model of the three vertebrae was imported into ScanCAD so as to create the intervertebral discs manually. These discs were created by using the cylinder default ScanCAD form, with two distinct parts each, the nucleus pulposus and the annulus fibrosus.

Once these cylinders, that were to be the discs, were created and put roughly into place, the whole model was then imported back into ScanIP and with the use of Boolean operations discs were shaped according to the upper and lower vertebrae (see figure 3.8). Once this was done, each mask was imported individually into ScanFE, where material properties were defined and meshes were created (see figure 3.9).

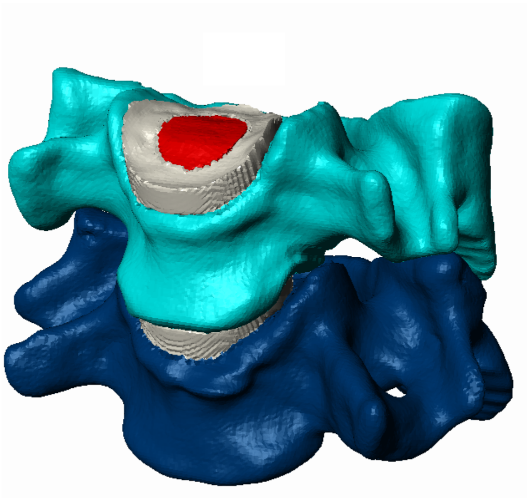

Figure 3.9: Created intervertebral discs with vertebrae C5 and C6.

The mechanical bone properties were also defined at this stage, where a distinction was made between cortical bone and trabecular bone. Depending on the HU level of the pixel in the created mask (ScanIP), the program would automatically allocate density, Elastic Modulus and Poisson's Ratio values to each element of the finite element (FE) model through the equations defined at this point.

As already mentioned, in ScanIP when the DICOM images of the CAT scan were imported the "bone" option was selected; by doing this the program set a default interval for all HU values ranging from -700 to 1300. This interval would later be divided into two intervals, in order to define material properties, one for the trabecular bone and another for the cortical bone.

By looking at the CT images and by observing the HU values of different pixels of the vertebrae an interval was determined for the cortical bone and another for the trabecular bone. It was determined that trabecular bone HU values would go up to 300. This value agreed with E.M.M.FONSECA's et. al. [22] study that determined that trabecular bone has an HU interval ranging from 45HU to 265HU. So for trabecular bone the interval would be [-700,300] and for cortical bone would be [300,1300].

After these intervals were established the equations for allocating density values were calculated. The maximum density for bone was considered as being $1.8g/cm^3$ [6], and the mimimum was $0g/cm^3$ (non bone condition).

ScanFE's default equation for density values was:

$$\rho = a + b * HU \tag{3.1}$$

The values for the constants "a" and "b" were determined through solving the following pair of simultaneous equations:

$$\begin{cases} \rho^{max} = a + b * HU^{max} \\ \rho^{min} = a + b * HU^{min} \end{cases}$$

$$\iff \begin{cases} 1.8 = a + b * (1300) \\ 0 = a + b * (-700) \end{cases} \iff \begin{cases} 1.8 = a + 1300b \\ a = 700b \end{cases} \iff \begin{cases} 1.8 = 700b + 1300b \\ a = 700b \end{cases}$$

$$\iff \begin{cases} b = 9x10^{-4} \\ a = 0.63 \end{cases}$$ Concluding that for this study the density equation was:

$$\rho = 0.63 + 9x10^{-4} * HU \tag{3.2}$$

The equations used for isotropic bone properties were the following:

$$E_c = 2065\rho^{3.09} \tag{3.3}$$

$$E_t = 1904\rho^{1.64} \tag{3.4}$$

where "E" (E_c and E_t) is the elastic modulus for cortical or trabecular bone in MPa, function of bone density ρ in g/cm^3 [22].

The Poisson coefficient was assumed equal to 0.3, for any bone tissues [22].

In order to associate these equations (3.2, 3.3 and 3.4) into the FE model two different greyscale materials were created for the one imported (from ScanIP) mask, then, for each material the HU interval was determined along with density, corresponding elastic modulus equations and Poisson ratio value.

In figure 3.10 the material properties for trabecular bone have been set. Similarly in figure 3.11 the material properties for cortical bone have also been defined.

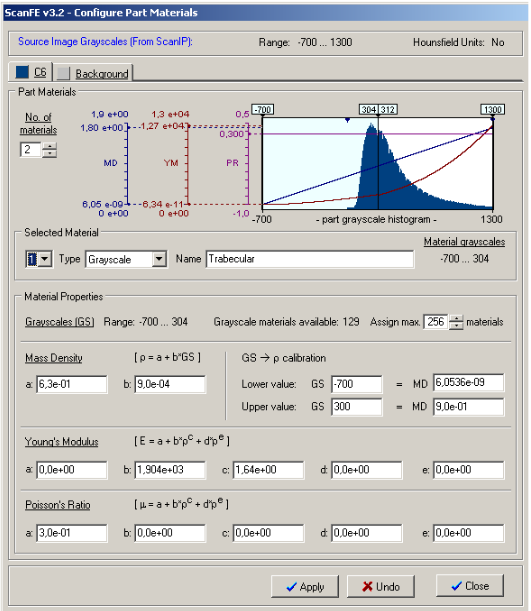

Figure 3.10: Trabecular mechanical properties in ScanFE.

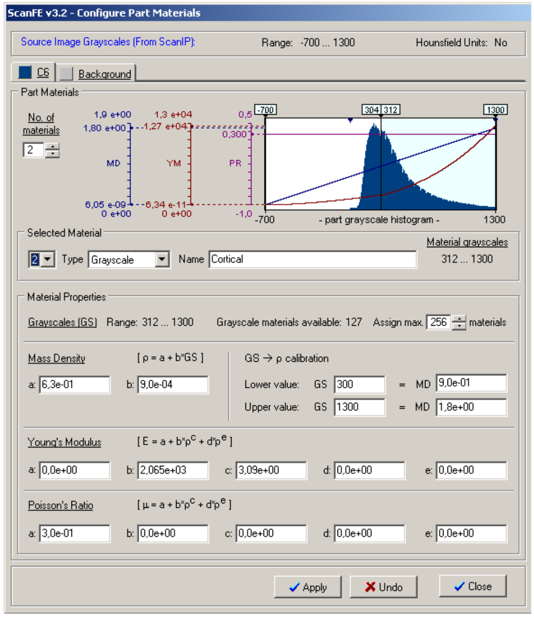

Figure 3.11: Cortical mechanical properties in ScanFE.

Each component of the model was then exported, in a Patran format, from ScanFE and opened individually in Marc. Once the whole model was put together (figure 3.12), boundary conditions were set, the considered compressive force was applied (axially on vertebra C4) and the simulation was run. For this Specific Patient Native Model simulation, in order for results to be more evident and since what was being evaluated were the differences between a simplified (discretized) bone model and a non simplified bone model (i.e. not the actual strain values), the applied force was of 100 N instead of the 50 N (that represent the force exerted by a human head on the cervical spine [25]). The Discretized Patient Model was also simulated with a loading of 100 N for this comparison to be made.

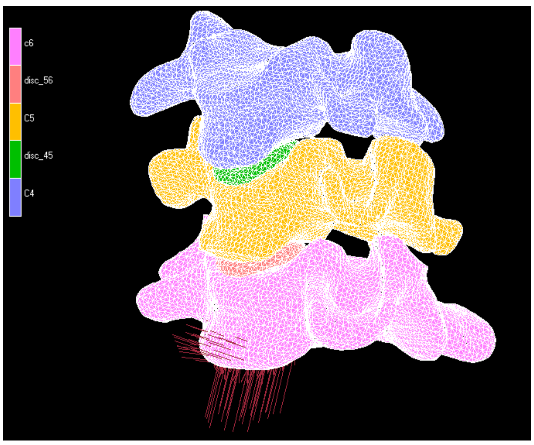

Figure 3.12: Marc Numeric Model.

In table 3.1 the number of elements and nodes of each body making up the Specific Patient

Native Model are displayed.

Table 3.1: Specific Patient Native Model - Elements and Nodes

Component	Number of Elements	Number of Nodes [N/m]
C4	101367	23240
C5	100906	23219
C6	123577	28265
Annulus Fibrosus C4/C5	3584	1012
Nucleus Pulposus C4/C5	1780	476
Annulus Fibrosus C5/C6	3137	902
Nucleus Pulposus C5/C6	1939	522

3.2.2.3 Discretized Patient Models

Discretized Patient Native Model

The masks for the three vertebrae and discs that were created for the Specific Patient Native Model with the use of ScanIP and ScanCAD were exported from ScanIP in STL format to the CAD program Catia. In the ScanIP program a second mask was created for each bone with a slightly lower threshold interval [107,300] so as to create a mask with the trabecular bone tissue (figure 3.13). This STL file (trabecular model) was also exported from ScanIP to Catia.

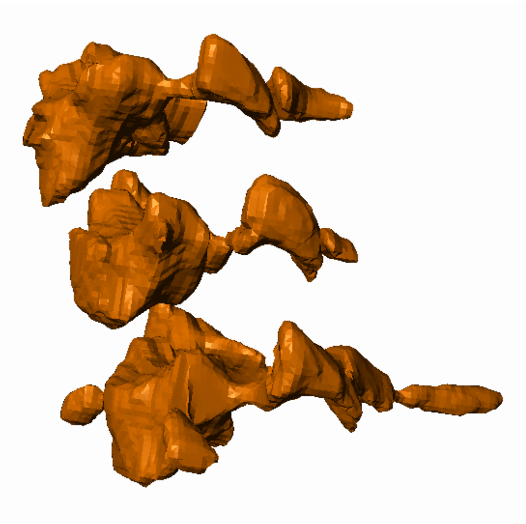

Figure 3.13: Trabecular bone mask: ScanIP.

STL stands for Standard Triangle Language, and it's a file format that possesses the information regarding the surface geometry of a 3D object.

These STL files were individually imported to Catia and from here, and with the use of different tools, solid models were created.

In figure 3.14 the various stages of the creation of the solid bone are visible, from the STL model (1) to a surface model (4), and finally the solid model (6).

Once all solid models had been created, the trabecular solid model was removed from its corresponding vertebrae. Then an assembly was created with the now partially hollow vertebrae (this part of the vertebrae now corresponds to the cortical bone), the trabecular bone solids and the solid intervertebral discs.

Cartilage was also created between superior articular surfaces of one vertebra with the inferior articular surfaces of another.

In figure 3.15 the Discretized Patient Native Model is partially assembled to allow a better visualisation of the various components in this model.

Lines were created on the surface of each of the vertebrae, in such a way that they would be as close to the area of the intervertebral disc/ProDisc-C/Cage as possible (see figure 3.16). These lines served as guidelines and didn't vary from one CAD model to another. The purpose of these guidelines was so that Principal Strain values could be extracted from these lines so that results for different models could be correctly compared.

Materials for each solid were then defined. For each of the three vertebrae a value for the cortical and another for the trabecular bone were determined using the material properties verified in the

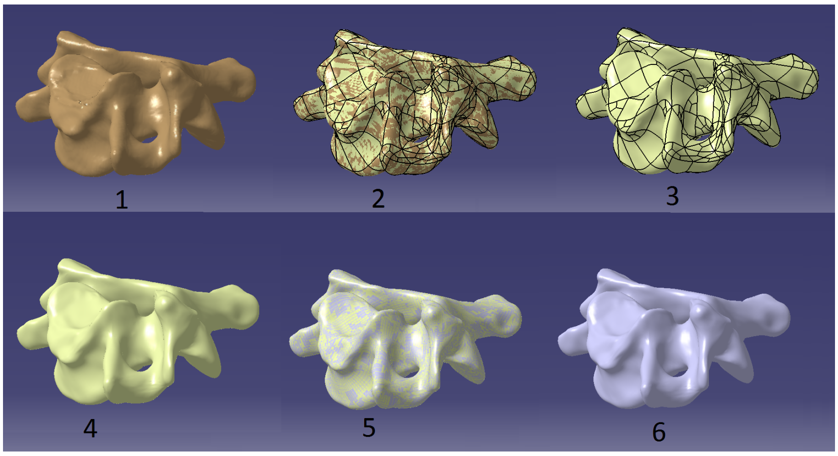

Figure 3.14: Vertebrae C6: STL to a sold model.

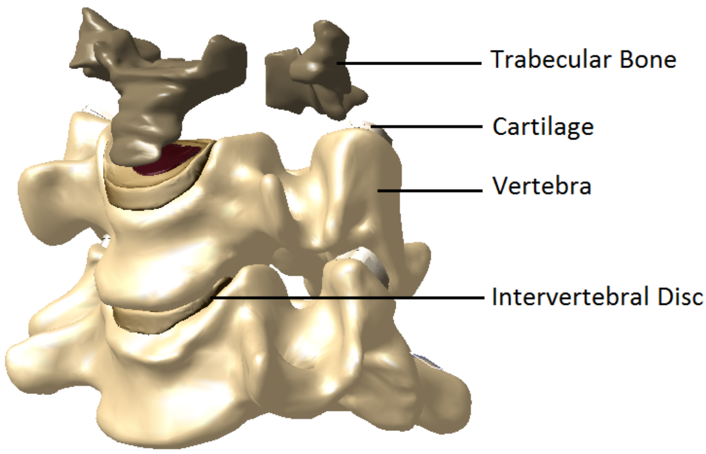

Figure 3.15: Partially assembled Discretized Patient Native Model.

Specific Patient Native Model. Since the Marc Model allocated material properties according to the grey scale value of the pixel/element a single vertebra had a varied range of material properties for both cortical and trabecular elements. By going through each one of these different material properties of one of the vertebrae and registering the Elastic Modulus and density values it was clearly visible which values belonged to cortical bone and which belonged to trabecular bone. Once this had been done an average of the Elastic Modulus was determined. This process was performed for each one of the vertebrae individually, so in principle each vertebra was allocated a different Elastic Modulus value. These calculated average values were then allocated to the solid bone components of all the Discretized Patient Models.

Once this was done, meshes were created and "forced" to incorporate the guidelines, loads and restrains were determined and the simulations were run. Once the simulations were run results were extracted from these guidelines. In other words the registered stress/strain/deformation/etc. results for each node that happened to be on that guideline were saved. This guaranteed that the results from one model to another were extracted from the exact same place in every one of these models.

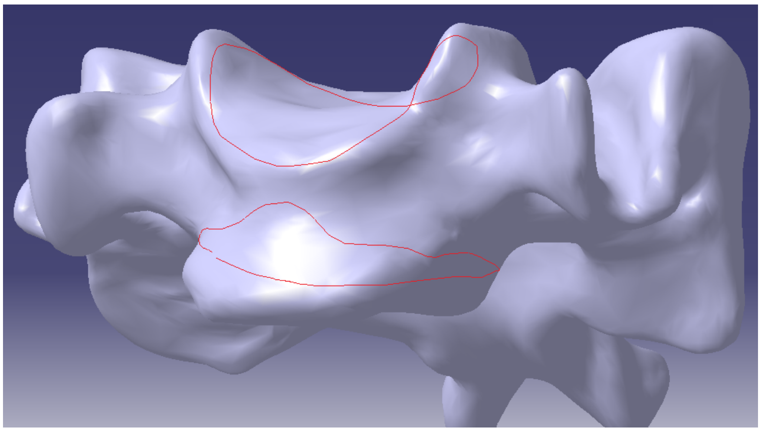

Figure 3.16: Guidelines represented in red on vertebra C5.

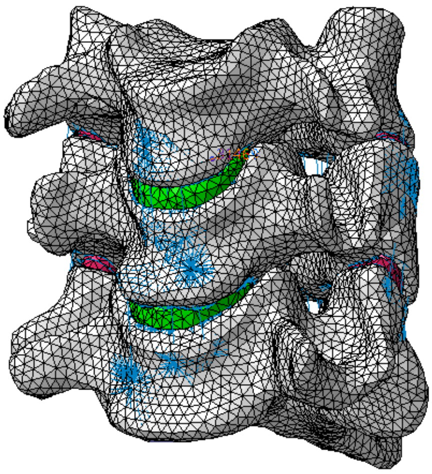

Figure 3.17: Discretized Patient Native Meshed Model.

There were two versions of this Discretized Patient Native Model, one with ligaments and another without. As indicated in the diagram in figure 3.2.

Ligaments considered were:

- Ligamentum Flavum (LF)
- Interspinous Ligaments (ISL)
- Anterior Longitudinal Ligament (ALL)
- Posterior Longitudinal Ligament (PLL)
- Capsular Ligament (CL)

An average of ligament stiffness was considered from a study performed by Paul C. Ivancic et. al. [46] and these values are presented in table 3.2.

Table 3.2: Ligament Stiffness Values

Ligament	Stiffness Value [N/m]
ALL	49000
PLL	62000
CL	64000
LF	97000
ISL	21000

Ligaments were considered in the model as spring-like components. These spring-like components were an approximation to the ligaments in a human neck since not many ligament connections were created, and also because ligaments don't normally behave as springs since they do not usually resist compressive forces. The springs' attachment on the bones was also an approximation since they were positioned according to anatomic pictures.

For the Discretized Patient Native Model without ligaments these were just eliminated from the previous model and the simulation was run again.

The loadings for the Discretized Patient Native Model were:

- 100N for the model without ligaments (so as to compare results with the Specific Patient Native Model)

- 50N for the model with ligaments (so as to compare results with all other Discretized Patient Models)

The direction and application point of the applied force is visible in figure 3.18. This force was applied in the same direction and location in all other Discretized Patient Models.

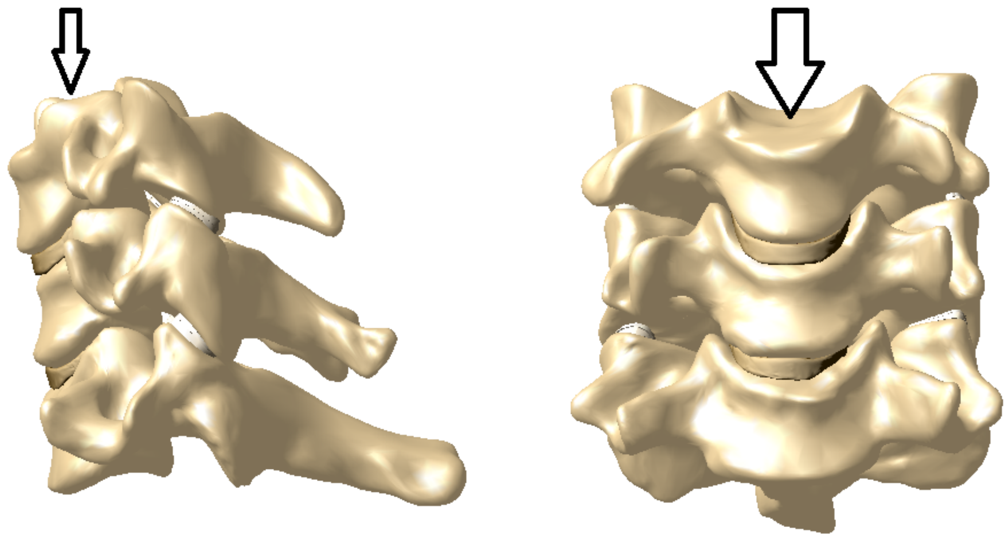

Figure 3.18: Lateral (left) and frontal (right) views of the Discretized Patient Native Model with an arrow representation the applied axial compressive force on vertebra C4.

All other Discretized Patient models were created from this native model.

Once all model properties were defined, simulations were run and results were extracted. Results were studied for both cortical bone (by means of the created guidelines) and trabecular bone. This made it possible to study not only what happens on the surface of the vertebrae but also what happens inside them.

The number of elements and nodes of each component for these two models (with and without ligaments) are present in table 3.3

Table 3.3: Discretized Patient Native Model - Elements and Nodes

Component	Number of Elements	Number of Nodes [N/m]
C4 Cortical	27713	44316
C4 Trabecular	4667	8345
C5 Cortical	27598	44103
C5 Trabecular	3667	6565
C6 Cortical	32345	51869
C6 Trabecular	5734	10178
Annulus Fibrosus C4/C5	1840	3353
Nucleus Pulposus C4/C5	554	1004
Annulus Fibrosus C5/C6	1008	1992
Nucleus Pulposus C5/C6	576	1030
Cartilage	1030	2470

Discretized Patient Cage Model

The Discretized Patient Cage Model was created from the Discretized Patient Native Model. The C5-C6 intervertebral disc was removed and in its place the CAD model of the Fidji Cage was inserted.

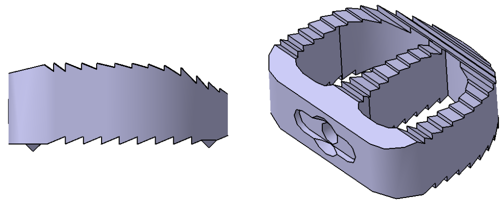

Figure 3.19: CAD Fidji Cage: lateral and perspective view.

Figure 3.19 represents the cervical cage used for this model. In the lateral view of the cervical cage an upper curvature is clearly visible in order for the cage to be better accommodated by the upper vertebra (C5).

The Fidji Cage possesses a serrated upper and lower surface to prevent the cage from sliding about on the vertebrae's surfaces.

Some bone was scraped of the top of vertebra C6 and bottom of vertebra C5 so that the Cage would be more stabled between these two bones. However, while smoothing out these surfaces care was taken not to remove so much cortical bone that the Fidji cage would be supported by trabecular bone, since if this were to happen then the Fidji cage would sink into the vertebrae (trabecular bone is spongier and more malleable than cortical bone, and wouldn't be able to support the implant).

The correct positioning of the Fidji cage in these vertebrae was a crucial point in order to replicate the real surgery as realistically as possible. Great care was taken to guarantee this, and with the help of Surgeon Dr. Abel Fernando Queirós e Nascimento[1] the Fidji cage was placed as well as possible in between vertebrae C5 and C6.

This Discretized Patient Cage Model is shown in figure 3.20.

After the model was assembled (figure 3.20), material properties were defined, meshes (figure 3.21) and ligaments were created (in the exact same way as with the previous Discretized Patient Models) and boundary and loading conditions were determined.

For this model, two different situations were simulated, one before ossification of the cage, and one after ossification.

Before ossification was considered the friction coefficient value was set as being 0.8 [8] between PEEK cage material and cortical bone so as to mimic the effect that the cage's small teeth have on vertebral surfaces.

[1]Invited Assistant Professor of the Mechanical Engineering Department of the University of Aveiro and Director of "Instituto de Cirurgia Reconstrutiva de Coimbra"

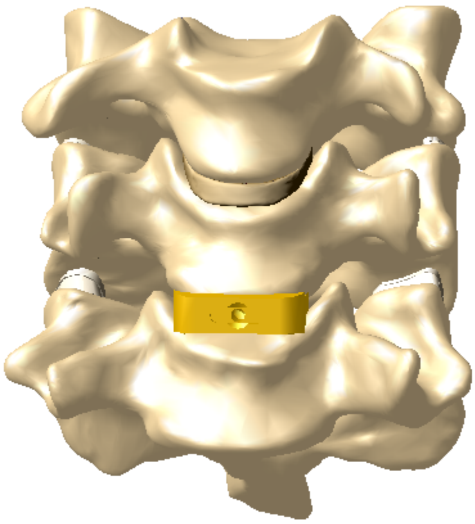

Figure 3.20: Discretized Patient Cage Model.

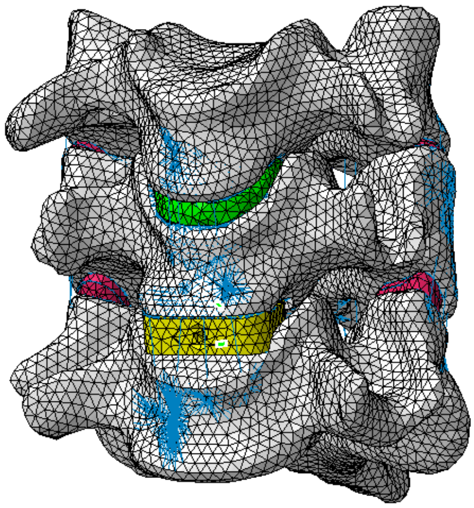

Figure 3.21: Discretized Patient Cage Meshed Model.

After ossification the contact between vertebrae and cage was defined as all other contacts in the model (rigidly fixed contact).

The simulation was then run (axial compressive force of 50N) and results were extracted using the guidelines for results regarding the cortical bone, and results were also observed for trabecular bone in each vertebrae.

Displayed in table 3.4 are the number of elements and nodes of the components in this model.

Table 3.4: Discretized Patient Cage Model - Elements and Nodes

Component	Number of Elements	Number of Nodes [N/m]
C4 Cortical	27336	43820
C4 Trabecular	5047	9012
C5 Cortical	27851	44527
C5 Trabecular	3659	6602
C6 Cortical	32732	52613
C6 Trabecular	5789	10371
Annulus Fibrosus C4/C5	1767	3287
Nucleus Pulposus C4/C5	651	1181
Fidji Cage	2450	4724
Cartilage	1016	2426

Discretized Patient ProDisc-C Model

The ProDisc-C Model was once again created from the Discretized Patient Native Model. The C5-C6 intervertebral disc was removed and in its place the CAD model of the ProDisc-C was inserted. For the ProDisc-C to be placed correctly some bone also had to be removed, more so than for the Discretized Patient Cage Model. In figure 3.22 the three components of the ProDisc-C are visible. The upper piece of the disc is inserted into vertebra C5, the central polyethelene piece is attached to the lower metal piece of the ProDisc-C and the latter is then inserted into vertebra C6. In figure 3.22 the metallic fins on the upper and lower surface of the ProDisc-C are visible. Slots were made in the vertebrae so as to incorporate the ProDisc-C.

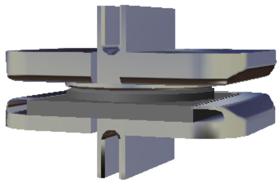

Figure 3.22: ProDisc-C CAD image.

The C5 and C6 vertebrae were also slightly separated in order to better fit the prosthetic disc. There are various sizes available for the ProDisc-C and by looking at the model with the ProDisc-C inserted in it, the size seemed to be acceptable for this particular vertebrae sample. In this case, since this "surgery" was not performed by a surgeon, a slight margin for error was taken into account for this step of the model construction.

Once more some bone was scraped off the top of vertebra C6 and bottom of vertebra C5 so that the ProDisc-C would be better stabilized between these two bones. The same care with not scraping away too much cortical bone was taken, for the same reasons as with the Fidji Cage. The procedure used here for positioning the cage and removing some bone was the same one used for the Fidji cage.

In figure 3.23 the Discretized Patient ProDisc-C Model is visible after bone removal.

The removal of bone was done by creating some basic rectangular prisms, some with the size of the fins and others with the size of the metallic plates of the ProDisc-C, and then performing various Boolean Subtracting operations. Once the different components were assembled (vertebrae, intervertebral disc, ProDisc-C and cartilage), material properties were defined (in the same way as for the Discretized Patient Native Model), the meshes (figure 3.24) were created as before so as to include the guidelines, ligaments were also created (in the same places as the ligaments in the Catia Native Model) and boundary and loading conditions (axial compression) were set (50N).

Here too, two different simulations were run. In reality, right after surgery the disc is only fixed to the vertebrae by the fins in the prosthetic disc. So for the first simulation a friction coefficient was considered between the ProDisc-C and the vertebrae.

According to H.Y. Yu et.al. [29] the coefficient of friction between the CoCr (cobalt chromium alloy) and bone is 0.23, whilst between CoCr and the polyethelene core (Ultra High Molecular Weight Polyethelene - UHMWPE) the friction coefficient is 0.08 [12].

Once the bone has had time to grow into the prosthetic disc (ossification) the ProDisc is totally fixed to the vertebrae. For the second simulation friction coefficient between the prosthetic disc and vertebrae was removed and this contact was defined as being rigidly fixed. Once again, after simulations were run, results were extracted from the surface of each vertebrae (cortical bone) and from the trabecular bone.

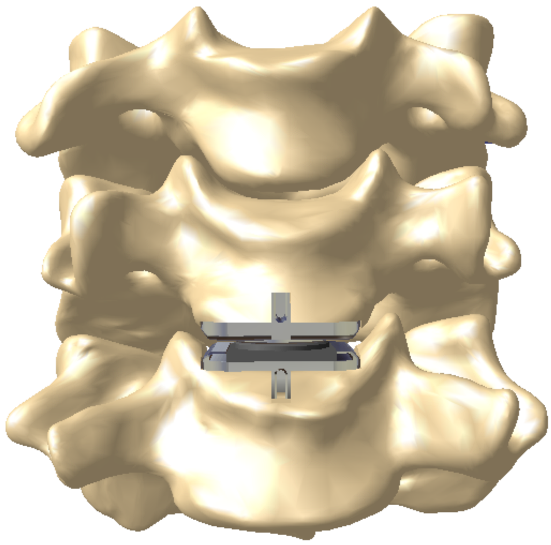

Figure 3.23: Discretized Patient ProDisc-C Model.

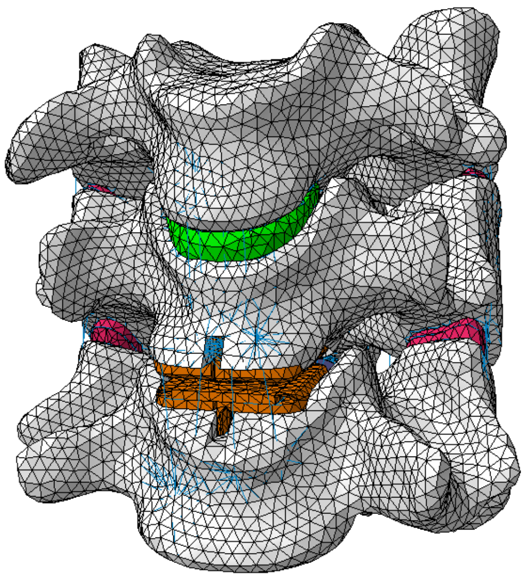

Figure 3.24: Discretized Patient ProDisc-C Meshed Model.

In table 3.5 the number of elements and nodes for each of the components of this model were recorded.

Table 3.5: Discretized Patient ProDisc-C Model - Elements and Nodes

Component	Number of Elements	Number of Nodes [N/m]
C4 Cortical	27607	6444
C4 Trabecular	5135	1459
C5 Cortical	26898	6337
C5 Trabecular	3803	1118
C6 Cortical	32497	7631
C6 Trabecular	6010	1745
Annulus Fibrosus C4/C5	1690	506
Nucleus Pulposus C4/C5	530	156
ProDisc-C	4097	1347
Cartilage	1022	480

3.2.2.4 Numerical Foam Models

Lastly these models were created in order to be able to compare the numeric models of this study to the experimental (physical) models. Since the experimental model consisted of Polyurethane rigid foam (PUR) vertebrae, and also since the experimental model consisted solely of vertebrae C5 and C6, a CAD model was created in order to recreate this segment from the Discretized Patient Native Model (no ligaments). Since the foam vertebrae were composed of only one material (no distinction between trabecular and cortical bone) PUR foam properties were applied to all bone components of vertebrae C5 and C6.

Numerical Foam Native Model

For the Numerical Foam Native Model the intervertebral C5/C6 disc was inserted between these two vertebrae, and meshes were created. For this model the above mentioned guidelines in this chapter were not necessary, seeing as results were taken from the anterior area of two vertebrae's body in the experimental approach.

The direction and application point of the applied force (50N) is visible in figure 3.25. This compressive force was applied in an axial direction on vertebra C5.

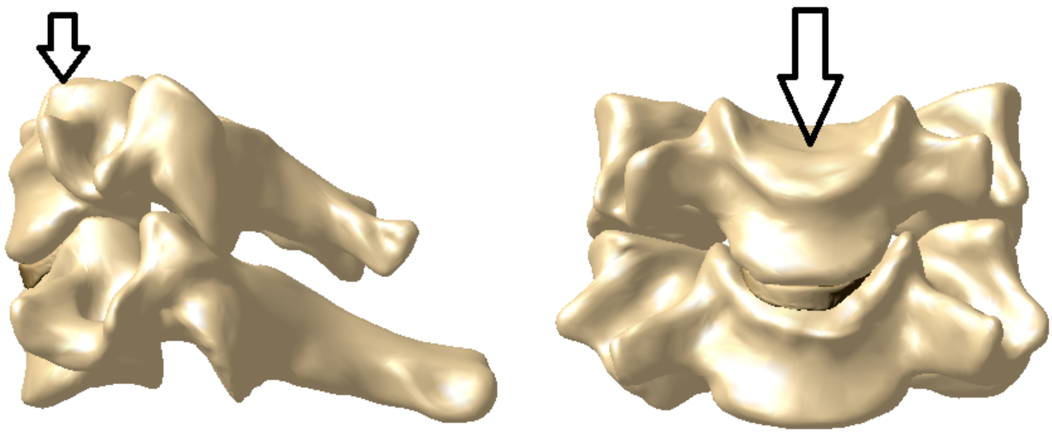

Figure 3.25: Lateral (left) and frontal (right) views of the Numerical Foam Model with an arrow representation the applied axial compressive

In table 3.6 the number of elements and nodes for this final model are represented.

Table 3.6: Numerical Foam Model - Elements and Nodes

Component	Number of Elements	Number of Nodes [N/m]
C5	31265	50668
C6	38079	62047
Annulus Fibrosus C5/C6	1008	1992
Nucleus Pulposus C5/C6	576	1030

Numerical Foam Cage Model

For the Numerical Foam Cage Model the Discretized Patient Cage Model pre ossification was used, vertebra C4 was removed along with ligaments, cartilage and the C4/C5 intervertebral disc. Material properties were altered to PUR mechanical properties and loading conditions (on vertebra C5) were set in the same way as for the Numerical Foam Native Model.

In table 3.7 the number of elements and nodes for this final model are represented.

Table 3.7: Numerical Foam Cage Model - Elements and Nodes

Component	Number of Elements	Number of Nodes [N/m]
C5	31510	51129
C6	38521	62984
Fidji Cage	2450	4724

Numerical Foam ProDisc-C Model

For the Numerical Foam ProDisc-C Model the Discretized Patient ProDisc-C Model pre ossification was used, vertebra C4 was once more removed along with ligaments, cartilage and the C4/C5 intervertebral disc. Material properties were altered to PUR mechanical properties and loading conditions (on vertebra C5) were set in the same way as for the Numerical Foam Native Model.

In table 3.8 the number of elements and nodes for this final model are represented.

Table 3.8: Numerical Foam ProDisc-C Model - Elements and Nodes

Component	Number of Elements	Number of Nodes [N/m]
C5	30701	7455
C6	38507	9376
ProDisc-C	4097	1347

3.2.2.5 Mechanical properties of all used materials

All the materials' mechanical properties used for these numerical models are represented in table 3.9.

Table 3.9: Material Mechanical Properties

Software ⇒	Catia		Marc		
Component ⇓	E [MPa]	Poisson	E [MPa]	Poisson	Density [g/cm^3]
C4 trabecular	1210	0,3 [22]	$E_c = 2065\rho^{3,09}$ (3.3) $E_t = 1904\rho^{1,64}$ (3.4) [22]	0,3 [22]	$\rho = 0,63 + 9.10^{-4}.HU$ (3.2)
C4 cortical	5906				
C5 trabecular	1218				
C5 cortical	5905				
C6 trabecular	1263				
C6 cortical	5905				
Nucleus Pulposus	3,4 [38]	0,49 [38]	3,4 [38]	0,49 [38]	-
Annulus Fibrousus	450 [38]	0,3 [28]	450 [38]	0,3 [28]	-
Cartilage	5 [23]	0,46 [23]	-	-	-
PEEK	4500 [17]	0,36 [17]	-	-	-
UHMWPE	2500 [34]	0,45 [19]	-	-	-
CoCr	70 [1]	0,3 [1]	-	-	-
PUR	1.19 [2]	0,24 [2]	-	-	-

3.3 Results

3.3.1 Specific Patient Model versus Discretized Patient Model

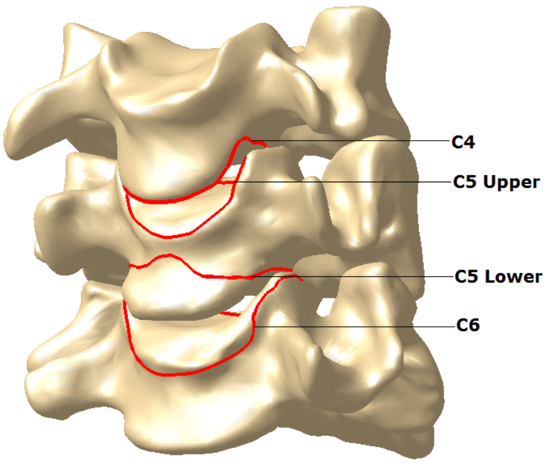

Figure 3.26: Four created guidelines.

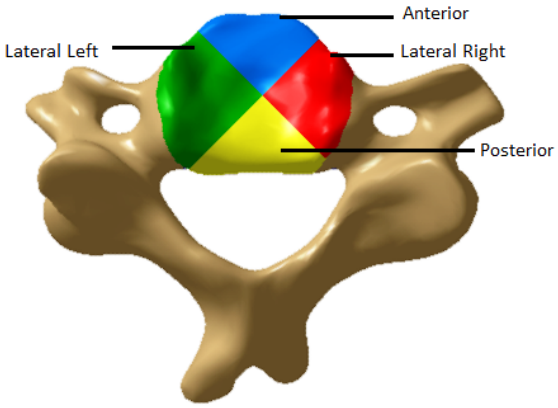

Figure 3.27: Colour division of the vertebral body.

The first results to be analysed were for the Specific Patient Native Model and Discretized Patient Native Model. Both these models consisted solely of the three vertebrae and respective intervertebral discs (i.e. no ligaments were used).

The results for the Discretized Model were extracted by means of the created guidelines. Four guidelines were created, one for the C4 vertebra, two for the C5 vertebra (C5 Upper guideline and C5 Lower guideline) and one for vertebra C6.

The results obtained from the Specific Patient Native Model were extracted from approximately the same place on the vertebra as those extracted from the Discretized Patient Native Model guidelines.

Figure 3.26 shows the four guidelines on the Catia Native Model; the guidelines were recreated as closely as possible in the Specific Patient Native Model, so that these two models could be better compared.

Bearing figure 3.27 in mind, the values were extracted from the vertebral body in a counterclockwise direction, starting at the center of the anterior section (blue), then through the left section of the vertebra (green) followed by the posterior (yellow) and right (red) sections, and then back to the anterior section of the vertebra.

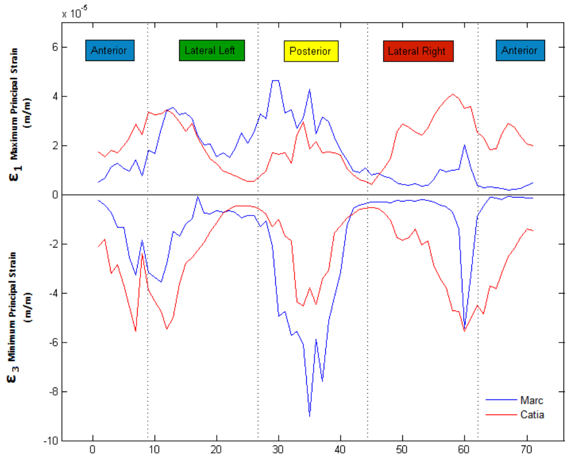

Figure 3.28: C4: Specific and Discretized Patient Native Model Strain Comparison - Cortical Bone.

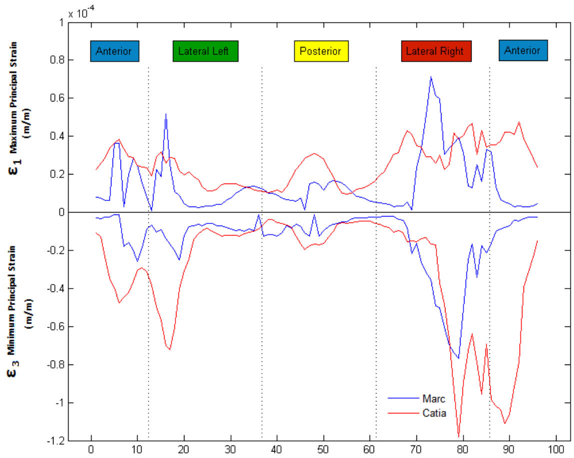

Figure 3.29: Upper C5: Specific and Discretized Patient Native Model Strain Comparison - Cortical Bone.

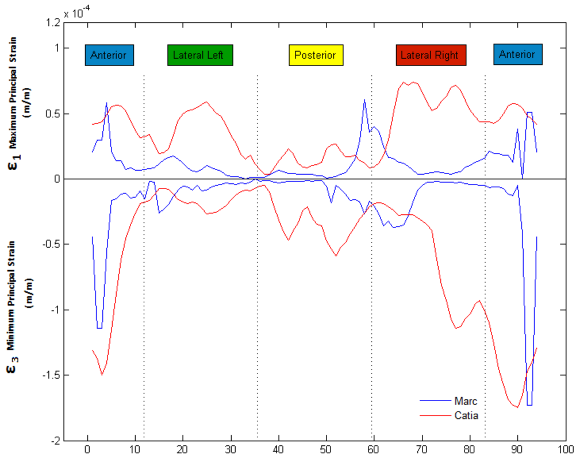

Figure 3.30: Lower C5: Specific and Discretized Patient Native Model Strain Comparison - Cortical Bone.

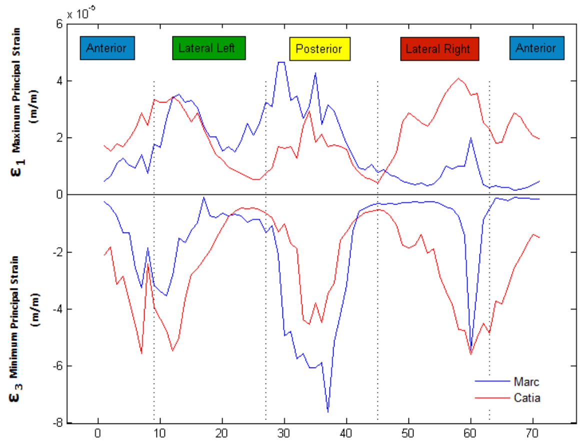

Figure 3.31: C6: Specific and Discretized Patient Native Model Strain Comparison - Cortical Bone.

This procedure was followed for all four guidelines, and the maximum and minimum principal strain values are represented in figures 3.28, 3.29, 3.30, 3.31 for vertebra C4, vertebra C5 (upper and lower guidelines) and vertebra C6 respectively.

For vertebra C4 (see figure 3.28) the greater differences between values for each model, were for the posterior and lateral right areas of the vertebral body. The biggest difference in values of both maximum and minimum principal strains, between the two models, was observed in the posterior area of the vertebra. In this area Specific Patient Native Model values of maximum principal strain were up to 3.3 times higher than Discretized Patient Native Model values (approximately $5.0x10^{-5}$ and $1.5x10^{-5}$ respectively). Minimum principal strains in the Specific Patient Native Model were up to double those in the Discretized Patient Native Model values (approximately $-9.0x10^{-5}$ and $-4.5x10^{-5}$ respectively).

For the vertebra C5 Upper guideline (see figure 3.29) absolute values were minimum in the posterior area of the vertebral body for both models, whilst the greater differences in values were for the posterior and lateral areas, particularly in the lateral right area towards the anterior section of the vertebral body.

The values of maximum principal strain for the Specific Patient Native Model were almost double those of the Discretized Patient Native Model (approximately $0.7x10^{-4}$ and $0.37x10^{-4}$ respectively). The value of minimum principal strain peaked at approximately $1.2x10^{-4}$ in the Discretized Patient Native Model, and, significanlty, the average rate of change of the gradient was smaller towards the anterior body (unlike the sharp decrease observed for the Specific Patient Native Model). Due to the seemingly slower response in the Discretized Patient Native Model, the difference in values between both models was up to 5 times greater in the Discretized Patient Native Model ($-1.0x10^{-4}$) when compared to the Specific Patient Native Model ($-0.2x10^{-5}$) in the lateral right/anterior area.

The values extracted from the lower guideline of vertebra C5 were, once again, lower in the posterior area and peaked in the lateral right/anterior area of the vertebral body. Maximum principal strain values in the Discretized Patient Native Model ($0.75x10^{-4}$) were up to approximately 7 times higher than in the Specific Patient Native Model ($0.1x10^{-4}$), while absolute minimum principal strain values in the Discretized Patient Native Model ($-1.2x10^{-4}$) were approximately up to 12 times higher than the values for the Specific Patient Native Model ($-0.1x10^{-4}$) in the lateral right area of the vertebral body.

In vertebra C6 values weren't as different from one model to the other as they were for vertebra C5. Greater differences in values between both models were observed in the lateral right area of the vertebral body. However even though maximum principal strain values were up to 4 times higher in the Discretized Patient Native Model ($1.0x10^{-5}$) compared to the Specific Patient Native Model ($4.0x10^{-5}$) in this area, greater differences in peak values for absolute minimum strain values were observed in the posterior area of the vertebra. These were practically doubled from the Discretized ($-4.0x10^{-5}$) to the Specific Patient Native Model ($-7.8.0x10^{-5}$).

The results for the Specific Patient Native Model (represented in a blue line[2]) generally vary in a more gradual way when compared to those for Discretized Patient Native Model (represented in a red line[2]). Even though the results for the Discretized Patient Native Model seem to vary more locally, (i.e. the results for the Specific Native Model are represented by a smoother curve), the overall rate of change in the curveâs gradient is higher in the case Specific Patient Native Model.

[2]The graphs' colours have no association with the color scheme used to indicate the location of the results' extraction on the vertebra.

3.3.2 Discretized Patient Models

In this section all the results regarding the different Discretized Patient Models were registered. It's important to bear in mind that all the following results were affected by the error (already determined in the previous section, section 3.3.1) associated to the bone material simplification that was performed in order to use Catia for numeric simulation.

3.3.2.1 Ligament Effect in the Native Model

The results regarding the effect of the ligaments on the studied Native Model are visible in figures 3.32 and 3.33. Results were again extracted from the vertebrae's guidelines, however since the same effect was noted for all four guidelines, for simplicity, only two of the four cases were registered and presented.

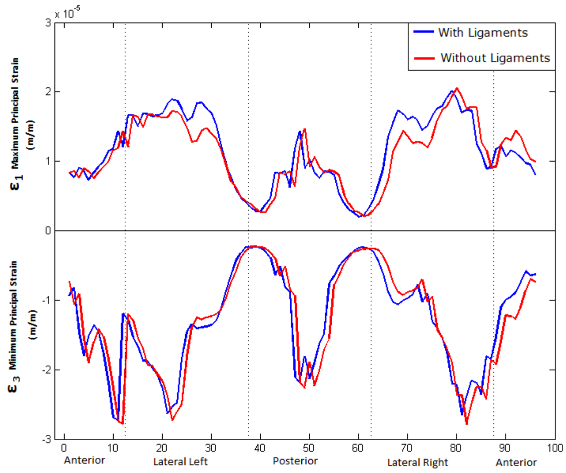

Figure 3.32: Upper C5: Ligament effect on Native model - Cortical Bone.

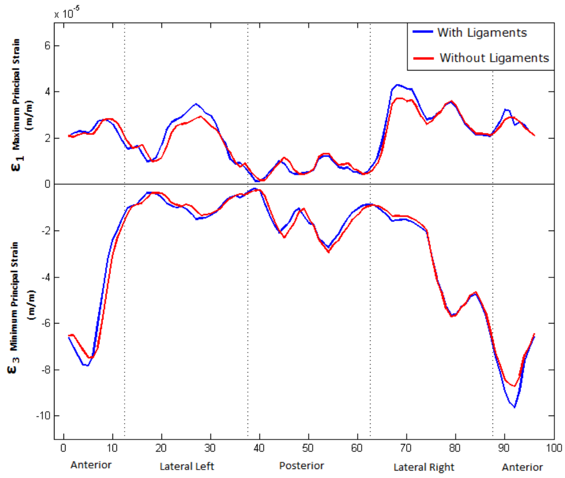

Figure 3.33: C6: Ligament effect on Native model - Cortical Bone.

Variations between these two models were most noticeable in the lateral areas of the vertebral bodies. However, these variations were small since the maximum difference between both models was of approximately 20%.

The values of the maximum and minimum principle strains are not very important in this comparison since what was required was the knowledge of whether or not ligaments have a very pronounced influence on the way the Catia models react to the load they were subjected to. By observing the graphs obtained from vertebrae C5 (Upper guideline) and C6 it's evident that ligaments do have some influence on the Principal strain values and that these strain values in Native Model with ligaments are overall slightly lower than those obtained for the Native Model without ligaments.

3.3.2.2 Native Model versus Arthrodesis Model

Figures 3.34, 3.35, 3.36 and 3.37 represent the results regarding the comparison between the Native Model (with ligaments) and implanted Fidji Cage Model (also with ligaments).

The two cases studied for the Fidji Cage are represented in green while the native model is represented in blue.

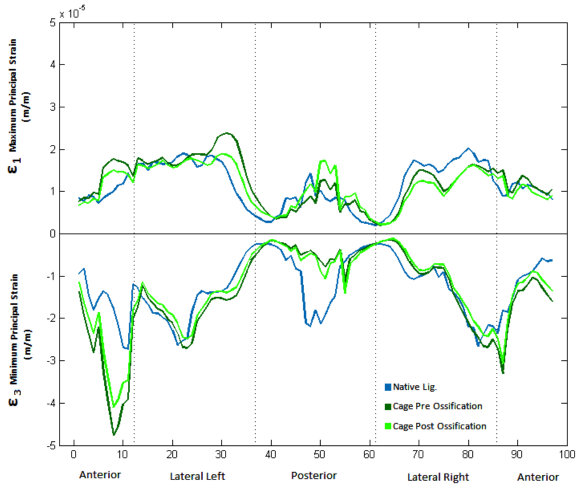

Figure 3.34: C4: Cage and Native Model Strain Comparison - Cortical Bone.

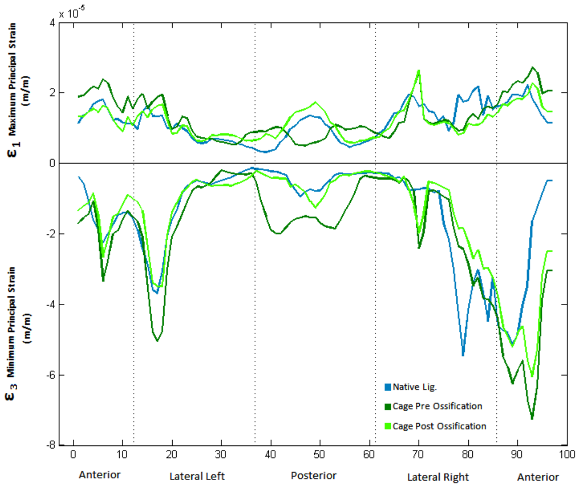

Figure 3.35: Upper C5: Cage and Native Model Strain Comparison - Cortical Bone.

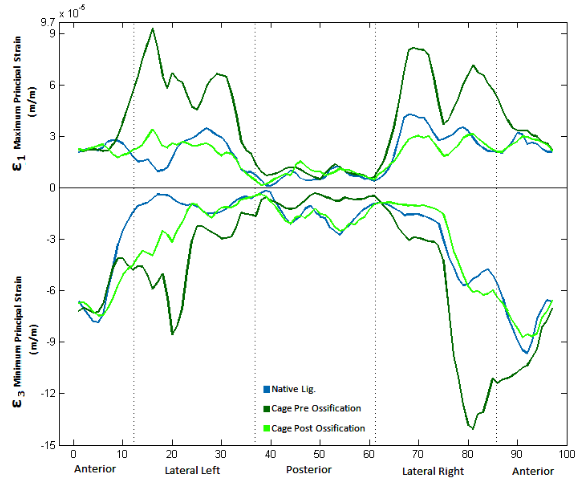

Figure 3.36: Lower C5: Cage and Native Model Strain Comparison - Cortical Bone.

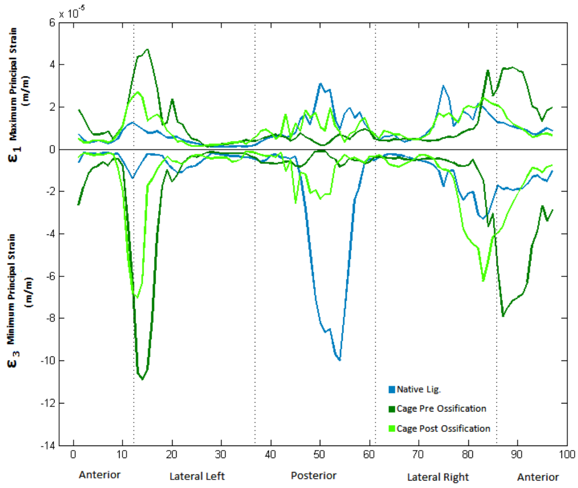

Figure 3.37: C6: Cage and Native Model Strain Comparison - Cortical Bone.

For vertebra C4 (see figure 3.34) the difference, in absolute value, between the case where the Cage has not yet had time to be "absorbed" by the bone (Pre Ossification case represented in a darker green) and the case where ossification had already taken place (Post Ossification case represented in a lighter green) ranges to about 15%, higher (for both maximum and minimum principal strain values) in the Pre Ossification case with the exception of the posterior area of the vertebra (where Post Ossification absolute values are higher). When comparing the Native Model to the Cage Model greater differences were visible in vertebra C4 in the posterior and anterior areas for absolute minimum principal strain values, since in the Cage Model these were practically double those registered in the Native Model. Maximum principal strain values were up to 20% greater in the Cage Model ($2.5x10^{-5}$) in the posterior area of the vertebra than the Native Model values ($2.0x10^{-5}$).

In the upper guideline of vertebra C5 (see figure 3.35), Pre Ossification maximum (ε_1) and minimum (ε_3) absolute principal strain values were always greater than Post Ossification values, with the exception of the maximum principal strain values in the posterior area of the vertebral body. Greater differences between these two cases (Pre and Post Ossification) were observed in the lateral left and posterior area for minimum principal strain values, and in the posterior area, for maximum principal strain values. This difference ranged up to 20% for both minimum and maximum strain values. When comparing the maximum principal strain values in the Pre Ossification case to the Native Model, even though peaks were observed in the lateral areas of the vertebral body, the highest variation (of 20%) was observed in the posterior area of the vertebra, where Native values were around $1.5x10^{-5}$ and the Pre Ossification values were $1.2x10^{-5}$. Differences in the absolute values of minimum principal strain (ε_3) between these two models were once again registered in the posterior area, where Pre Ossification values ($-2.0x10^{-5}$) were practically 4 times higher to those in the Native Model($-0.5x10^{-5}$). Principal strain values in the Post Ossification case practically coincided with the ones for the Native Model, in all areas of the vertebral body

When comparing the Pre and Post Ossification cases in the lower guideline of vertebra C5 (figure 3.36), it was observed that Pre Ossification absolute values for ε_1 and ε_3 were generally much higher than the same values for the Post Ossification case, particularly in the lateral areas, where ε_1 values tripled and ε_3 values doubled. For this guideline, when comparing the Native Model with the Post Ossification Model, absolute values peaked in the anterior area and the biggest difference between these two curves was in the lateral left area where Post Ossification values were double those observed for the Native case. As for the Pre Ossification case versus Native Model comparison, absolute values for ε_1 and ε_3 peaked in the lateral areas of the vertebral body and were around 9 times higher in the lateral left area in the Pre Ossification case (ε_1 reached just over $9.0x10^{-5}$ and ε_3 reached $-9.0x10^{-5}$) when compared to the native model (ε_1 reached $1.5x10^{-5}$ and ε_3 reached $-1.0x10^{-5}$). In this guideline the maximum compressive strain value (ε_3) was registered at approximately $14.0x10^{-5}$.

In the last of these graphs (figure 3.37) vertebra C6 is analysed. When comparing the Pre Ossification case to the Post Ossification case, absolute values of ε_1 and ε_3 were higher for the Pre Ossification case just about everywhere on the vertebra with the exception of the posterior area.

In the lateral and anterior areas the values of ε_1 and ε_3 were 35% higher for the Pre Ossification case compared to the Post Ossification case. In the posterior area, ε_1 values in the Post Ossification case were double those obtained in the Pre Ossification case, and ε_3 values in the Post Ossification case were up to triple those obtained in the Pre Ossification case.

Greater differences were observed in the Pre Ossification Model vs Native Model comparison than in the Post Ossification Model vs Native Model comparison.

When comparing the Pre Ossification Model to the Native Model three main peaks stand out, one in the anterior-going-on-to-lateral-left area, one in the posterior area and in the lateral-right-going-on-to-the-anterior area. Bigger differences in strain values between these models were seen in the lateral left and posterior areas. The absolute values of ε_3 for the former, in the Pre Ossification Model ($11.0x10^5$), were up to 11 times higher than those for the Native Model ($1.0x10^5$), whereas the values of ε_3 for the latter, in the Native Model ($11.0x10^5$), were up to 11 times higher than those of the Pre Ossification Model ($-1.0x10^{-5}$).

The absolute values of ε_1 weren't as high as those obtained for ε_3.

The biggest difference in ε_1 values between these two models was in the lateral left area of the vertebral body, where ε_1 values in the Pre Ossification case ($4.0x10^{-5}$) were up to 4 times higher than in the Native case ($1.0x10^{-5}$).

In the Post Ossification case differences (with the Native Model) were also greater in the lateral left and posterior area of the vertebra. However, the values of ε_3 were only 7 times higher between models, unlike in the Pre Ossification case where they were 11 times higher (than the results in the Native Model). The biggest difference for ε_1 values between these two models was also observed in the lateral left area of the vertebral body where values for the Post Ossification Model ($4x10^{-5}$) were double those of the Native Model ($2x10^{-5}$).

In all four cases, the highest absolute values for minimum strain (ε_3) were higher than those of maximum principal strain values (ε_1).

Results show that, as a general rule, strain values for the case where the Cage has not yet had time to be "absorbed" by the bone are higher than the ones obtained for the case where ossification had already taken place.

Of the four cases, the ones that present higher peak values are the C5 lower vertebral area and the C6 vertebra, these results correspond to the points on the guidelines closer to the implant, therefore indicating that the presence of this implant affects principal strain values.

These results also enable a clear view of the location, on the vertebral body, where the absolute value of principal strain is maximised. The right and left lateral areas of the vertebral body are the ones most affected in the Fidji Cage models, whilst the anterior and posterior generally show lower absolute values of principal strain. This is due to the positioning of the Cage on the vertebrae.

For trabecular bone, only compression strain was evaluated since usually the cervical spine is subjected to compressive forces, as opposed to extension forces. In figure 3.38 the three studied vertebrae are visible along with their respective trabecular bone. Four views are shown so as to show what happens in the trabecular bone at the C4/C5 interface and at the C5/C6 interface, hence the two views for vertebra C5. Figure 3.39 shows trabecular bone for the native model and the cage model (post ossification).

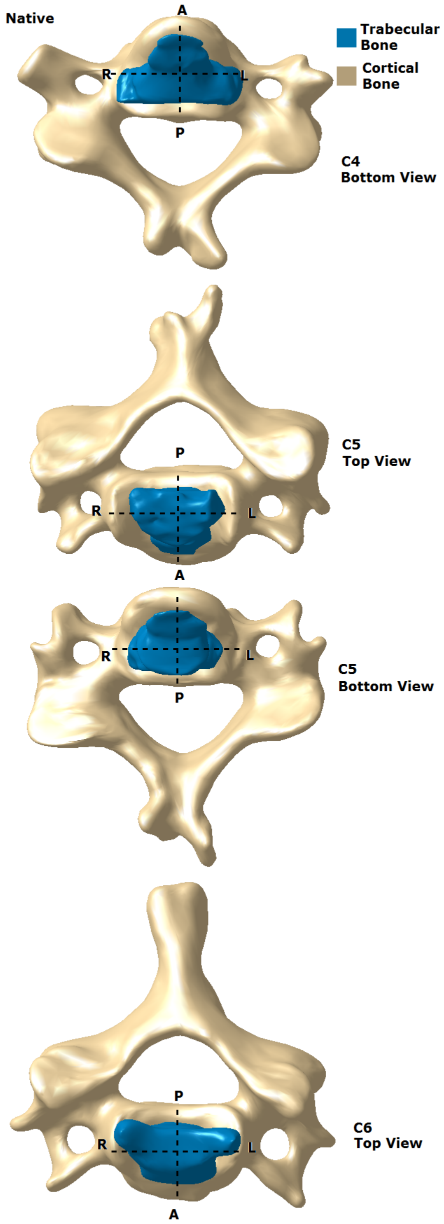

Figure 3.38: Analysed trabecular bone's location in the vertebrae.

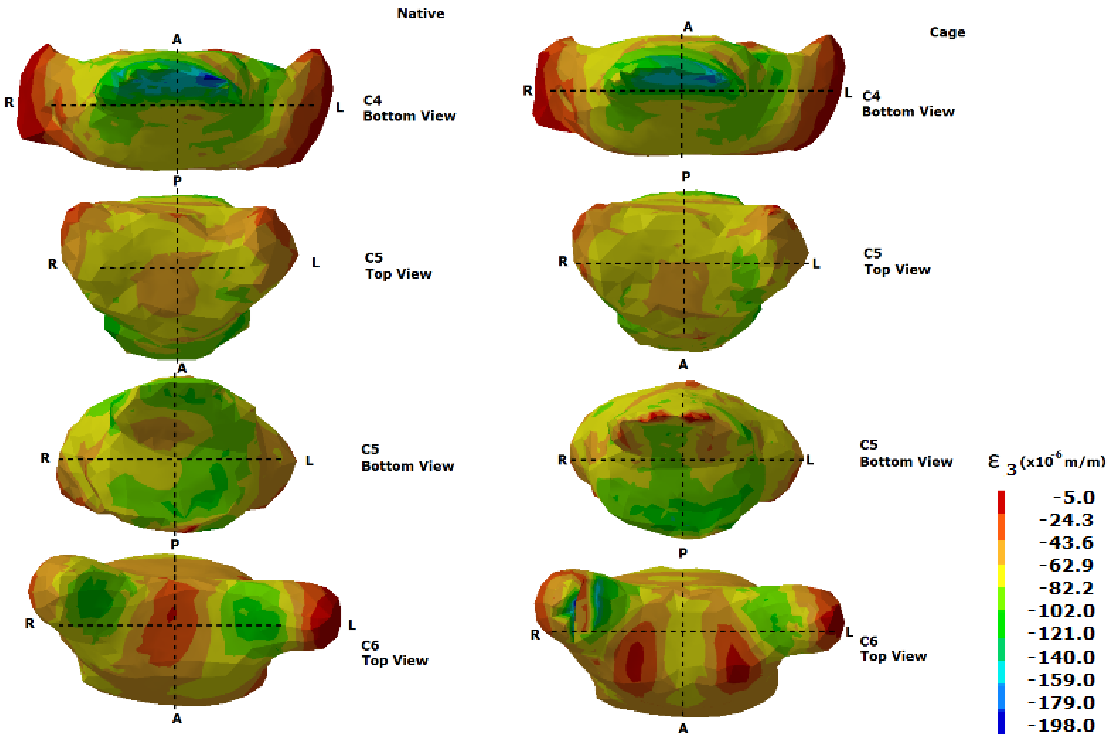

Figure 3.39: Cage and Native Model Strain Comparison - Trabecular Bone.

By looking at this last figure the differences between one model and the other are clearly shown to occur mostly in the C5 Bottom View and the C6 Top View, where an increase in strain on the trabecular bone in the posterior and lateral areas is shown. These areas are where the Fidji Cage is mostly supported on the cortical bone, thus seeming to affect the same areas on the trabecular bone. In vertebra C6 in the Cage Model ε_3 values reach $-179.0x10^{-6}$ whereas in the Native Model (for the same vertebra) values onlly reach $-121x10^{-6}$.

3.3.2.3 Native Model versus Arthroplasty Model

Figures 3.40, 3.41, 3.42 and 3.43 represent the results regarding the comparison between the Native Model (with ligaments) and implanted ProDisc-C Model (also with ligaments).

The two cases (pre and post ossification) for the ProDisc-C are represented in orange and yellow respectively, whilst the native model is represented in blue.

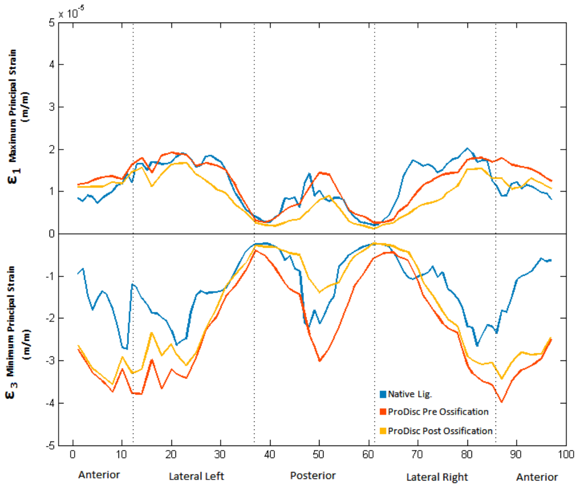

Figure 3.40: C4: ProDisc-C and Native Model Strain Comparison - Cortical Bone.

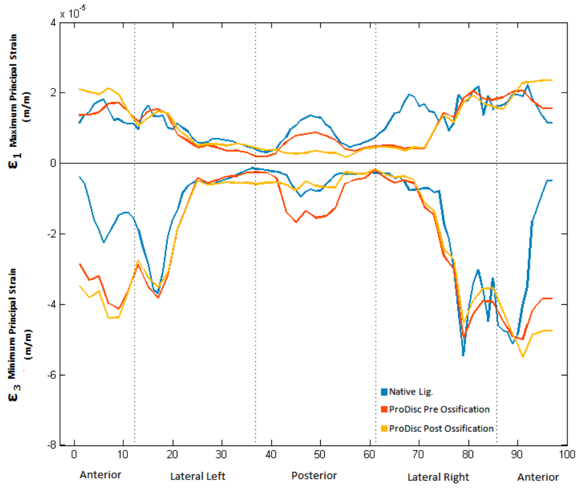

Figure 3.41: Upper C5: ProDisc-C and Native Model Strain Comparison - Cortical Bone.

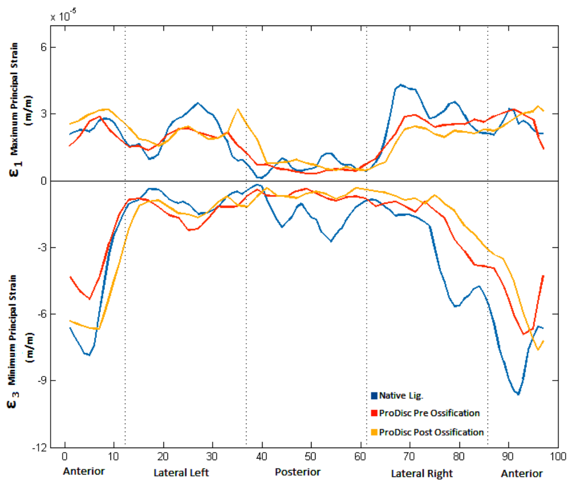

Figure 3.42: Lower C5: ProDisc-C and Native Model Strain Comparison - Cortical Bone.

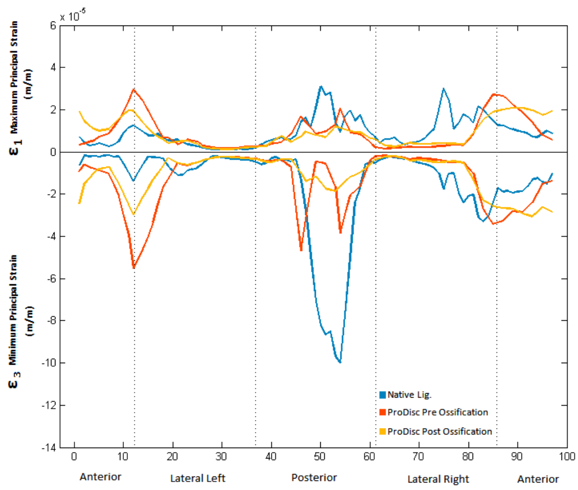

Figure 3.43: C6: ProDisc-C and Native Model Strain Comparison - Cortical Bone.

The results for vertebra C4 are displayed in figure 3.40. Absolute values were generally higher in the lateral areas reaching $-4.0x10^{-5}$ for ε_3 (Pre Ossification Cage Model) and $2.0x10^{-5}$ for ε_1. When comparing the Pre Ossification Model with the Post Ossification Model absolute values for the Pre Ossification Model are higher than those for the Post Ossification Model. The biggest difference between these two models was in the posterior section. For ε_1, values for the Pre Ossification Model ($1.0x10^{-5}$) were 50% higher than those of the Post Ossification Model ($1.5x10^{-5}$). For ε_3 absolute values in the Pre Ossification Model ($1.5x10^{-5}$) were double those obtained for the Post Ossification Model ($3.0x10^{-5}$). Comparing the Pre Ossification Model with the Native Model, absolute values of ε_3 were practically always higher in the former than in the latter, while ε_1 values were practically the same in these models. The biggest difference between ε_3 values in these two models was in the lateral right area where Pre Ossification Model values ($-4.0x10^{-5}$) were twice as large as those in the Native Model ($-2.0x10^{-5}$). ε_1 values were practically the same for both these models. The biggest difference between these two models for ε_1 values was in the lateral right/anterior area, where Native Model values ($1.5x10^{-5}$) were up to 30% higher than the values in the Pre Ossification Model ($1.0x10^{-5}$). Comparing the Post Ossification Model with the Native Model, absolute values of ε_3 were always higher than those of the Native Model, except in the posterior area. The biggest difference between ε_3 values in these two models was in the anterior area since Post Ossification Model values ($-3.0x10^{-5}$) were triple the value of those in the Native Model ($-1.0x10^{-5}$). Absolute values of ε_1 were practically the same in both models. The biggest difference between these two models for ε_1 values was in the lateral right area since Native Model values ($-1.5x10^{-5}$) were also triple those of Post Ossification Model ($-0.5x10^{-5}$).

In figure 3.41 results for the upper guideline of vertebra C5 are visible. All values were generally the same for this case. Peaks were registered in the lateral areas reaching $-5.5x10^{-5}$ for ε_3 and $2.0x10^{-5}$ for ε_1. When comparing the Pre Ossification Model with the Post Ossification Model values are practically the same for both these models. The biggest difference between these two models was in the posterior section. For ε_1, values for the Pre Ossification Model ($1.0x10^{-5}$) were double those of the Post Ossification Model ($0.5x10^{-5}$). For ε_3 absolute values in the Pre Ossification Model ($-1.6x10^{-5}$) were also double those obtained for the Post Ossification Model ($-0.8x10^{-5}$). Comparing the Pre Ossification Model with the Native Model, absolute values were practically the same in both these models. The biggest difference between ε_3 values in these two models was in the anterior area since Pre Ossification Model values ($-4.0x10^{-5}$) were up to 8 times higher than those registered in the Native Model ($-0.5x10^{-5}$). ε_1 values were also practically the same in both these models and the biggest difference for ε_1 values was in the lateral right area where Native Model values ($2.0x10^{-5}$) were up to 4 times higher than the values in the Pre Ossification Model ($0.5x10^{-5}$). Comparing the Post Ossification Model with the Native Model, absolute values of ε_3 were also practically the same in both models. The biggest difference between ε_3 values in these two models was in the anterior area, where Post Ossification Model values ($-5.0x10^{-5}$) were up to 10 times higher than the values registered for the Native Model ($-0.5x10^{-5}$). ε_1 values were practically the same in both models. The biggest difference between these two models for ε_1 values was in the lateral right area since Native Model values ($-2.0x10^{-5}$) were up to 4 times higher than those registered for the Post Ossification Model ($-0.5x10^{-5}$).

In figure 3.42 results for the lower guideline of vertebra C5 are visible. All values were also generally the same for this case. Peaks were registered in the anterior area reaching $-9.0x10^{-5}$ for ε_3 and $4.5x10^{-5}$ for ε_1 in the Native Model. When comparing the Pre Ossification Model with the Post Ossification Model greater differences were noted in the lateral left and posterior areas for ε_1 values since these were practically twice as high in the Post Ossification Model than in the Pre Ossification Model, however the greater difference in these models in the ε_3 absolute values was in the anterior area of the vertebra where Post Ossification values were 30% higher than the Pre Ossification values. Comparing the Pre Ossification Model with the Native Model, absolute values were higher in the Native Model in the anterior area of the vertebral body. This difference was greater when Native Model values ($-9.0x10^{-5}$) were up to 22% higher than those registered in the Pre Ossification Model ($-7.0x10^{-5}$). ε_1 values were practically the same in both these models, except for in the lateral right area of the vertebra where the value of ε_1 for the Native Model ($4.5x10^{-5}$) was 33% higher than that for the Pre Ossification Model ($3.0x10^{-5}$). Comparing the Post Ossification Model with the Native Model, the maximum value of ε_3 was noted in the right/anterior area of the Native Model ($9.0x10^{-5}$), which was double that registered for the Post Ossification Model ($5.0x10^{-5}$). ε_1 values were practically the same in both models with the exception of the values registered in lateral right area of the vertebra, which were almost double in the Native Model ($4.5x10^5$) compared to the Post Ossification Model ($2.5x10^5$). Lastly, in vertebra C6 (figure 3.43) the highest peaks were observed for the Native Model curve, in the posterior area of the vertebral body, with values of ε_3 and ε_1 of $-10x10^{-5}$ and $3.0x10^{-5}$ respectively. When comparing the Pre Ossification Model with the Post Ossification Model it was noted that ε_1 was 50% higher in the Pre Ossification Model, in the the anterior/lateral left areas of the vertebra. In these two areas as well as in the posterior area the absolute values of ε_3 were double in the Pre Ossification Model compared to the Post Ossification Model. Comparing the former with the Native Model, higher absolute values were noted for the Native Model, in the posterior area and lower in the anterior/lateral left areas of the vertebral body. The maximum value of ε_3 registered in the posterior area was twice as big in the Native Model ($-10.0x10^{-5}$) compared to that in the Pre Ossification Model ($-5.0x10^{-5}$). The highest value for ε_1 was noted in the posterior area of the Native Model ($3.0x10^{-5}$), and was 3 times than that registered in the same area for the Pre Ossification Model ($1.0x10^{-5}$). Comparing the Post Ossification Model with the Native Model, absolute values were, once more, higher in the latter, in the posterior area, and lower in the anterior/lateral left areas of the vertebral body. The maximum value of ε_3 was registered in the posterior area, where the value for the Native Model ($10.0x10^5$)was 5 times greater than that registered for the Post Ossification Model ($2.0x10^5$). The biggest difference for ε_1 values was also registered in the posterior area, where Native Model values $3.0x10^5$) were up to 3 times higher than those for the Post Ossification Model $1.0x10^5$).

Results show that, as a general rule, strain values for the case where the ProDisc-C has not yet had time to be "absorbed" by the bone (pre ossification, represented in orange) are higher than the ones obtained for the case where ossification had already taken place (represented in yellow).

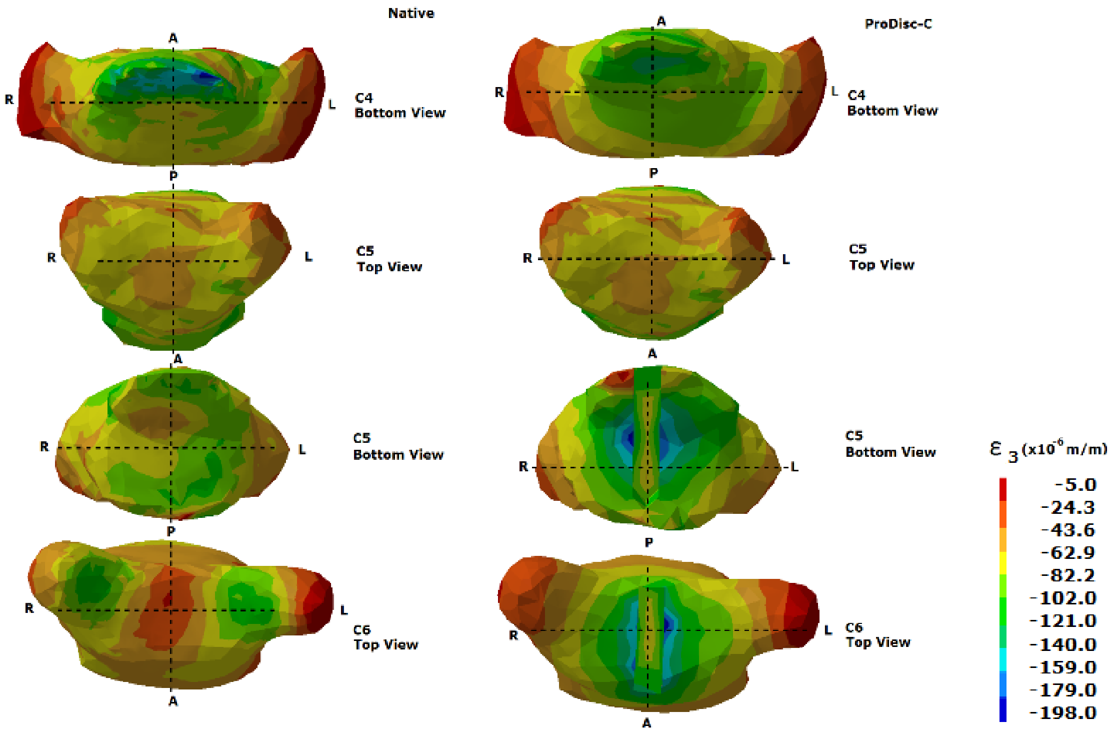

Figure 3.44: Native and ProDisc-C Model Strain Comparison - Trabecular Bone.

In figure 3.44 the comparison between the Native and ProDisc-C Models in the trabecular bone is shown.

The main difference between these two models is due to the fact that some of the trabecular bone had to be removed from vertebrae C5 and C6 in order to accommodate the implant's fixating fins. This resulted in an increase in strain in the trabecular bone of these two vertebrae in the central area (trabecular bone/ProDisc-C interface).

Once more in this comparison, compressive values in vertebra C6 are higher in the ProDisc-C Model ($-198.0x10^{-6}$) than in the Native Model ($-121.0x10^{-6}$).

3.3.2.4 Arthrodesis Model versus Arthroplasty Model

The last comparison to be made between models was between the ProDisc-C Model and the Fidji Cage Model. The same colour scheme was used for the graphs, where ProDisc-C models are represented in orange and yellow, while Fidji Cage Models are represented in light and dark green. Again, one graph was created for each one of the guidelines.

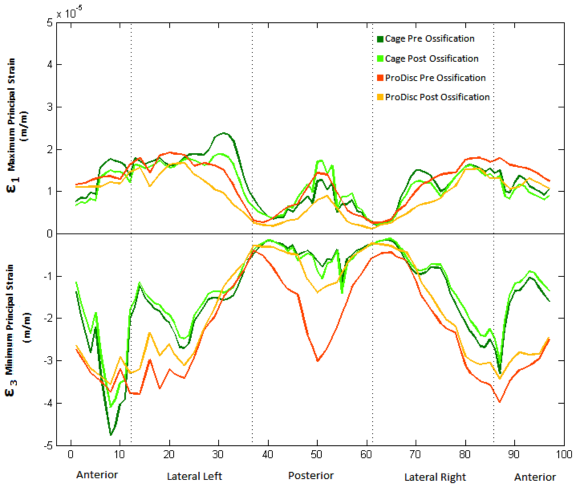

Figure 3.45: C4: ProDisc-C and Fidji Cage Model Strain Comparison - Cortical Bone.

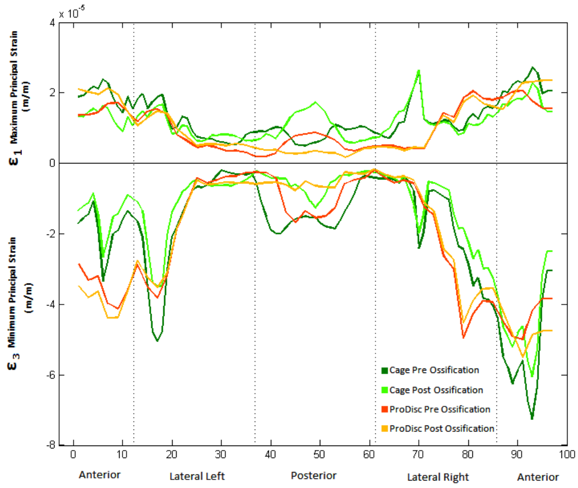

Figure 3.46: Upper C5: ProDisc-C and Fidji Cage Model Strain Comparison - Cortical Bone.

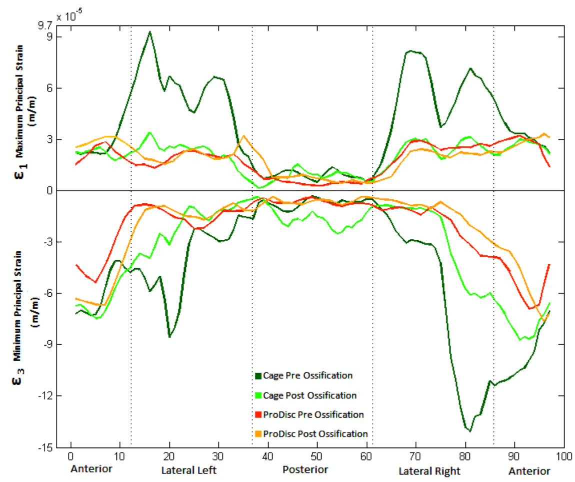

Figure 3.47: Lower C5: ProDisc-C and Fidji Cage Model Strain Comparison - Cortical Bone.

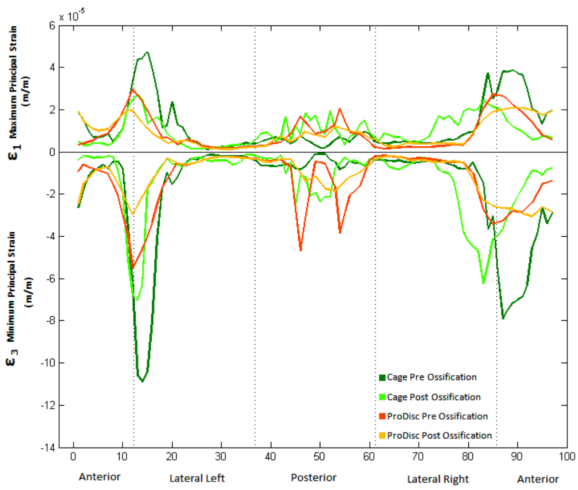

Figure 3.48: C6: ProDisc-C and Fidji Cage Model Strain Comparison - Cortical Bone.

In figure 3.45 the values for the four models (Pre and Post Ossification Cage Models and Pre and Post Ossification ProDisc-C Models) obtained for vertebra C4 are presented. Values were higher in the lateral and anterior areas of the vertebral body. Absolute peak values were obtained for the Pre Ossification Cage Model, $2.3x10^{-5}$ and $-4.8x10^{-5}$ for ε_1 and ε_3 respectively. The biggest difference between the Cage and ProDisc-C Models was in the value of $\varepsilon 3$ in the posterior area of the vertebral body where values for the Pre Ossification ProDisc-C Model were as high as $-3.0x10^{-5}$ and all other models present values close to $-1.0x10^{-5}$.

In figure 3.46 peak values were once more observed in the lateral areas of the superior surface of the C5 vertebral body. Maximum values were obtained for the Pre Ossification Cage Model ($3.0x10^{-5}$ and $-7.0x10^{-5}$ for ε_1 and ε_3 respectively). Analysing firstly the Pre Ossification Models, peak absolute values of principal strain were generally higher in the Cage Model than in the ProDisc-C Model. This was also true when analysing the Post Ossification Models.

In the lower surface of the C5 vertebra (see figure 3.47) peak values were observed in the lateral areas of the vertebral body for the Cage Models, and in the anterior area for the ProDisc-C Models. When analysing the two cases of Pre Ossification, the peak values for ε_1 and ε_3 for the Cage Model were $9.0x10^{-5}$ and $-14.0x10^{-5}$, while for the ProDisc-C model they were $3.0x10^{-5}$ and $-6.0x10^{-5}$ respectively,. When analysing the two cases of Post Ossification, the peak values for ε_1 and ε_3 for the Cage Model were $3.0x10^{-5}$ and $-9.0x10^{-5}$, while for the ProDisc-C model they were $3.0x10^{-5}$ and $-7.0x10^{-5}$ respectively. The results obtained for the Pre Ossification Cage Model were the furthest away from the other three models.

In the last graph (see figure 3.48) values for the C6 vertebra are presented. Peak values were observed in the anterior/lateral left and lateral right/anterior areas. However, in the posterior area, compressive values for the Pre Ossification ProDisc-C Model also peaked.

The ε_3 values for the ProDisc-C Model ($-6.0x10^-5$) were up to double those for the Cage Model ($-12.0x10^{-5}$), in the lateral areas. The higher absolute values were observed for the Cage Models. Similarly, the maximum values of ε_1 were $4.0x10^{-5}$ and $2.0x10^{-5}$ for the Cage and ProDisc-C models respectively.

When comparing the Pre Ossification Models, the posterior area of the vertebra was the only place where principal strain absolute values were higher in the ProDisc-C Model than in the Cage Model.

By observing these results, and even though implanted models seem to follow more or less the same patterns, there seems to be a greater discrepancy between Cage models and ProDisc-C models in the Lower C5 (figure 3.47)and C6 (figure 3.48) cases for the right and left lateral areas. For these two graphs the absolute values for maximum and minimum principal strain appear to be significantly greater for the Fidji Cage models than for the ProDisc-C models.

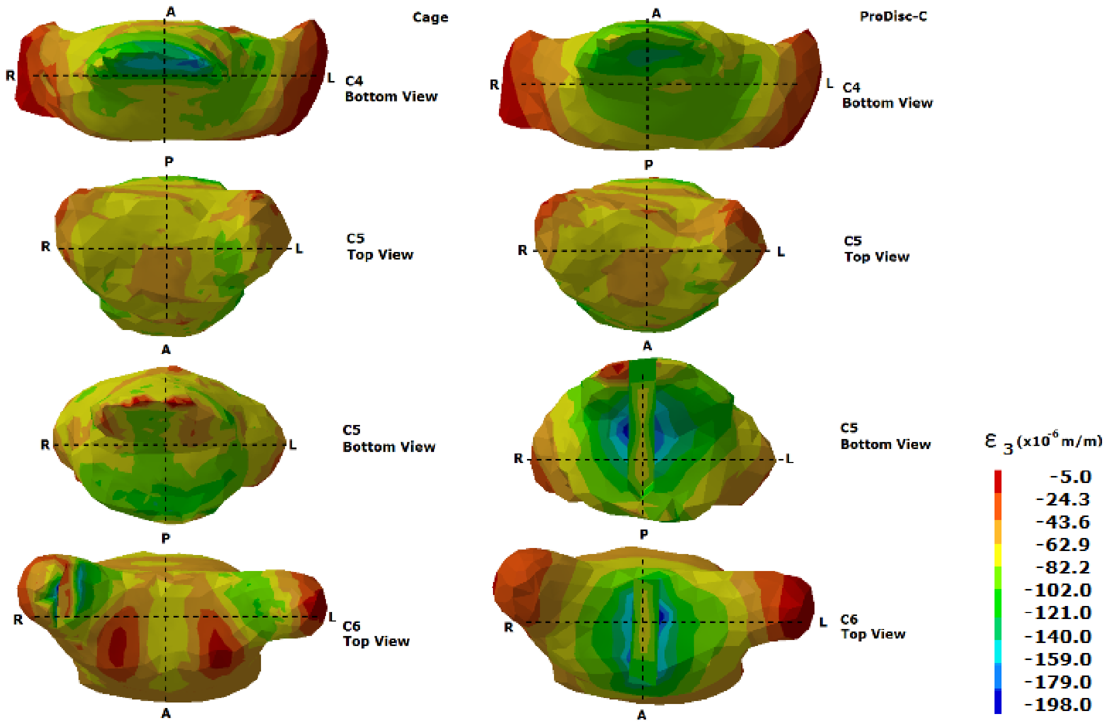

Figure 3.49: Cage and ProDisc-C ModelsStrain Comparison - Trabecular Bone.

In figure 3.49 the comparison between the Cage and ProDisc-C Models in the trabecular bone is shown. Geometrically, the main difference in these two models is due to the fact that the trabecular components have been altered so as to better accomodate each implant.

Due to the fact that more bone was removed in both cortical and trabecular components from the C5 and C6 vertebrae to accommodate the ProDisc-C model, the trabecular bone shown in figure 3.49 for this model is the one that presents higher absolute values for minimum principal strain. In the ProDisc-C model compressive strain values of up to $-198x10^{-6}$ are visible in Lower C5 and C6 images, while the highest value of compressive strain recorded for the trabecular bone for the Cage was $-159x10^{-6}$.

3.4 Discussion

When creating the numerical models for simulation, it's important to mention that a lot of time (due to the trial and error approach) was required in reaching the decisions concerning what simplifications would be made and what programmes would be used for simulation. There was hardly any information regarding the use of the required software, and multiple versions and the programmes were tried (Simpleware programmes and Marc). Three different Simpleware programmes were used to create a numeric model (ScanIP, ScanCAD and ScanFE), and numerous permutations were tried, unsuccessfully, so as to be able to use only Marc for simulation, thus leading to the discretization of the model (computed in Catia).

As far as the results obtained are concerned, the comparison between the Specific and Discretized Patient Models will be discussed first. As observed, even though both models were composed of three vertebrae and two discs obtained from the exact same initial model, there were clear differences between Principal Strain levels. In some sections of the graphs Specific Patient Native Model's results are higher than those of the Discretized Patient Native Model, but in other sections the opposite applies. This difference may be justified by the fact that material properties of the Specific Patient Native Model vary, cortical bone values vary from 2GPa to 12 GPa.

Considering that each value was taken from nodes in a particular location from which results were extracted for the Discretized Patient Native Model, the variation of Principal Strain values could only be justified by the difference in material properties. Bearing this in mind and after verifying the material properties of a couple of elements in the Specific Patient Native Model it was concluded that for the areas in the graph where absolute values, for this model, were higher than those obtained for the Discretized Patient Native Model, these coincided with elements that possessed an Elastic modulus superior to the Elastic modulus allocated to the Discretized Patient Native Model cortical bone. The same principle applies for areas of the graphs where the Specific Patient Native Model absolute values were inferior to those of the Discretized Patient Native Model, seeing as when this happens, the elements in the Specific Model mesh possess an inferior Elastic modulus to that of the equivalent Discretized Model elements.

Seeing as the Specific Patient Native Model's elements had a variation in their mechanical properties, this made the model more susceptible to Principal Strain variations than the Discretized Patient Native Model (that had a constant Elastic modulus value for all elements in a vertebra). Kumaresan et. al. [54] reported values of micro strain of approximately 200, 400, 500 and 700, for compressive forces of 200, 400, 600 and 800 N applied on a C4-C6 numerical segment respectively. In other words, strain increased with the load applied. Since the Specific and Discretized Patient Native Models were simulated with a load of 100 N, and registered peak compressive strain values of approximately 120 me, these Specific and Discretized Native Models seem to be in agreement with Kumaresan et. al.'s findings.

Results for the ligament analysis were clear and predictable. Imagining a ligament as a vertical elastic string, if a compressive load were applied to the ligament along its length, the ligament would not counter-react the compressive force at all. However if it were an extension force then the ligament would naturally oppose this force and limit it.

In the models created the ligaments were created as spring-like bodies (since this was the only option available at the time), meaning that they would react to both compressive and extension forces. Bearing in mind that ε_1 represents an extension strain and ε_3 represents compression strain, this was verified since ligaments affected both ε_1 and ε_3 values. Ideally, if ligaments had been created for limiting the node's extension only, then graphically there would be a difference in the ε_1 values for each model but no difference would have been visible for ε_3 values.

Once this error was accounted for, and knowing that ligaments would restrain the model's movement it was predicted that the model with ligaments would have greater absolute Principle Strain values. By observing the resulting graphs for this part of the study, this point is clear since the red line (model with no ligaments) corresponds to values inferior to those of the blue line (model with ligaments).

In the comparison between the Native Model and the Cage model there was a distinct difference for the posterior area of the C6 vertebra. This may be due to the positioning of the cervical cage on the vertebra. It's possible that the area occupied by the intervertebral disc on the posterior part of the vertebral bodies wasn't the same as the one occupied by the Fidji Cage. In other words, if the nodes on the guideline in the posterior section of the C6 vertebra were very close to the C5/C6 intervertebral disc, but then were further away from the implanted Cage, when the force is transferred from C5 to C6 through the disc (or cage) these nodes will be affected in a different way. The nodes closer to the load transfer (case of the Native Model) will show higher strain values than those that are further away from it (case of the Cage Model).

The Cage's geometry is also an important factor in this discussion. Even though the upper surface of the Fidji Cage is curved, the contact area between vertebrae (C5 and C6) and the Cage is never as big as the contact area between these vertebrae and the intervertebral disc. For this reason strain will be bigger for the cervical Cage case, particularly where the Cage is actually in contact with the vertebrae. In this case the Cage was supported by the lateral sides of the vertebral bodies so these were the areas with the highest absolute values of principal strain. This fact also explains the increase in strain in the lateral areas of the trabecular bone.

Similar observations were made for the ProDisc-C model comparison with the Native model. And the same justification regarding the positioning of the implant is valid.

The trabecular bone presented a decrease in strain in the central part of of the C5 and C6 vertebral bodies, since once the ProDisc-C had been implanted most of the strain was transferred to the cortical bone.

The ProDisc-C's main advantage is that, in theory, it doesn't alter the biomechanics of the cervical spine as much as a cervical fusion Cage. The results, for the ProDisc-C/Cage comparison, indicate that at the implant interface (C5/C6) the absolute values of Principal Strain seem generally higher in the Cage model, confirming the theoretical advantage of the ProDisc-C over the cervical Cage.

Chapter 4

Experimental models of C5-C6 segment

4.1 Introduction

This chapter concerns the experimental part of this study. The experimental models were created with the purpose of being compared to the computational models, so as to ascertain if the latter could be considered a valid recreation of a "real" physical model.

The construction process of the various experimental models is explained in this chapter. The results obtained from these models were then discussed.

4.2 Materials and Methods

Only three basic models were recreated and studied experimentally. These models all consisted of vertebrae C5 and C6. The three different models are represented in figure 4.1. These are:

- C5 and C6 with an intervertebral disc - Experimental Native Model
- C5 and C6 with the ProDisc-C - Experimental ProDisc-C Model
- C5 and C6 with the Fidji Cage - Experimental Cage Model

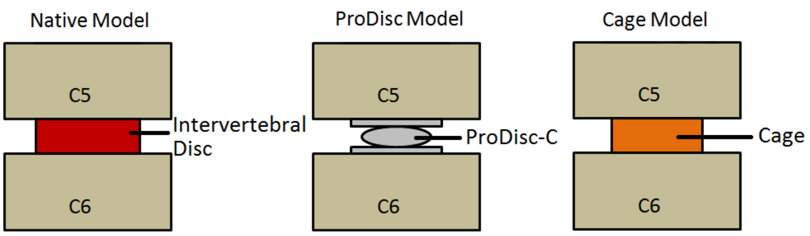

Figure 4.1: Simple representation of experimental models

These models were created from a Syntes Foam Cervical Model. Initially this experimental part of this study was to be performed using human cervical bones; however, due to lack of time and resources this option was quickly put aside. Using the cervical spine of another animal was also considered, but cattle, swine or sheep were the only options available, and the geometry of the cervical vertebrae of these animals is so very different from that of the Human cervical vertebrae that the implants considered were incompatible with any of these.

Another option would have been to obtain a synthetic bone model, made of a material with the same mechanical properties as bone, such as a composite material composed of a mixture of short glass fibers and epoxy resin pressure-injected around a foam core (resembling trabecular bone). However this was not possible since there is no such cervical spine model available at present, and won't be until January 2012 (developed by Sawbone).

So the only option available was a Rigid Polyurethane (PUR) Foam model developed by Synebone[1]: 9334 Spine cervical Occiput.

Figure 4.2: Synbone PUR foam model (www.synbone.ch)

Since the intervertebral discs were made of a material whose mechanical properties were very different to those of a human intervertebral disc, there was no visible point in using the same segment of the cervical spine that was used for the numerical models and analyzing stress/strain levels on the C4 vertebrae since force transfer would be very different. Therefore the studied experimental segment was C5-C6.

4.2.1 Experimental Native Model

This model was created from the Cervical Model represented in figure 4.2. In figure 4.3 a white strip is clearly visible on the anterior surfaces of the vertebrae's model. This strip was removed and the C5 and C6 segment were separated from the rest of the vertebrae. Any bits of foam or glue (see figure 4.3) that may have been left over from the rest of the model were removed with a file.

Once this was done it was necessary to create a structure to allow the model to be placed correctly on the loading machine, ensuring the force was applied in the correct place and direction, and preventing it from collapsing or breaking.

In figure 4.4 all pieces used for the assembly of the Native Model are visible. The upper vertebral support (far left), bottom cylinder for supporting C6 vertebrae screwed to the base, screw, and a ring to make up for the space between the model and the loading machine.

Once these different pieces were obtained the experimental model was assembled. Vertebrae C5 and C6 were glued (Araldite Super Strength epoxy adhesive) to the upper vertebral support and bottom cylinder.

[1]SYNBONE [Anatomical Models for Education]

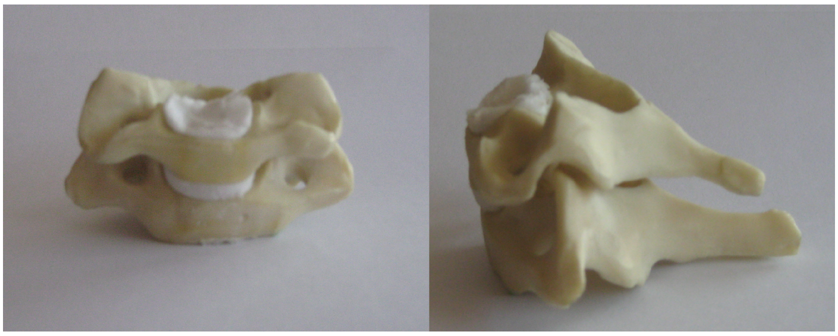

Figure 4.3: Frontal and Lateral view of the separated segment.

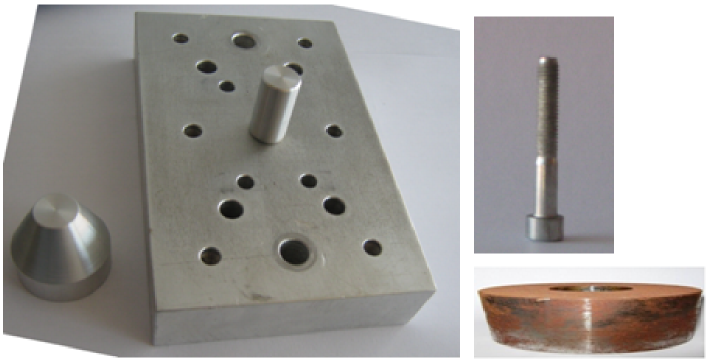

Figure 4.4: All pieces used for experimental assembly.

So as to equally analyze how each model behaved in terms of principal strain, a pair of strain gauges were placed on the PUR model. A strain gauge is a transducer capable of measuring deformations on the body they have been attached to.

The principal strain levels were measured on the "cortical" surface of the vertebrae.

Figure 4.5 shows the assembled model with the strain gauges fixed to the vertebrae.

When a strain gauge has been attached to the model, and a force is applied on this model that causes it to shrink or extend, any shrinkage or extension of the model will affect the length of the filaments in the strain gauges' rosette, thus altering the diameter of this rosette and consequently its electrical resistance.

Therefore, by measuring the variation of the electric resistance of the conductive filaments, we can obtain a continuous and precise reading of the strain felt on the body when any loads are applied.

Tri-axial strain gauges (KFG-3-120-D17-11L3M2S, Kyowa Electronic Instruments Co, Ltd, Tokyo, Japan) were chosen as the measurement system.

The tri-axial strain gauge contains three filaments aligned at a 45° angle to each other, which allows enough information to completely describe Cauchy's stress tensor on the models.

The minimum and maximum principal strains (ε_1 and ε_2) were the main variables assessed in this part of the study.

For each vertebrae, the principal strains were calculated using each strain filament (ε_a, ε_b and ε_c) of each strain gauge.

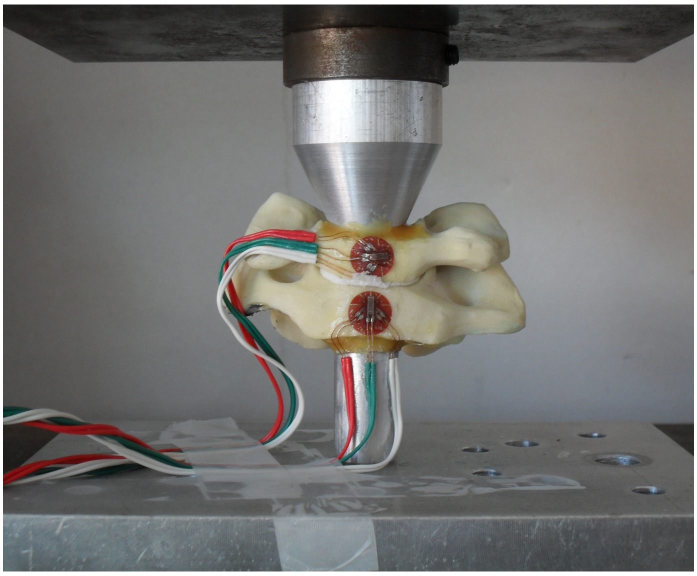

Figure 4.5: Assembled native experimental model.

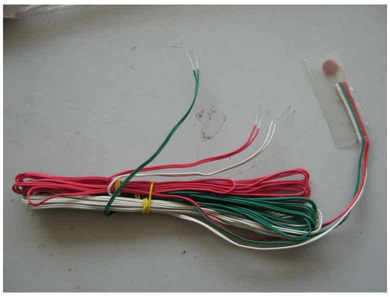

Figure 4.6: A single strain gauge.

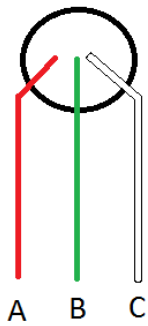

Figure 4.7: Representation of strain gauge colours and corresponding letters.

The values obtained in each filament were registered and using the mathematical expressions 4.1 and 4.2 the maximum and minimum principal strains were calculated.

$$\varepsilon_1 = 0,5(\varepsilon_a + \varepsilon_c) + 0,5\sqrt{(\varepsilon_a - \varepsilon_c)^2 + (2\varepsilon_b - \varepsilon_c - \varepsilon_a)^2} \tag{4.1}$$

$$\varepsilon_2 = 0,5(\varepsilon_a - \varepsilon_c) + 0,5\sqrt{(\varepsilon_a - \varepsilon_c)^2 + (2\varepsilon_b - \varepsilon_c - \varepsilon_a)^2} \tag{4.2}$$

In figure 4.7 the letters A, B and C correspond to the variables ε_a, ε_b and ε_c respectively.

For each different case five measurements were made for each of the experimental models.

The positions of the strain gauges were selected with the purpose of measuring the strains on the anterior surface of the vertebral body, since the vertebrae were quite small in relation to the strain gauges' rosette and didn't fit anywhere else that would allow a correct fixation of the rosette on the vertebrae.

Once the vertebral surfaces were filed and clean of any dust, a little portion of glue was applied on the back of the gauges and then these were placed on the vertebral surfaces by pressing the rosettes against the surface of each one of the vertebrae. Pressure was applied on the rosettes for about a minute so as to ensure correct fixation.

Note that on vertebra C5 the central filament of the strain gauge is in a horizontal position, whilst the C6 central filament of the strain gauge is in a vertical position (see figure 4.5). Considering a vertical load was applied on vertebra C5 ideally both strain gauges would have been placed in a vertical position (i.e. placement on C6), so as to maximize measured strain levels. However this was not possible due to the lack of space on the anterior surface of the C5 vertebra. If the gauge had been placed vertically, the filaments wouldn't have been correctly placed on the vertebrae and would certainly all have been destroyed when the ProDisc-C was inserted.

Once strain gauges were attached to the vertebrae, each one was identified according to what vertebrae it was attached to.

Before the connection between strain gauges and the acquisition data software was done, the internal resistance of the strain gauges was checked, and the internal resistance of 120Ω (recommended by the supplier) was confirmed.

Figure 4.8: Multimeter used to measure resistance.

After this, all the components of the experimental setup were connected. This procedure was done with great care, and double checked, to ensure that none of the wires were mistaken for each other, since this would have led to serious errors.

All strain gauges were connected to the National Instruments PXI 1050 acquisition data system, which in turn was connected to a computer where the results were stored and processed by a Lab View Signal Express application.

The Experimental Native Model was then inserted in the loading machine and the force of 50N was applied vertically to the model. This system as a whole is represented in figure 4.9.

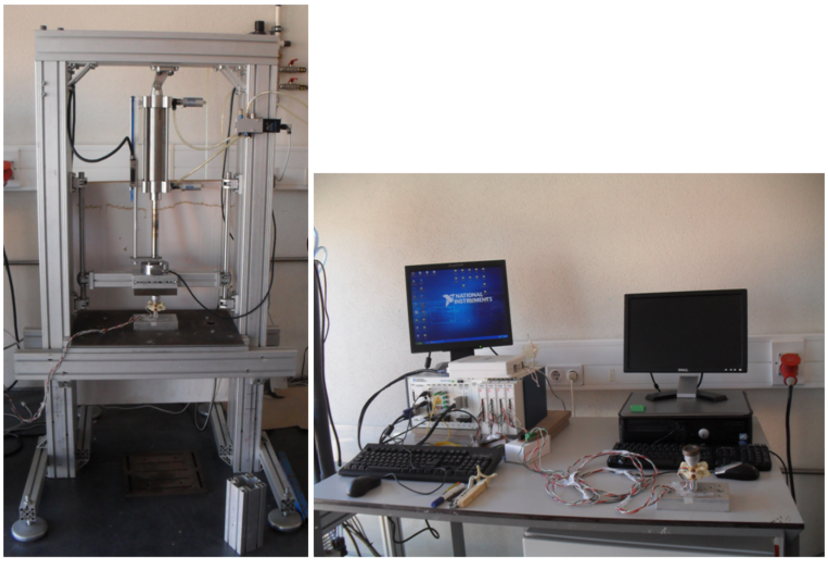

Figure 4.9: Left: Experimental Native Model during loading test. Right: National Instruments PXI 1050 acquisition data system and necessary computers.

Once the 5 tests were performed and results extracted and saved, the Experimental Cage Model was created.

4.2.2 Experimental Cage Model

For the Experimental Cage Model, the Experimental Native Model was used and altered. The intervertebral disc foam was carefully removed so as not to damage strain gauges.

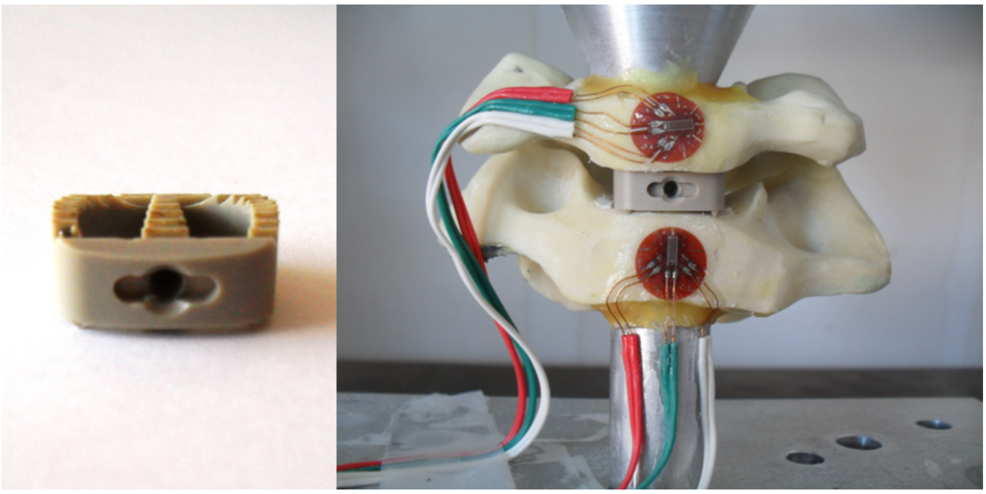

Figure 4.10: On the left: Fidji Cervical Cage; On the right: Experimental Cage Model.

Once again, a file was used to remove any remains of disc foam. The Fidji Cage (see figure 4.10) was placed in the intervertebral space so as to determine where some of the "bone" would have to be removed to ensure its correct placement. Once it was ascertained where the Cage would rest on the bones, the appropriate amount of "bone" was removed with a file. Material was removed mostly from the lateral area of the vertebral body to better accommodate the cervical Cage. A very small amount of super-glue was applied to the upper and bottom surfaces of the C6 and C5 vertebra respectively so ensure fixation of the Cage.

No other alterations, other than those mentioned above, were done to the original model (Experimental Native Model).

Loading conditions were applied and results obtained in the same way as before. After the 5 tests were performed, the Cage was removed and the ProDisc-C was inserted.

4.2.3 Experimental ProDisc-C Model

For this model the Experimental Cage Model was taken apart so that the Cage could be removed. Once the Cage was removed the vertebrae had to be cut and scraped so that the ProDisc-C could be placed properly between them.

With the help of a pencil some marks were made on the vertebrae to ensure that the cut for the ProDisc-C's fins were done as accurately as possible.

Firstly, vertebra C6 was cut and shaped in order to accommodate the bottom part of the ProDisc-C (figure 4.11).

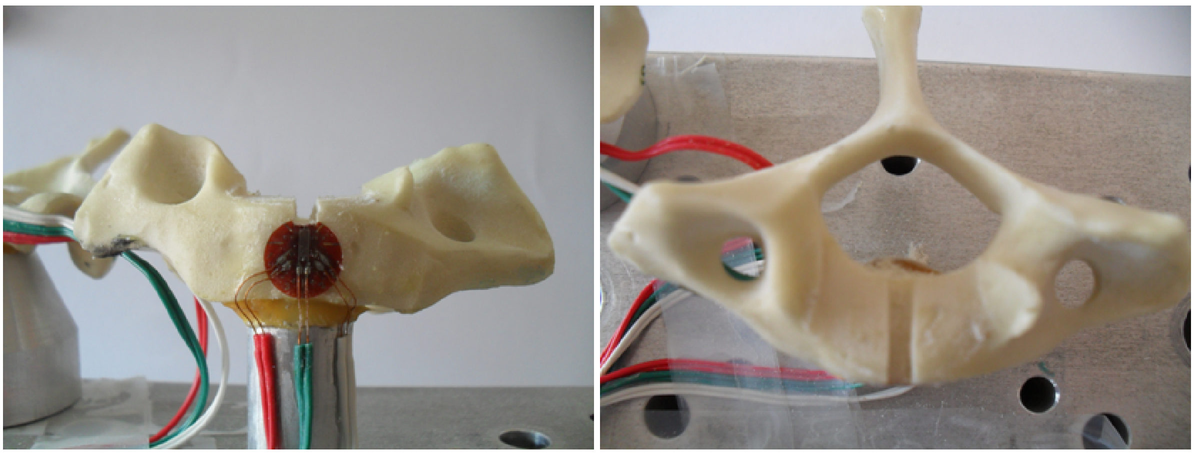

Figure 4.11: Cut and shaped vertebra C6 - frontal and upper view.

Once C6 was shaped, the inferior part of the ProDisc-C was inserted. This can be observed in figure 4.12.

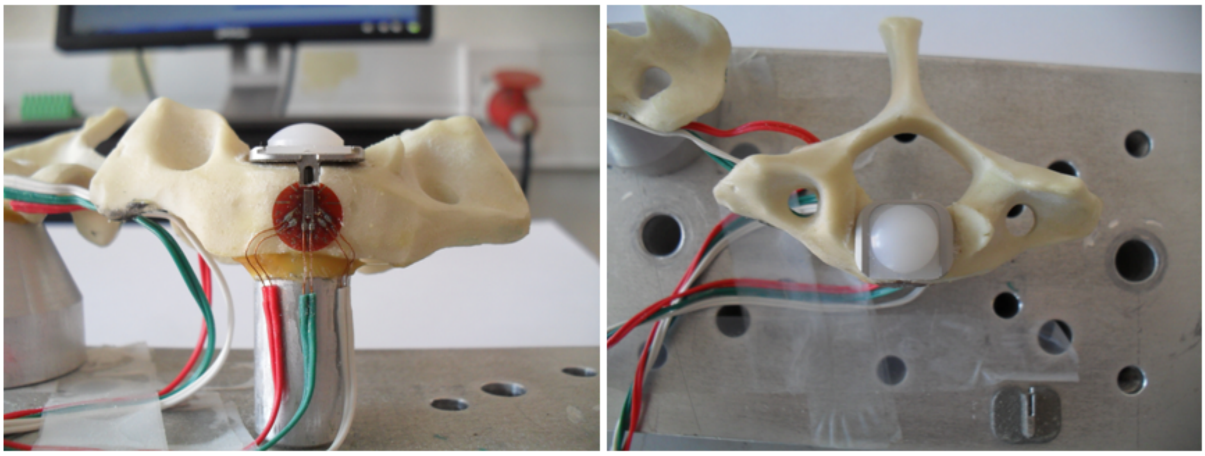

Figure 4.12: Vertebra C6 with ProDisc - frontal and upper view.

The same procedure was applied to vertebra C5.

During this process, one of the filaments of the C5 strain gauge was sacrificed so that the ProDisc-C's upper fin could be properly inserted into this vertebra.

To ensure the accuracy of the results obtained the measurements taken by the damaged filament were no longer considered.

In figure 4.13 the final experimental model is visible: C5 and C6 vertebrae with the ProDisc-C.

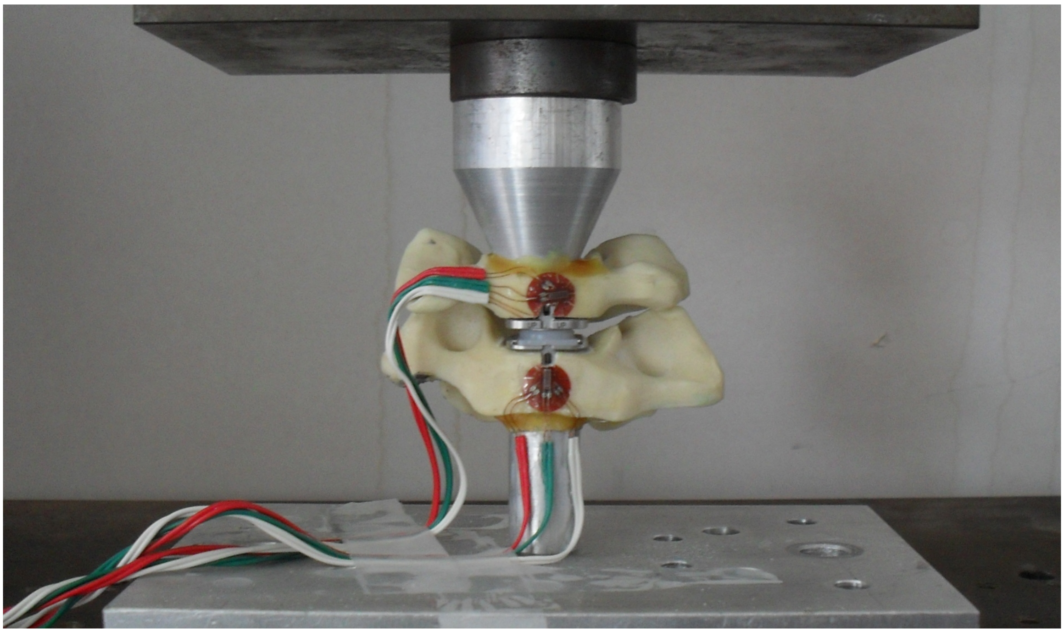

Figure 4.13: Experimental ProDisc-C Model.

4.3 Results

In this section all experimental results are presented. A comparison between numerical and experimental foam models was done so as to ascertain how well the former recreated the latter. Figure 4.14 represents the area where the strain gauges were attached, and consequently also the area from which results were extracted in the numerical foam models.

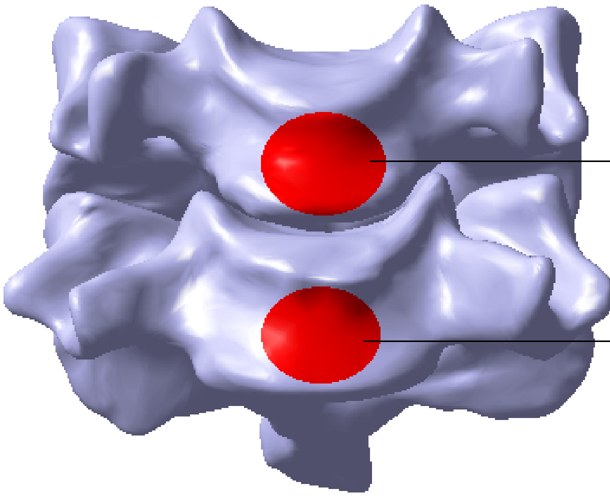

Figure 4.14: Representation of the area from which results were extracted.

In table 4.1 experimental results obtained for all models (with corresponding standard deviations) from each of the strain gauges (C5 and C6) are presented. Three different comparisons will be made between these results:

- Experimental Native Model vs Experimental Fidji Cage Model
- Experimental Native Model vs Experimental ProDisc-C Model
- Experimental Fidji Cage Model vs Experimental ProDisc-C Model

Table 4.1: Principal Strain Values ($x10^{-6}m/m$) - Experimental Results

Strain Gauge		Native Model		Cage Model		ProDisc-C Model	
		Mean Value	Standard Deviation [%]	Mean Value	Standard Deviation [%]	Mean Value	Standard Deviation [%]
C5	ε_2	-8.25	-31.50	-74.14	-44.20	-195.44	-31.50
	ε_1	20.36	7.70	70.02	11.30	220.91	3.30
C6	ε_2	-63.12	-67.80	-110.10	-42.50	-137.15	-13.10
	ε_1	386.57	-7.50	127.51	6.00	127.24	8.70

4.3.1 Numerical Analysis versus Experimental Analysis

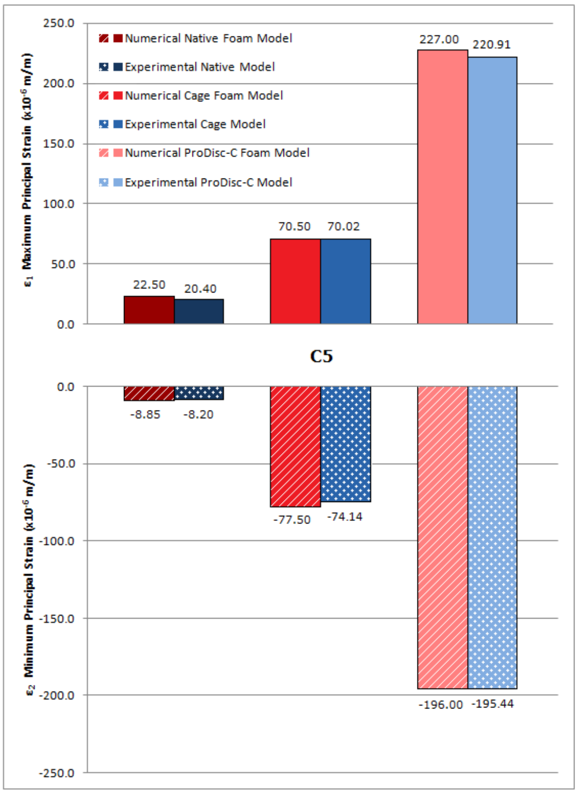

Figure 4.15: C5: Experimental vs Numerical principal strain results.

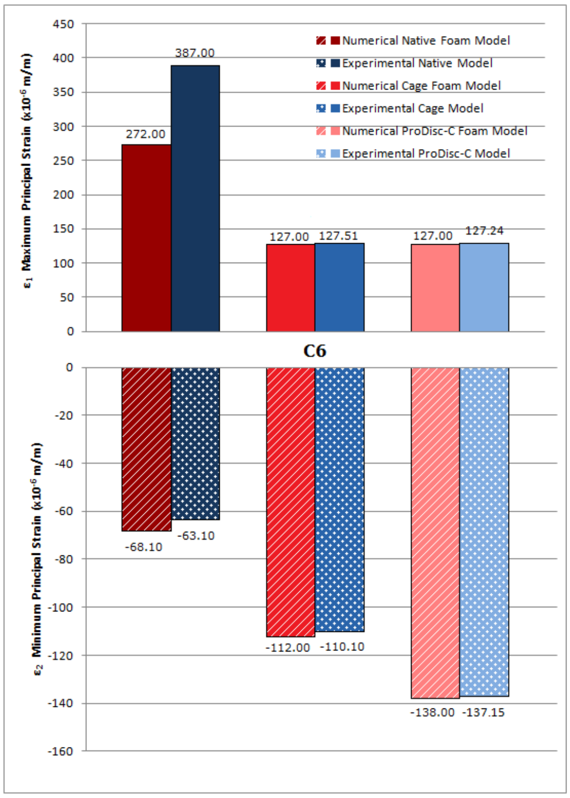

Figure 4.16: C6: Experimental vs Numerical principal strain results.

Experimental values were obtained for each one of the five loading cycles for the Native Model. Once these values were obtained maximum and minimum principle strain values (ε_1 and ε_2) were calculated and an average value was obtained. This experimental average value was then compared with values observed in the numerical foam models (Native, Cage and ProDisc-C Foam Models, C5-C6 segment) and can be viewed in figures 4.15 and 4.16.

In vertebra C5 (figure 4.15) all absolute values for ε_1 and ε_2 are higher in the numerical models than in the experimental models.

The biggest differences between ε_1 and ε_2 values across the three different models were registered in the Native Model, where ε_1 in the Experimental Native Model ($20.4x10^{-6}$) was 10% lower than in the Numerical Native Model ($22.5x10^{-6}$).

ε_2 decreased 7% in value from the Numerical Native Model ($-8.8x10^{-6}$) to the Experimental Native Model ($-8.2x10^{-6}$).

In the Cage Models this decrease was of 1% for ε_1, and of 4.3% for the absolute values of ε_2 . In the ProDisc-C Models the decrease was of 2.7% for ε_1, and of 0.3% for the absolute values of ε_2 .

In vertebra C6 (figure 4.16) all absolute values for ε_1 were higher in the Experimental Models, but all ε_2 were higher in the Numerical Models.

The biggest differences between ε_1 and ε_2 values across the three different models in this vertebra was also registered in the Native Model, where ε_1 in the Experimental Native Model

($387.0x10^{-6}$) was 40% higher than in the Numerical Native Model ($272.0x10^{-6}$). ε_2 decreased 7% in value from the Numerical Native Model ($68.1x10^{-6}$) to the Experimental Native Model ($63.1x10^{-6}$).

In the Cage Models this decrease was of 14% for ε_1, and of 2% for absolute values of ε_2. In the ProDisc-C Models the decrease was of 0.2% for ε_1, and of 0.6% for absolute values of ε_2.

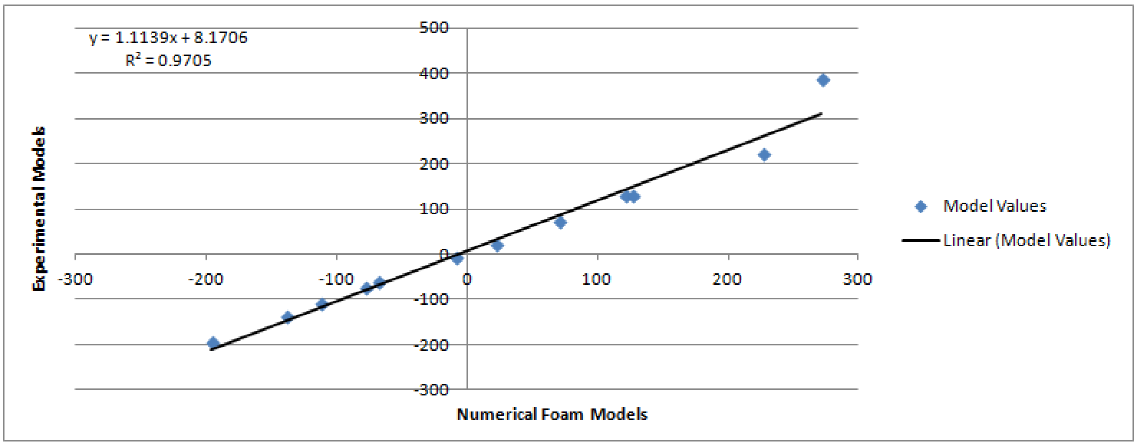

Figure 4.17: Numerical Model validation.

In figure 4.17 the linear regression of this comparison between Numerical and Experimental Models is presented. The value of the coefficient of determination R^2 is very near 1 (0.9705), $m = 1.1139$ and $b = 8.1706$ (when considering the linear regressions equation as $y = m * x + b$).

4.3.2 Native Model versus Implanted Models

Experimental Native Model vs Experimental Cage Model

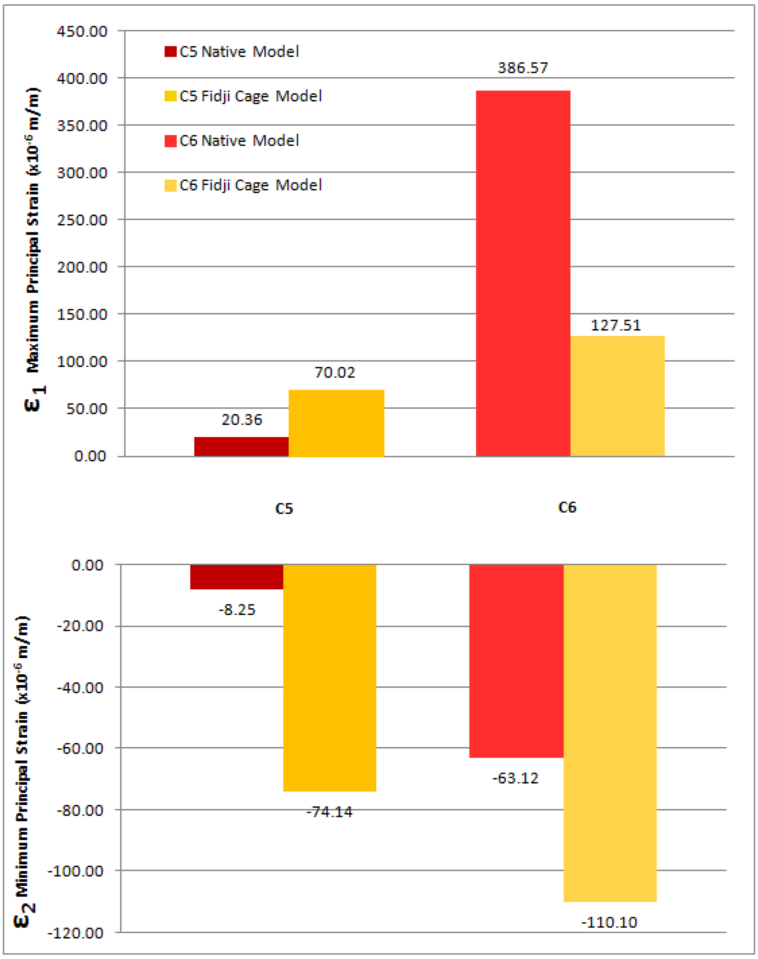

Figure 4.18: Strain results Native vs Cage model.

The Native and Cage models are compared in figure 4.18.

Compressive strain values increased in both vertebrae when inserting an implant.

The extension strain value (ε_1) in vertebra C5 and compressive strain value (ε_2) on the anterior surfaces of the vertebral bodies increased considerably from the Native model to the Cage model.

The value of ε_1 and ε_2, in vertebra C5, increased from the Native Model to the Cage Model by approximately 3.5 and 9 times respectively, for vertebra C5.

In vertebra C6 ε_1 values tripled from the Cage Model to the Native Model. However, ε_2 values in the Native Model were practically half those registered for the Cage Model.

Experimental Native Model vs Experimental ProDisc-C Model

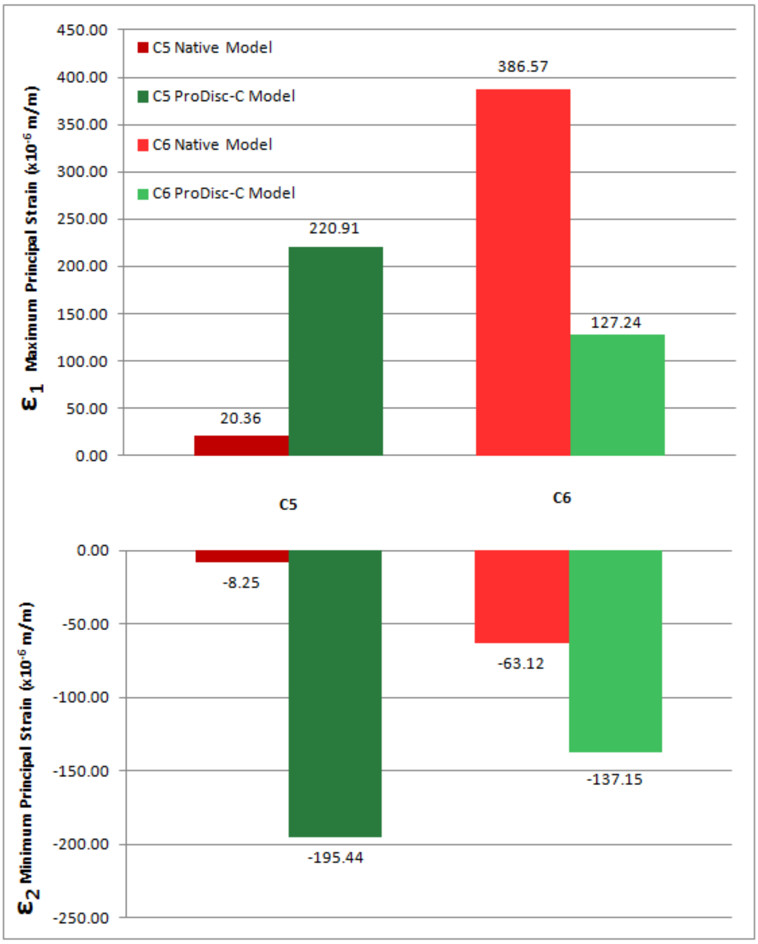

Figure 4.19: Strain results Native vs ProDisc-C model.

In this comparison, (see figure 4.19) the absolute values of strain were greater in the implanted model, with the exception of ε_1 for vertebra C6.

Contrary to the Cage Model comparison (see figure 4.18), where an increase in strain values from C5 to C6 was made evident in both models, in the comparison above (see figure 4.19) the absolute values of ε_1 and ε_2 for the ProDisc-C decrease.

Between these two models, in vertebra C5, ε_1 values increased by approximately a factor of 10 and ε_2 by a factor of 20, from the Native Model to the ProDisc-C Model. In vertebra C6 ε_1 values tripled from the ProDisc-C Model to the Native Model. However, ε_2 values in the Native Model were half those registered in the Cage Model.

Experimental Cage Model vs Experimental ProDisc-C Model

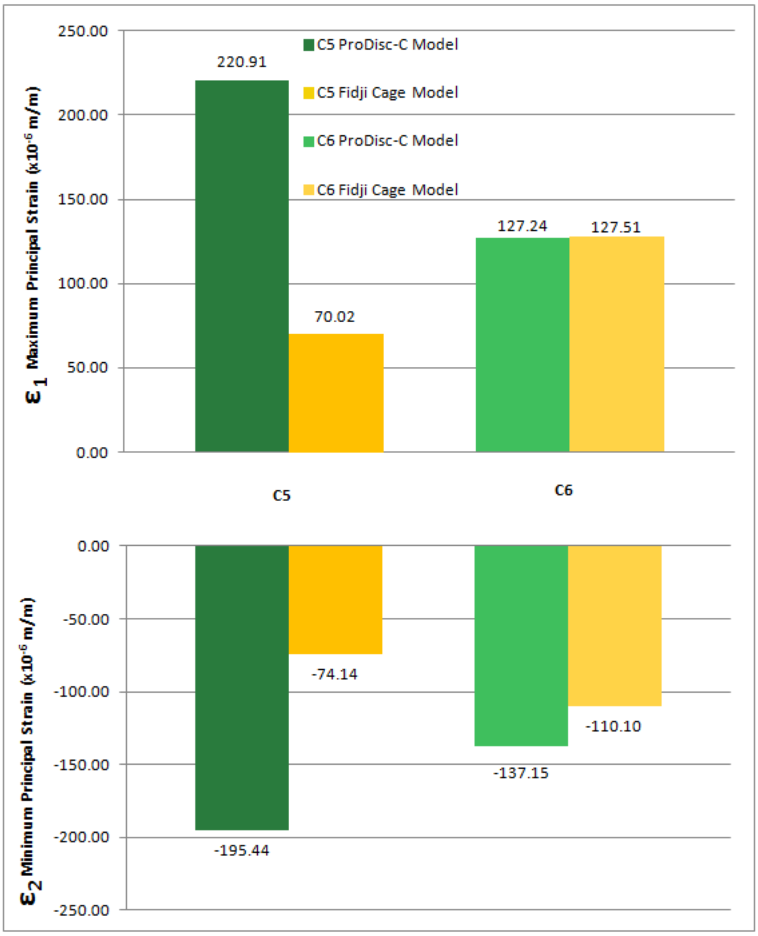

Figure 4.20: Strain results ProDisc-C vs Cage model.

In the last experimental comparison, both implanted models were compared. For both vertebrae, differences between these two models weren't as great as the differences observed between each of these implanted models and the Native Model. In vertebra C5 the absolute values of ε_1 and ε_2 were 3 and 2.6 times greater, respectively, in the ProDisc-C Model than in the Cage Model.

The value of ε_1 for vertebra C6 in the Cage Model were practically the same as those for the ProDisc-C Model, where the value for the former was 0.2% greater than for the latter. The absolute values of ε_2 were 20% greater in the ProDisc-C Model compared to the Cage Model.

4.4 Discussion

These experimental models were essential for the validation of the results obtained from the numerical models. However, important differences between the two types of models (experimental and numerical) had to be take into account.

The Catia Foam Models were created so as to minimize the differences between the numerical bone models and the Experimental Models.

As mentioned, the Numerical Foam Models and the Experimental Models were fundamentally different. Numerical Models were obtained from CT images of a male patient, while the Experimental Models were created from a basic cervical spine model purchased from SYNBONE [Anatomical Models for Education]. Intervertebral disc material properties weren't the same (between the Numerical Foam Model and the Experimental Models) and results were taken approximately from the same area on the vertebra in the Numerical and Experimental models, but there was no precision regarding the exact location of where the strain gauges were measuring results (so that Numerical results could be extracted in this same exact location).

Despite these differences results appeared to be acceptable, since the R^2 is approximately 1 and $m = 1.1139$ (also $\simeq 1$). These values mean that a correlation between experimental and numerical models was achieved. In other words, both maximum and minimum principal strain values obtained for the Numerical Foam Models followed practically the same behaviour of the maximum and minimum principal strain values of the experimental models. Since the Numerical Foam Models were validated it's safe to conclude that the other Numerical Models in this study (Specific Patient Native Model and the Discretized Patient Models) were valid.

In a study performed by Kumaresan et. al. experimental and numerical C4-C6 segment models were studied when subjected to an anterior compressive force. Results for these forces showed that compressive forces in the numerical models were typically slightly higher than the results for the experimental studies [54].

There was a bigger difference between the two models (experimental and numerical) for vertebra C6 in the Native Models, and observing that for vertebra C5 (also in the Native Models), values were practically the same, it stands to reason that forces applied weren't transferred in the same way from vertebra C5 to C6 in the Experimental and Numerical Native Models. This difference in values may be due to the fact that in the Numerical Native Foam Model, the mechanical properties of the intervertebral disc were determined for a realistic intervertebral disc (mechanical properties for annulus fibrosus and nucleus pulposus) and for the Experimental Native Model the intervertebral disc was but a very soft uniform spongy material. So the intervertebral disc in the Numerical Native Foam Model behaved more like a shock absorber than the one in the Experimental Native Model, seeing as the maximum principal values for vertebra C6 were lower in the Numerical Foam Native Model than in the Experimental Native Model.

In the Experimental Native Model versus Experimental Cage Model comparison, vertebra C6 presented a much higher value of extension strain for the Native model compared to the Cage Model. This may be due, once again, to the fact that the intervertebral disc in the Native Model was practically nonexistent. In other words, if the intervertebral disc had been made of a material closer to that of a real intervertebral disc then it would have likely performed better as a shock absorber. Had this been the case then the value of ε_1 for vertebra C6, in the Native Model, would have been lower, and might even well have been below that of the Cage Model.

The fact that values were higher in the C5 vertebra, for the ProDisc-C Model, may have been due to the fact that not only was one of the C5 Strain Gauge's filaments damaged, (therefore requiring a calculated approximation for the values of this damaged filament) but also because the strain gauge in vertebra C5 was directly on the part of the vertebra where the ProDisc-C was in contact with the vertebra. In theory strain values would be higher in the ProDisc-C/vertebra interface when compared to any other section of the vertebra. Since the strain gauge in vertebra C6 was positioned solely on the "cortical bone" of the vertebra it stands to reason that these absolute strain values would be inferior to the absolute strain values of the strain gauge positioned at the ProDisc-C/"bone" interface. So the increase in absolute strain values from vertebra C5 to vertebra C6 in the ProDisc-C model may be justified in this way.

When comparing the Cage model to the ProDisc-C model, absolute strain values were generally higher for the ProDisc-C model. The absolute principal strain values for vertebra C5 were greater for the ProDisc-C Model than for the Cage Model. This may have been due to the positioning of the strain gauge in the C5 vertebra in relation to the location of the implant. Even though the ProDisc-C is, in theory, better suited to the mechanics of the cervical spine (going hand in hand with lower absolute principal strain values), it requires more bone extraction than the Fidji Cage. For this reason the ProDisc-C would generally be associated to higher absolute strain values in the anterior area of the vertebral body than the Fidji Cage.

When performing the two different "surgeries" (implanting the Fidji Cage and the ProDisc-C) there was a significant difference noted regarding the stabilization of the implants. Even though the ProDisc-C had the fins that guarantee it wouldn't slide on the vertebrae, the cervical Cage's geometry seemed better suited to the vertebral body geometry. The topsurface of the Fidji Cage was convex and fit better in vertebra C5, than the ProDisc-C (with flat surfaces) did.

Chapter 5

Conclusions

This study was performed with the purpose of studying the biomechanics of the cervical spine, and to ascertain how it is affected by an implant. Not only is the spine an extremely intricate and complex structure, but it also varies slightly from one healthy person to another, these factors only add a degree of difficulty when trying to find solutions for spinal injuries or illnesses. When trying to find solutions for anomalies in living/breathing beings it's important to be aware of the fact that there isn't much space for error, and that every case is different. In the case of cervical implants, different patients will react in different ways to a same implant, inserted in the same part of the spine.

The results obtained in this study for the Numerical Native Models were inferior (in magnitude) to those obtained in a study by Bozkus et. al. [25] who studied the C4-C6 spinal segment by using an Occiput-T1 human cadaver model. In this study strain gauges were used and applied on vertebrae C4, C5 and C6. A compressive force of 50 N was applied on vertebra C1.

The compressive strain values obtained by Bozkus et. al. were approximately -440, -880 and -760 for vertebrae C4, C5 and C6 respectively. These higher strain values may have been due to the fact that all cervical components were kept in the cadaver's cervical spine, thus increasing strain values in this model. Bearing this in mind the results obtained here are in agreement with those in the aforementioned study.

It was concluded that there are significant alterations to the cervical spine's biomechanics when any implant is inserted. By simulating the effect of ossification between implant and vertebra it was made clear that once the bone has had time to grow into the implant strain levels decreased. This is in agreement with a study performed by Faizan et. al. who studied the artificial disc influence in the biomechanics of the C3-C7 cervical spine segment. Faizan et. al. also described an increase in strain levels when inserting an implant in the studied segment of the cervical spine [3].

Numerical results for all Discretized Patient Models were affected by the simplification of the material properties. Even though a wide range of results was observed, the features in all respective graphs are still smoother than those that would have been obtained had all models been simulated with Marc. However, these results are still in agreement with other studies [54].

It would be interesting and pertinent to procure the means to simulate these different cases (implanted models) with a programme that recognizes grey scale information from a programme such as ScanIP so that models would be closer to a realistic model.

For the numerical models, results were extracted from a ring-like line round the intervertebral disc area, whilst in the experimental models the results were extracted from the anterior surface of the vertebral bodies.

For the ring-like results, the greater differences in strain values between the different models were undoubtedly for vertebrae C5 and C6 since these were the ones in direct contact with the implant.

The biggest variation in strain values between any of the implanted models to the Native Model in vertebra C4 was $2x10^{-5}$ m/m. However, for vertebrae C5 and C6 these differences were greater: $3x10^{-5}$ and $5x10^{-}5$ for the ProDisc-C model and $7x10^{-5}$ and $10x10^{-5}$ for the Cage Model respectively.

The greatest differences in peak values verified for both cortical and trabecular bone were in the lateral areas of the vertebrae, which suggest that by altering the geometry of both implants these may be better fitted on the vertebral body, and decrease strain level values.

In the experimental part of the study the maximum strain values were clearly obtained for the ProDisc-C model, due to the area on the vertebral body where results were extracted from. Finally, it's important to bear in mind that when the ProDisc-C has been inserted into a patient's cervical spine, bone tissue growth should take place, and once this has happened strain values in the anterior area of the vertebral body would decrease in theory. By assessing the experimental results it seemed that the vertebra suffers significant alterations in this anterior area, when an implant is inserted, especially in the case of the ProDisc-C. If the vertebrae are in any way damaged, (thus leading to surgery), and by evaluating these results, the Fidji cervical cage may be a safer option when compared to the ProDisc-C implant since the cervical cage wouldn't require much bone removal that could lead to fractures in the vertebrae.

Cervical implants still have room for improvement. Long term results on studies regarding implanted prosthetic discs are still needed to better assess the biomechanical effect of these implants in the cervical spine [20]. However, in general, cervical arthroplasty seems to be a better option for most cases of degenerative disc disease than cervical arthrodesis. If more than one disc has suffered degeneration, then, and depending on the location of these damaged intervertebral discs a cervical cage, as well as a cervical prosthetic disc, may be inserted, since even though movement would be restricted in one area of the spine, the prosthetic disc could make up for this restriction without suffering as much degeneration as a natural disc would.

It would be interesting to perform an experimental study with a fresh cadaver cervical spine segment (C4-C6) and, by measuring strain values on the anterior surfaces of the vertebral bodies, compare the strain levels to those obtained for the three cases which were the object of study of this thesis (Native, Fidji Cage and ProDisc-C). In this study there was no focus on the fact that the human body is in constant regeneration of human tissues; this process may be slower or quicker depending on the patient, but even if a fresh cadaveric model of the C4-C6 segment were to be studied, this model would still be affected by an error associated to the lack of tissue regeneration.

Another suggestion towards the improvement of prosthetic implants would be to ascertain how a prosthetic disc with convex upper and lower surfaces (as opposed to the case of the ProDisc-C) would behave in the cervical spine.

Bibliography

[1] Catia software: Material library.

[2] www.matweb.com/.

[3] S. R. Garfin C. M. Bono H. Serhan A. Biyani H. Elgafy M. Krishna-T. Friesem A. Faizan, V. K. Goel. Do design variations in the artificial disc influence cervical spine biomechanics? a finite element investigation. *European Spine Journal*, 18:1211–1216, 2009.

[4] U. Simona E. Hartwigb L. Kinzlb L. Claesa H.-J. Wilke A. Kettlera, H. Schmitta. A new acceleration apparatus for the study of whiplash with human cadaveric cervical spine specimens. *Journal of Biomechanics*, 37(10):1607–1613, October 2004.

[5] P. L. Kuflik M. G. Neuwirth A. L. Wollowick, A. M. Casden. Rheumatoid arthritis in the cervical spine: What you need to know. *The American Journal of Orthopedics*, 46(8):400–406, August 2007.

[6] Yuehuei An. *Internal Fixation In Osteoporotic Bone.* Thieme, 2002.

[7] A. Jafarigol V. Vihko Asg. Rezasoltani, A. Ahmadi. The reliability of measuring neck muscle strength with a neck muscle force measurement device. *Journal of Physical Therapy Science*, 14(1):7–12, 2003.

[8] Z. C. Zhong S. H. Chen C. Hung C. C. Lo, K. J. Tsai. Biomechanical differences of coflex-f and pedicle screw fixation combined with tlif or alif - a finite element study. *Computer Methods in Biomechanics and Biomedical Engineering*, 14(11):947–956, 2011.

[9] R. J. Nelson N. H. Metcalf J. T. Robertson C. C. Wigfield, S. S. Gill. The new frenchay artificial cervical joint: Results from a two-year pilot study. *Spine*, 27(22):2446–2452, 2002. Department of Neurosurgery, The Academic Centre, Frenchay Hospital, Bristol, United Kingdom.

[10] B. Costachescu C. E. Popescue, J. Muller. 1 year experience with solis peek cages in cervical disectomy and fusion. *Romanian Neurosurgery*, 16(2):27–33, 2010.

[11] S. R. Garfin C. M. Bono. History and evolution of disc replacement. *The Spine Journal*, 4:145S–150S, 2004.

[12] R. M. Hall J. Fisher T. D. Brown C. M. Goreham-Voss, P. J. Hyde. Cross-shear implementation in sliding-distance-coupled finite element analysis of wear in metal-on-polyethylene total joint arthroplasty: Intervertebral total disc replacement as an illustrative application. *Journal of Biomechanics*, 43:1674–1681, 2010.

[13] B. L. Currier J. P. Dormans J. Dvorak F. Eismont S. R. Garfin-H. N. Herkowitz C. G. Ullrich A. R. Vaccaro C. R. Clark, E. C. Benzel. *The Cervical Spine: Cervical Spine Research Society Editorial Committee.* Lippincott Williams and Wilkins, 4th edition, November 2004.

[14] H. Choi. Analysis of human neck loads during isometric voluntary ramp efforts: Emg-assisted optimization modelling approach. *KSME International Journal*, 14(3):338–349, 2000.

[15] Hyeonki Choi. Quantitative assessment of co-contraction in cervical musculature. *Medical Engineering & Physics*, 25(2):133–140, 2003.

[16] M. G. Fehlings D. C. Baptiste. Pathophysiology of cervical myelopathy. *The Spine Journal*, 6:190S–197S, November 2006.

[17] S. M. Kurtz D. J. Jaekela, D. W. MacDonalda. Characterization of peek biomaterials using the small punch test. *Journal of the Mechanical Behavior of Biomedical Materials*, 4(7):1275–1282, 2011.

[18] R. Delamarter J. Goldstein J. Zigler B. Tay B. Darden D. Murrey, M. Janssen. Results of the prospective, randomized, controlled multicenter food and drug administration investigational device exemption study of the prodisc-c total disc replacement versus anterior discectomy and fusion for the treatment of 1-level symptomatic cervical disc disease. *The Spine Journal*, 9:275–286, 2009.

[19] T. D. Brown D. R. Pedersen, J. J. Callaghan. Activity-dependence of the "safe zone" for impingement versus dislocation avoidance. *Medical Engineering & Physics*, 27:323–328, 2005.

[20] N. Duggal. Cervical disc arthoplasty: A practical overview. *Current Orthopaedic Practice*, 20(3):216–221, 2009.

[21] H. W. Ng E. C. Teo. Evaluation of the role of ligaments, facets and disc nucleus in lower cervical spine under compression and sagittal moments using finite element method. *Medical Engineering & Physics*, 23:155–164, 2001.

[22] L. M. S. Barreira E. M. M. Fonseca, M. J. Lima. Human femur assessment using isotropic and orthotropic materials dependent of bone density. 3rd international conference on integrity, reliability and failure, porto/portugal, Polytechnic Institute of Bragança, Bragança, Portugal, July 2009.

[23] M. A. Martinez D. Palanca M. Doblare E. Pena, B. Calvo. Finite element analysis of the efect of meniscal tears and meniscectomies on human knee biomechanics. *Clinical Biomechanics*, 20:498–507, 2005.

[24] H. Gray. *Anatomy Of The Human Body.* Philadelphia: Lea & Febiger, 20th edition, 1918.

[25] E. Sunbuloglu E. Tanyeli A. C. Sarioglu M. Hanci H. Bozkus, E. Bozdag. Surface strain and stress analysis of the mid-cervical vertebrae bony compartments: A biomechanical pilot study. *Turkish Neurosurgery,*, 14(1-2):1–11, 2004.

[26] L. Pimenta H. D. Link, P. C. McAfee. Choosing a cervical disc replacement. *The Spine Journal*, 4:294S–302S, 2004.

[27] D. Kopansky-Giles C. Hagino S. Fuligni H. T. Vernon, J. Piccininni. Chiropractic rehabilitation of spinal pain patients: Principles, practices and outcome data. *Journal of the Canadian Chiropractic Association*, 39(3):147–153, 1995.

[28] S. K. Ha. Finite element modeling of multi-level cervical spinal segments (c3-c6) and biomechanical analysis of an elastomer-type prosthetic disc. *Medical Engineering & Physics*, 28:534–541, 2006.

[29] Z.R. Zhoua H.Y. Yua, Z.B. Caia. Fretting behavior of cortical bone against titanium and its alloy. *Wear - 15th International Conference On Wear Of Materials*, 259:910–918, 2005.

[30] A. D. Sharan J. A. Goldstein. Cervical artificial disc replacement technologies. Master's thesis, NYU-Hospital for Joint Diseases; Seaport Orthopaedic Associates Spine Center, 2006.

[31] F. V. Calenbergh J. Goffin, J. V. Loon. Cervical arthroplasty with the bryan disc, 4-year results. *The Spine Journal*, 6(5):62S–63S, September/October 2006. Supplement 1.

[32] K. Baker J. Marzluff, J. Highsmith. Long-term clinical experience with secure-c cervical disc arthroplasty. *The Spine Journal*, 9(10):189S, October 2009.

[33] R. Bock D. E. Harrison B. Holland J. McAviney, D. Schulz. Determining the relationship between cervical lordosis and neck complaints. *Journal of Manipulative and Physiological Therapeutics*, 28(3):187–193, 2005.

[34] Z. Sun B. K. Tay G. Q. Yu F. Y. Zhu D. Z. Zhu-H. J. Xu J. S. Chen, S.P. Lau. Structural and mechanical properties of nitrogen ion implanted ultra high molecular weight polyethylene. *Surface and Coatings Technology*, 138:33.38, 2001.

[35] I. A. Kapandji. *Fisiologia Articular: Esquemas Comentados de Mecânica Humana - Vol. 3.* Manole, São Paulo, 1987.

[36] K. P. Singer L. G. F. Giles. *Clinical Anatomy And Management Of Cervical Spine Pain.*, volume 3. Butterworth-Heinemann, January 1998.

[37] P. C. McAfee A. Cappuccino A. Crockard B. Cunningham F. Bellera L. Pimenta, M. Leon. Single- versus multilevel cervical disc replacements: Two-year follow-up of the pcm discs. Technical report, America Association of Neurological Surgeons, 2005.

[38] D. S. Cronin M. B. Panzer. C4-c5 segment finite element model development, validation, and load-sharing investigation. *Journal of Biomechanics*, 42:480–490, 2009.

[39] D. Tejszerska M. Gzik, W. Wolanski. Experimental determination of cervical spine mechanical properties. *Acta of Bioengineering and Biomechanics*, 10(4):49–54, 2008.

[40] R. R. Pelker T. Videman G. E. Friedlaender W. O. Southwick M. M. Panjabi, D. J. Summers. Three-dimensional load-displacement curves due to forces on the cervical spine. *Journal of Orthopaedic Research*, 4(2):152–161, 1986.

[41] J. F. Loss M. O. Melo M. Torre R. E. Silva R. B. Teixeira-G. B. Delwing M. Pasini, C. T. Candotti. A biomechanical model of the cervical spine during cycling. Master's thesis, University of Vale do Rio dos Sinos, SÃ£o Leopoldo, Brazil, 2007.

[42] S. M. Papadopoulos M. S. Gerber, R. M. Galler. Spinal disk arthroplasty. *Barrow Quarterly*, 19(1):1–9, 2003.

[43] G. M. McKhann. *Clinical Neurosurgery: A Publication Of The Congress of Neurological Surgeons.*, volume 53. Lippincott Williams and Wilkins, 1st edition, December 2006.

[44] D. J. Maiman J. F. Cusick A. Sances P. R. Walsh N. Yoganandan, F. A. Pintar. Human head-neck biomechanics under axial tension. *Medical Engineering and Physics*, 18:289–294(6), 1996.

[45] The Board of Trustees. *Back Pain: Overview.* PhD thesis, University of Illinois, 2010.

[46] A. B. Ndu Y. Tominaga E. J. Carlson W. Rubin F. H. Dipl-Ing M. M. Panjab P. C. Ivancic, M. P. Coe. Dynamic mechanical properties of intact human cervical spine ligaments. *The Spine Journal*, 7:659–665, 2007.

[47] E. A. Malkia H. Kautiainen A. H. Hakkinen P. K. Salo, J. J. Ylinen. Isometric strength of the cervical flexor, extensor, and rotator muscles in 220 healthy females aged 20 to 59 years. *Journal of Orthopaedic & Sports Physical Therapy*, 36(7):495–502, 2006.

[48] K. C. Hayes P. M. Barton. Neck flexor muscle strength, efficiency and relaxation times in normal subjects and neck pain and headache. *Archives of Physical Medicine and Rehabilitation*, 77:680–687, 1996.

[49] C. Yomtob R. Brynin. Missed cervical spine fracture: Chiropractic implications. *Journal of Manipulative and Physiological Therapeutics*, 22(9):610–614, November 199.

[50] G. Hoffman R. Hoffman. Single-site comparison of one and two level mobi-c cervical disc replacement and anterior cervical discectomy and fusion control: Preliminary outcomes of investigational fda trial. *The Spine Journal*, 9(10):43S, October 2009.

[51] G. R. Trost R. Moftakhar. Anterior cervical plates: A historical perspective. *Neurosurg Focus*, 16 (1)(8):1–5, January 2004.

[52] M. Ronthal. On the coincidence of cervical spondylosis and multiple sclerosis. *Clinical Neurology and Neurosurgery*, 108(3):275–277, March 2006.

[53] M. G. Fehlings S. Carette. Clinical practice. cervical radiculopathy. *The New England Journal of Medicine*, 353:392–399, 2005.

[54] F. A. Pintar D. J. Maiman S. Kumaresan, N. Yoganandan. Finite element modeling of the cervical spine: Role of intervertebral disc under axial and eccentric loads. *Medical Engineering & Physics*, 21:689â700, 1999.

[55] D. D. Ohnmeiss S. L. Blumenthal. Intervertebral cages for degenerative spinal diseases. *The Spine Journal*, 3(4):301–309, July 2003.

[56] North American Spine Society. Cervical stenosis & myelopathy. North American Spine Society - Public Education Series, 2006.

[57] M. K. Steven. Implantable peek polymers: A decade of progress in spine: Device manufacturers continue to expand their peek product offerings. *Orthopedic Design & Technology*, 18:1–7, January 2010.

[58] E. C. Benzel V. Gonugunta, A. A. Krishnaney. Anterior cervical plating. *Neurology India*, 53(4):424–432, 2005.

[59] K. R. Tripuraneni W. D. Yu. Cervical interbody cage fusions. *Seminars In Spine Surgery*, 16:2–8, 2004.

[60] T. Sato Y. Tanaka, S. Kokubun. Cervical roots as origin of pain in the neck or scapular regions. *SPINE*, 31(17):E568–E573, November 2006.